Section I

RESEARCH IN PROGRESS

Structure of the A=6-14 Nuclei Calculated with an Effective Interaction

Paul S. Hauge and S. Maripuu

Numerous properties of the normal parity states for all 0p shell nuclei are being calculated with the shell model computer codes of French, Halbert, McGrory and Wong.[1] The Hamiltonian is diagonalized in the full 0p basis, and the effective two-body interaction used in the calculation is computed directly from the relative Sussex matrix elements.[2] Corrections to the two-body matrix elements (2BME's) involving intermediate states up to $2\hbar\omega$ in excitation energy are computed to second order in the perturbation theory. As seen in Table I, the second order corrections change the 2BME's significantly and are definitely needed, if one is to obtain satisfactory agreement between experiment and theory. The effective 2BME's shown in the last column are found to be similar to those determined from the least squares fittings of Cohen and Kurath[3] and of Goldhammer and coworkers.[4]

The only two parameters that one could possibly consider in the present calculation are the harmonic oscillator size parameter (b), and the energy separation between the $p_{3/2}$ and $p_{1/2}$ single particle states (ε). Recent experimental data has shown (somewhat surprisingly) that all 0p shell nuclei have approximately the same rms radius.[5] We therefore choose to fix b at a value of 1.7 fm for all nuclei, and not vary this parameter. On the other hand, the average potential well depth should increase considerably as one proceeds from mass A=6 to A=14, and this should affect the energy separation of the single particle orbits. Consequently, we allow ε to vary from mass number to mass number.

A comparison of calculated with experimental energy spectra is very encouraging, and much better than one might expect for a one parameter theory. Two minor, but noticable discrepancies between the theoretical and experimental spectra were the following:

1. We calculate the three lowest states in ^{8}Be around 2.0 MeV too high. Also, two low-lying states in ^{12}C (at 7.66 and 10.1 MeV) are observed much lower than theoretically predicted.
2. The lowest $J^{\pi}T=0^{+}1$ states in masses A=6, 10, and 14 are predicted about 2.0 MeV too low.

The first discrepancy is not serious, since the five experimental states involved have high reduced α decay widths, and are known to be collective states of highly deformed α-structures.[6] In order to accurately describe these states in the shell model, we would need a larger configuration basis for constructing the Hamiltonian. The second discrepancy is a common problem that arises in many calculations with realistic 2BME's.[7] It could presumably be rectified by (1) introducing an attractive monopole shift into the effective diagonal T=0 2BME's, or (2) including higher order corrections into the perturbation calculation.

Table II shows the values of ε that yield the best agreement with the experimental levels for each mass number considered. The number shown for mass A=5 is an experimental number.[8]

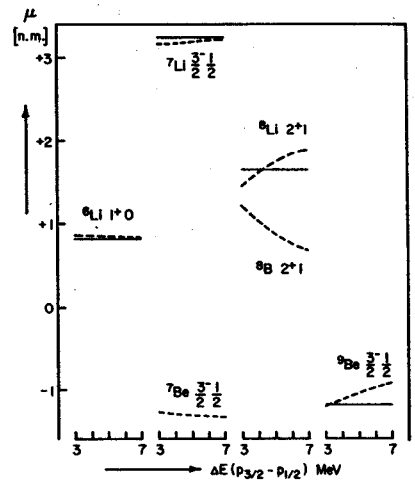

Fig. 1 Magnetic moments for $6 \leq A \leq 9$. Solid lines denote experimental numbers, and the dashed lines show how the theoretical moments vary with ε.

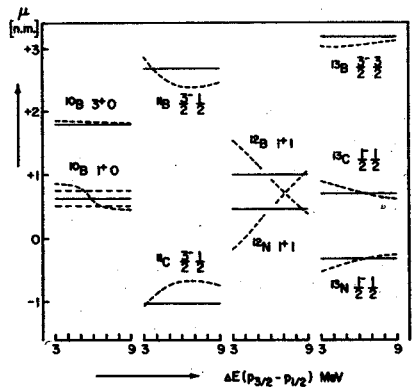

Fig. 2 Magnetic moments for $10 \leq A \leq 13$.

Using the eigenvectors found from the energy-level fitting, we computed magnetic dipole moments, M1 transition strengths, β-decay matrix elements, and single nucleon spectroscopic factors. Most results are in good agreement with experiment. Typical results are shown in Figs. 1 and 2, where we show how the magnetic moments vary with increasing ε. In a few nuclei, it was found that some observables agreed with the experimental numbers at slightly different values of ε. An example of such a variance is shown in Fig. 3 for the mass A=13 nuclei. Most observables are predicted best at ε=6.8 MeV, but the β-decay rates favor a value of ε=5.0 MeV

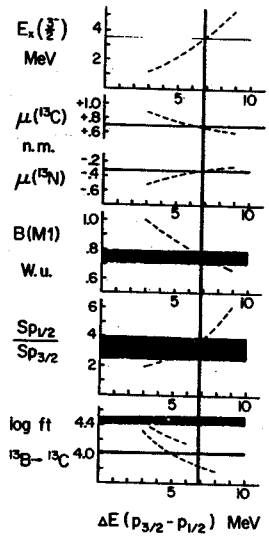

Fig. 3 Various observables for the mass A=13 nuclei. Horizontal solid lines denote measured quantities, their width implying experimental uncertainty. Dashed lines show how theoretical values vary with ε.

We find it encouraging, indeed, that our calculation, essentially without parameters and derived from first principles, does just as well as those works[3,4] which deduce the effective 2BME's from a least-squares fitting and which have upwards of thirteen free parameters.

References

1. J.B. French, E.C. Halbert, J.B. McGrory, and S.S.M. Wong, in Advances in Nuclear Physics, Vol. 3, edited by M. Baranger and E. Vogt (plenum Press, New York, 1969), pp. 193-257.
2. J.P. Elliott, A.D. Jackson, H.A. Mavromatis, E.A. Sanderson, and B. Singh, Nucl. Phys. A121, 241(1968).
3. S. Cohen and D. Kurath, Nucl. Phys. 73, 1(1965).
4. P. Goldhammer, J.R. Hill, and J. Nachamkin, Nucl. Phys. A106, 62(1968); J.L. Norton and P. Goldhammer, Nucl. Phys. A165, 33(1971).
5. D.H. Wilkinson and M.E. Mafethe, Nucl. Phys. 85, 97(1966).
6. T. Kanellopoulos and K. Wildermuth, Nucl. Phys. 14, 349(1960); H. Morinaga, Phys. Letters 21, 78(1966).
7. M. Dworzecka and H. McManus, BAPS 17, 554(1972).
8. P. Fessenden and D.R. Maxson, Phys. Rev. 133, B71(1964).

TABLE I

The 2BME's, in the form <ab;JT|V|cd;JT>, are shown for the 0p shell along with their most important perturbative corrections. The quantum numbers abcd represent $2J_a$, $2J_b$, $2J_c$, and $2J_d$ respectively. All matrix elements are expressed in MeV's.

Quantum Numbers		Second-Order Corrections			
a b c d - J T	<V>	$\langle V_{3p-1h}\rangle$	$\langle V_{4p-2h}\rangle$	$\langle V_{2p}\rangle$	$\langle V_{eff}\rangle$
3 3 3 3 - 1 0	-1.541	-0.055	-0.112	-0.838	-2.546
- 3 0	-4.060	-0.158	-	-0.764	-4.982
- 0 1	-3.020	-0.276	-0.303	-0.414	-4.013
- 2 1	-1.453	+0.315	-	-0.170	-1.308
3 3 3 1 - 1 0	+3.528	+0.059	+0.316	+0.562	+4.465
- 2 1	-1.539	-0.276	-	-0.127	-1.942
3 3 1 1 - 1 0	+1.676	+0.026	-0.138	+0.437	+2.001
- 0 1	-3.606	-0.643	-0.214	-0.176	-4.639
3 1 3 1 - 1 0	-4.770	+0.196	-0.888	-0.923	-6.385
- 2 0	-5.350	+0.156	-	-1.255	-6.449
- 1 1	-0.728	+0.544	-	-0.051	-0.235
- 2 1	-2.542	+0.522	-	-0.261	-2.281
3 1 1 1 - 1 0	+0.942	+0.256	+0.389	-0.174	+1.413
1 1 1 1 - 1 0	-1.843	+0.065	-0.170	-0.722	-2.670
- 0 1	-0.470	+0.264	-0.152	-0.289	-0.647

TABLE II

Values of the Separation Energy, ε, which yield Optimum Agreement with the Experimental Energy Levels for each Mass Number in the Region $5 \leq A \leq 14$.

A	5	6	7	8	9	10	11	12	13	14
ε(MeV)	2.6 ± 0.4	3.0	3.0	4.8	4.0	7.0	7.0	7.0	6.5	7.0

Proton Capture by ^{7}Be, and the Solar Neutrino Problem

R.G.H. Robertson

The recent experiments of Davis[1] have set an upper limit of 1.0 SNU on the neutrino flux from the sun (1 SNU=10^{-36} captures per target atom per sec.), in sharp disagreement with the theoretical prediction of 9 SNU, calculated by Bahcall and Ulrich.[2] The rare termination of the p-p chain ^{7}Be(p,γ)^{8}B($e^+\nu$)2α results in energetic neutrinos and is calculated to contribute 7.3 SNU. It is therefore important to have an accurate estimate of the rate of this reaction in the solar interior. Very detailed measurements of the cross-section for ^{7}Be(p,γ)^{8}B have been carried out by Kavanagh *et al.*[3,4] at laboratory energies E_p=0.165 to 10.0 MeV. A theoretical extrapolation to lower energies based on a calculation by Tombrello[5] yielded a zero-energy cross-section factor[6] S(0) of 0.034 keV-b, where, if σ is the cross section and E_p the lab proton energy in MeV,

$$S(E_p)=0.8744 l \sigma E_p \exp(3.9734\ E_p^{-1/2})$$

for the ^{7}Be(p,γ)^{8}B reaction. A calculation by Aurdal[7] similar to that of Tombrello gave S(0)= 0.044 keV-b, but the new data of Kavanagh *et al.* were not used in that extrapolation. The value S(0)=0.030 keV-b actually adopted by Bahcall and Ulrich[2] is lower than either of these, and is presumably the result of an empirical extrapolation.

Proton capture by ^{7}Be involves the radiative transition of a proton in a continuum state to the 2^+ ground state of ^{8}B, bound by 137.2 keV. Only dipole radiation is of importance at the energies considered here. Because the spin and parity of ^{7}Be are $\frac{3}{2}^-$, capture from the s and d partial waves leads to E1 radiation, and from the p wave, M1. Higher partial waves cannot contribute to dipole radiation. The calculations of Tombrello[5] and Aurdal[7] assumed that only s wave capture was significant. Re-examination of the ^{7}Be(p,γ)^{8}B reaction shows that while this is approximately true in the solar environment ($E_p \sim 20$ keV), it is not the case at laboratory energies, even as low as 150 keV. The small binding energy of ^{8}B results in a spatially extended wave function, enhancing capture from the p and d partial waves.

Detailed calculation (Fig. 1), in which particular attention was paid to the choice of s wave potential and to the influence of nearby p wave resonances, has yielded a revised cross-section factor at E_p=0.02 MeV of

$$S(.02)=.031 \text{ keV-b.}$$

This value is lower than the previous theoretical results,[5,7] and very close to the empirical value actually used by Bahcall and Ulrich.[2] Thus there is no appreciable change in the predicted ^{8}B neutrino flux from the sun.

References

1. R. Davis, Jr., BAPS 17, 527(1972).
2. J.N. Bahcall and R.K. Ulrich, Astrophys. J. 170, 593(1971).
3. R.W. Kavanagh, T.A. Tombrello, J.M. Mosher, and D.R. Goosman, BAPS 14, 209(1969).
4. C.A. Barnes, in "Advances in Nuclear Physics" ed. M. Baranger and E. Vogt (Plenum Press 1971) Vol. 4, p. 133.
5. T.A. Tombrello, Nucl. Phys. 71, 459(1965).
6. W.A. Fowler, G.R. Caughlan, and B.A. Zimmerman, Ann. Rev. Astron. Astrophys. 5, 525(1967).
7. A. Aurdal, Nucl. Phys. A146, 385(1970).

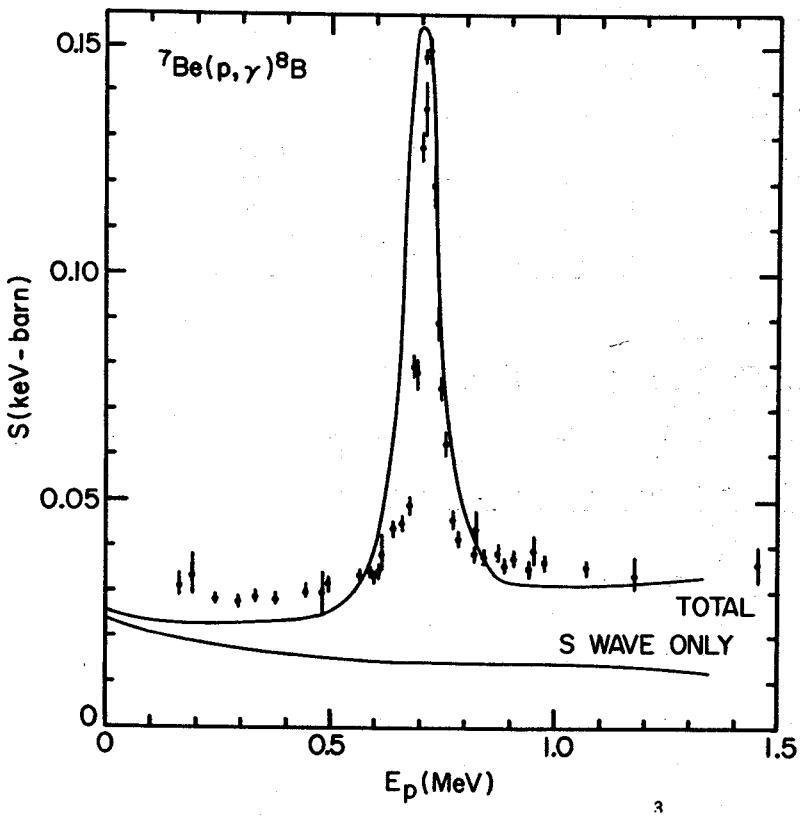

Fig. 1 Comparison between the experimental measurements of the ^{7}Be(p,γ)^{8}B cross-section by Kavanagh *et al.* and the theoretical calculation (smooth curves). The calculation is shown here in absolute form, without normalization to the data. The abscissa is the lab proton energy. The sharp resonance at 720 keV is M1 capture through an unbound 1^+ state in ^{8}B.

A Survey of the (^{3}He,^{7}Be) Reaction

W.F. Steele, G.M. Crawley, and S. Maripuu

During the past year, work has continued[1] on the α-pickup reaction, (^{3}He,^{7}Be). To date, the effort has been directed primarily toward developing an effective, reliable position sensitive gas proportional counter system[2] for the focal plane of the laboratory's split-pole broad range magnetic spectrograph. The basic counter employs a gas chamber 25x1x1 cm with an axial nichrome wire 10μ in diameter. Because ^{7}Li^{3+} and ^{7}Be^{4+} ions have similar differential energy loss for a given momentum, a ΔE signal from the counter provides insufficient information for unambiguous particle identification. Consequently, a plastic scintillator photomultiplier detector is used behind the proportional counter. The scintillator yields both a total energy signal and a signal proportional to the time-of-flight in the spectrometer. Using the ΔE, E, and time-of-flight information, excellent particle identification is routinely achieved.

So far, spectra have been obtained at several angles for ^{12}C, ^{16}O, ^{24}Mg, ^{26}Mg, ^{40}Ca, and ^{48}Ca targets using a 70 MeV incident ^{3}He beam. Spectra from the ^{24}Mg target at 10° and 40° are displayed in Figs. 1 and 2. The doublet structure of each ^{20}Ne level, which is caused by the 432 keV first excited state of ^{7}Be, is clearly resolved. At all angles, the dominant level in ^{20}Ne is the 5.62 MeV 3$^-$. This result is rather surprising if the reaction goes predominantly by α-pickup. The 10° spectrum shows the 4.97 MeV 2$^-$ to be weakly excited. It is essentially absent at larger angles. The 0$^+$ ground state is somewhat weaker than the 1.63 2$^+$, 4.25 4$^+$, and 5.62 3$^-$. Around 7 MeV, there is a cluster of unresolved states. However, it appears from the preliminary energy calibration, that neither the 6.72 nor 7.17 MeV 0$^+$ states are strongly excited as the peak energy is 7.01 MeV. Higher lying states are not clearly resolved. As the resolution is target thickness limited, further work will be undertaken with a thinner target to resolve more states. In addition the survey will be extended to heavier targets in coming months.

References

1. G.M. Crawley et al., A Survey of the (^{3}He,^{7}Be) Reaction, Annual Report 1970-71, Cyclotron Laboratory, Dept. of Physics, Michigan State University.

2. W.A. Lanford et al., A Charge Division Position Sensitive Proportional Counter System, Abstract submitted for the Seattle Meeting of the APS, Nov. 2-4, 1972.

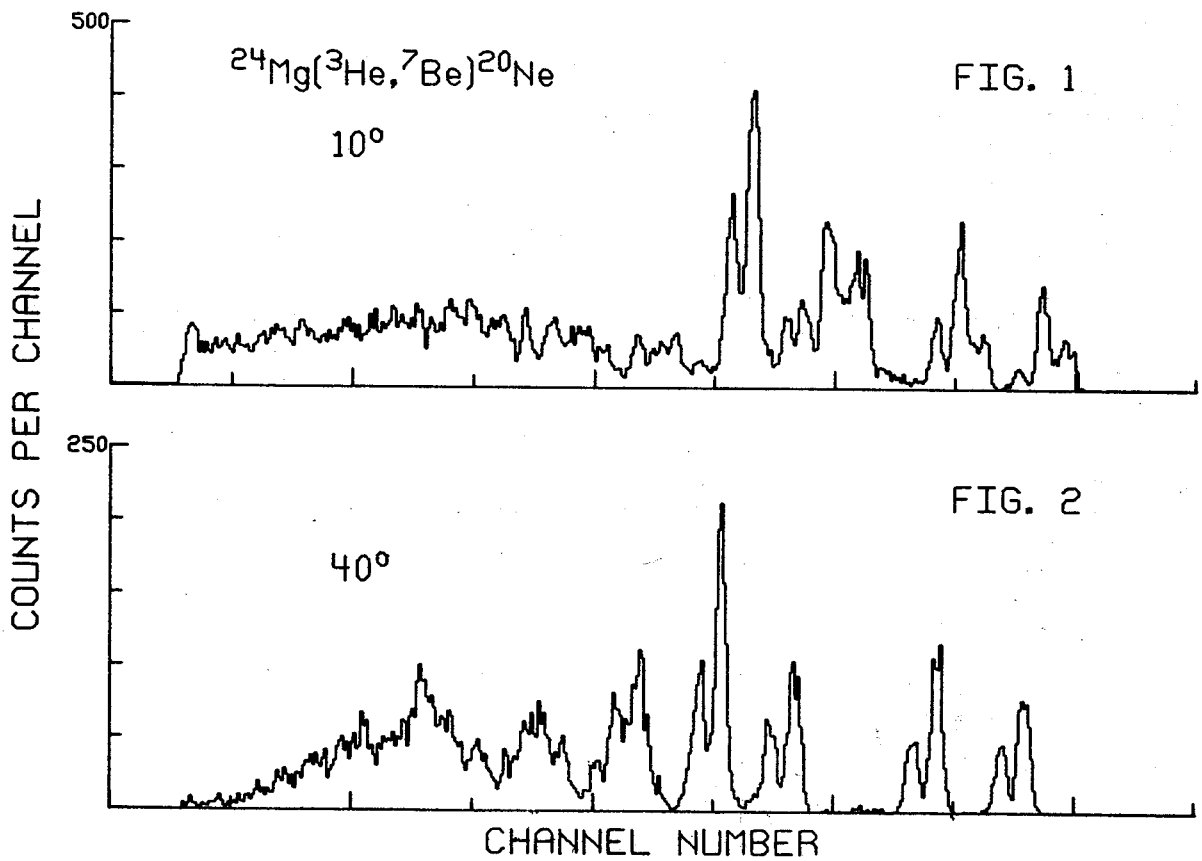

FIG. 1

FIG. 2

A Comment on j-Dependence of ℓ=2 Angular Distributions in the sd-Shell

D.L. Show, J.A. Nolen, and B.H. Wildenthal

Angular distributions of direct single nucleon transfer reactions have shapes which depend in definitively characteristic ways upon the orbital angular momentum (ℓ) transferred in the reaction. Lee and Schiffer pointed out several years ago that in many cases the shapes of the angular distributions depend also, in more subtle ways, on the total spin (j) transferred.[1] Such effects were first noted for ℓ=1 transfers in (d,p) reactions, while subsequent studies[2,3] showed that j-dependence could be discerned in different types of reactions and for several ℓ-values. We concern ourselves here with ℓ=2 transfer via the (p,d) reaction in the sd-shell and the differences in shape between j=5/2 and j=3/2 angular distributions. Several investigations[3-6] have noted that for (d,p) and (p,d) reactions characterized by deuteron energies in the range 7-18 MeV, those transitions transferring j=5/2 have "fatter" angular distributions than those transferring j=3/2. That is, the differential cross-sections for j=5/2 transfer do not decrease as the detection angle is moved away from the main ℓ=2 maximum as rapidly as do those for j=3/2 transfer.

We have studied the $^{30}Si(p,d)^{29}Si$ reaction using a 35 MeV proton beam from the MSU Cyclotron and a wire proportional counter in the focal plane of a split-pole spectrograph. The first five states of ^{29}Si have energies and J^{π} of 0.000 MeV-$1/2^+$, 1.273 MeV-$3/2^+$, 2.032 MeV-$5/2^+$, 2.427 MeV-$3/2^+$, and 3.069 MeV-$5/2^+$. Thus we have deuteron energies about 50% and more larger than those for which j-dependence of the present type has been previously reported. The first two excited states are strongly populated in the (p,d) reaction with ℓ=2 angular distributions. The shapes are compared in Fig. 1. The normalizations of the distributions have been adjusted to make the forward maxima coincide. The curve is calculated for the j=5/2 reaction according to the prescription of Ref. 5.

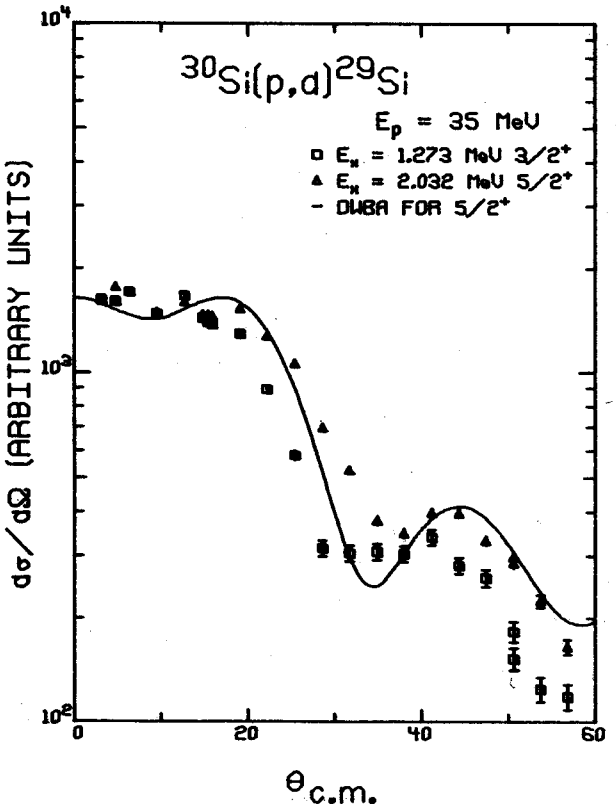

One can see from Fig. 1 that the distribution for the first $3/2^+$ state (which must correspond to j=3/2 transfer) falls off markedly faster from the first maximum than the distribution for the first $5/2^+$ state. This same trend is evident in the distributions for the weakly populated 2.427 MeV and 3.069 MeV states, which ensures that the effect is not merely an effect of different Q-values, but the statistical scatter keeps this higher excitation energy pair from forming an equally conclusive example.

Thus, we observe in the present study j-dependent effects for ℓ=2 transfer which are completely consistent with those outlined by Lee and Schiffer. The qualitative difference between the present shapes of different j-values are smaller than those observed at lower energies, which is also consistent with the extrapolation of the various results obtained at lower energies. The stability of this j-dependent effect and its magnitude seem to be such that reliable s-d shell spectroscopic information can be extracted from reasonably precise (p,d) or (d,p) angular distributions measured at any of a rather wide range of energies.

References

1. L.L. Lee, Jr. and J.P. Schiffer, Phys. Rev. Letters 12, 108(1964).
2. L.L. Lee, Jr. and J.P. Schiffer, Phys. Rev. 136, B405(1964).
3. J.P. Schiffer, L.L. Lee, Jr., A. Marinov, and C. Mayer-Broicke, Phys. Rev. 147, 829(1966).
4. C.M. Glashausser, Thesis, Princeton Univ.
5. M.C. Mermaz, C.A. Whitten, Jr., J.W. Champlin, A.J. Howard, and D.A. Bromley, Phys. Rev. C4, 1778(1971).
6. B.H. Wildenthal and P.W.M. Glaudemans, Nucl. Phys. A108, 49(1968).

← Fig. 1

Mass Multiplets in the sd Shell

W. Benenson, E. Kashy, and I.D. Proctor

The study of mass multiplets in the sd shell has three distinct facets; a) mass measurements of T_z=-3/2 nuclei with the (^{3}He,^{6}He) reaction, b) remeasurements with higher precision of the T=3/2 levels of T_z=±1/2 nuclei, c) shell model calculations of the T_z dependence of the masses of the members of multiplet. The results are expressed in terms of the isobaric mass multiplet equation (IMME) which is usually written as,

$$M(T_z) = a + bT_z + cT_z^2.$$

Since there are four members of a T=3/2 multiplet, the IMME predicts that d, the coefficient of the cubic term required to fit the masses, will be zero. In terms of the four masses $M(T_z)$ the d-coefficient can be written

$$d = \frac{1}{6}[M(3/2)-M(-3/2)+3M(1/2)-3M(-1/2)].$$

The T_z=±3/2 levels are necessary for a determination of d, but the accuracy of the T_z=±1/2 masses is three times more important. That is the reason for adding remeasurements of the T=3/2 levels in the T_z=±1/2 nuclei. During the past year the following experiments have been completed.

i) mass of ^{25}Si[1] and ^{37}Ca using (^{3}He,^{6}He).
ii) the energies of the T=3/2 levels in ^{25}Al, ^{25}Mg, ^{37}Ar, and ^{37}K, using (p,t) (p,h), and (p,d).
iii) the mass of ^{25}Na using (d,^{3}He).
iv) the energy level schemes of ^{25}Si[1] and ^{21}Mg using (^{3}He,^{6}He).
v) mass of ^{29}S using (^{3}He,^{6}He).

All data is taken in the spectrograph. A single-wire resistive-readout proportional counter is the most frequently used detection device. Particle identification is performed by time-of-flight and energy loss information obtained from a plastic scintillator placed behind the wire counter. A position sensitive silicon detector is used frequently also. The method for determining Q-values, mass excesses and excitation energies consists in measuring the magnetic fields required to place the reaction of interest and a calibration reaction at the same position on the focal plane counter. Whenever possible, the calibration reaction is on a nucleus already present in the target. Forward angles (4-10°) are used to minimize kinematic energy shifts.

The T=3/2 levels in the A=25 system are given in Table I below. There are now three complete multiplets, and there is an evident state dependence to the coefficients. The state dependence is due to mixing of the T=3/2 state in the T_z=±1/2 nuclei with T=1/2 states of the same spin and parity. The shell model calculations give effects of this type, but fail in predicting in detail the T_z dependence.

The A=37 system has changed drastically because of the improvement in accuracy over the previous measurements. This is shown in Table II.

Experiments which are presently in progress include the mass of ^{33}A and a study of the T=3/2 levels in T_z=±1/2 nuclei of A=29 and 33. The shell model calculations will be extended to all of the A=4n+1 multiplets in the sd shell.

References

1. W. Benenson, J. Dreisbach, I.D. Proctor, G.F. Trentelman, and B.M. Preedom, Phys. Rev. C5, 1426(1972).

J	^{25}Na	^{25}Mg	^{25}Al	^{25}Sc	b	c	d
5/2$^+$	0.0	*	†	0.0	-4405(8)	221(4)	4.5(4.2)
3/2$^+$	90	80	71(1)	40(5)	-4395(8)	216(4)	7.3(4.3)
1/2$^+$	1068	1009	940(15)	815(15)	-4319(18)	204(6)	4.4(9.0)

*E_x=7780(5) †E_x=7904(5)

TABLE I

A=25,T=3/2 Levels

All energies in keV with errors in parenthesis.

	^{37}Ar(E_x)	^{37}K(E_x)	^{37}Ca(ME)	b	c	d
Present	4993(6)	5045(4)	13144(20)	-6200(8)	200(5)	-2.4(4.9)
Previous*	5010(30)	5048(3)	13230(50)	-6189(30)	182(30)	5(17)

*From J. Cerny, Ann. Rev. of Nuc. Sci., Vol. 18, p. 27.

TABLE II

A=37,T=3/2 Excitation Energies and Mass Excesses

All energies in keV with errors in parenthesis.

Shell Model Calculation for ^{24}Ne

R.G.H. Robertson and B.H. Wildenthal

A large basis shell model calculation for the A=24, T=2 system, with particular emphasis on ^{24}Ne, has now been completed. Recent investigations of ^{24}Ne via the ^{22}Ne(t,pγ)^{24}Ne reaction[1] have provided reliable spin assignments and electromagnetic decay properties for many levels. Interestingly, the ^{24}Ne spectrum resembles the two-particle spectrum of ^{18}O, and is in sharp contrast to the highly rotational isobar ^{24}Mg. One of the principal objectives of the calculation, then, was to see whether the same Hamiltonian[2] which was successful for ^{24}Mg could account for the properties of ^{24}Ne. The Hamiltonian used was one derived by adjustment of the Kuo matrix elements to fit various energy levels in the A=18-22 mass region. No data from A≥23 was employed in the fit. In order to keep the dimensionality of the basis space manageable, at least four particles were required to occupy the $d_{5/2}$ shell, and no more than two were allowed in the $d_{3/2}$ shell.

Figure 1 shows the shell model calculation for ^{24}Ne compared with experiment and with the projected Hartree-Fock calculation of Khadkikar et al.,[3] and the projected Hartree-Bogoliubov calculation of Goeke et al.[4] The agreement between the shell model calculation and experiment is sufficiently good to warrant a 3^+ assignment for the 4.89 MeV level. This is in accord with the experimental observation that the state is very weak in (t,p), as would be expected for an unnatural parity transition.

Results of electromagnetic transition rate calculations are shown in Table I. Standard effective charges of 0.5e have been added to the proton and neutron charges for calculation of E2 rates, and free-nucleon g-values have been used for the M1 rates. The agreement with experiment is excellent.

References

1. A.J. Howard, R.G. Hirko, D.A. Bromley, K. Bethge, and J.W. Olness, Phys. Rev. C1, 1446(1970); K. Bharuth-Ram, K.P. Jackson, K.W. Jones, and E.K. Warburton, Nucl. Phys. A137, 262(1969).
2. J.B. McGrory and B.H. Wildenthal, Phys. Letters 34B, 373(1971).
3. S.B. Khadkikar, S.C.K. Nair, and S.P. Pandya, Phys. Letters 36B, 290(1971).
4. K. Goeke, A. Faessler, and H.H. Wolter, Nucl. Phys. A183, 352(1972).

TABLE I

Electromagnetic Decay Properties and Lifetimes of ^{24}Ne Levels

INITIAL LEVELS				FINAL LEVELS			
J^π	E_x(MeV)	τ(ps) Calc.	τ(ps) Exp.	J^π	E_x(MeV)	Branch(%) Calc.	Branch(%) Exp.
2^+	1.9808	0.71	$1.0^{+0.2}_{-0.4}$	0^+	0.00	100	100
2^+	3.867	0.02	<0.1	0^+	0.00	4	10
				2^+	1.9808	96	90
4^+	3.96	0.90		2^+	1.9808	100	100
0^+	4.6757	3.53	>1.5	2^+	1.9808	98	100
				2^+	3.867	2	0
3^+	4.89	0.04		2^+	1.9808	93	100 (weak)
				2^+	3.867	6	0
				4^+	3.96	1	0
2^+	5.58	0.03		0^+	0.00	3	<5
				2^+	1.9808	95	100
				2^+	3.867	2	<5
3^+	5.64	0.02		2^+	1.9808	34	
				2^+	3.867	54	
				4^+	3.96	11	

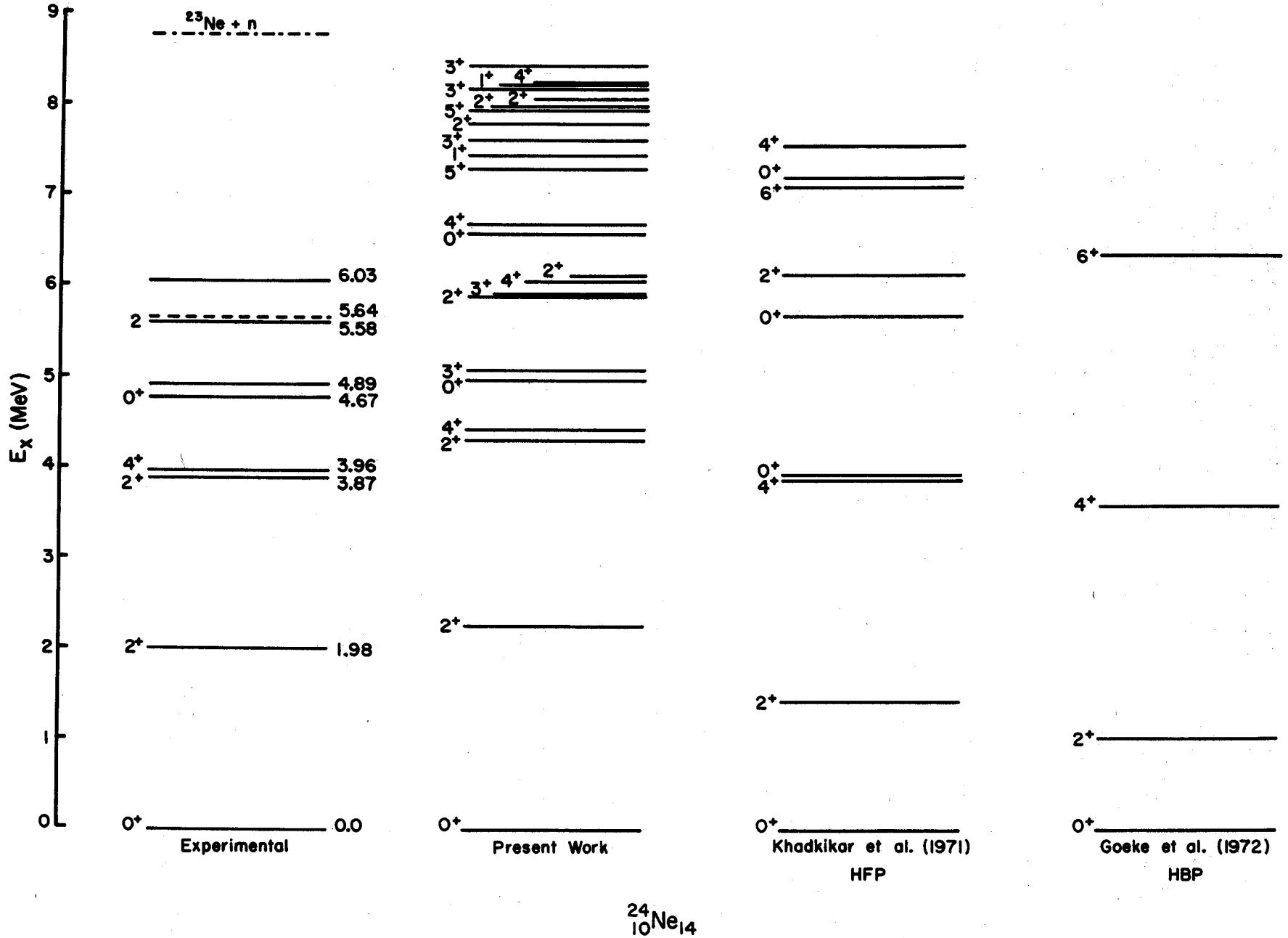
E_x (MeV)
^{23}Ne + n
6.03
5.64
5.58
4.89
4.67
3.96
3.87
1.98
0.0
Experimental
Present Work
Khadkikar et al. (1971)
HFP
Goeke et al. (1972)
HBP
$^{24}_{10}Ne_{14}$

Fig. 1

Three-Neutron Transfer Reaction Mechanism

E. Kashy, W. Benenson, and I.D. Proctor

In the course of our investigation of proton rich nuclei via the (^{3}He,^{6}He) reaction, we have been struck by the large variation in some of the measured cross sections, and by the fact that the $f_{7/2}$ shell cross sections are as large and sometimes greater than those in the 1p and 2s-1d shell. For example the (0.25 μb/ster) cross section in the ^{40}Ca to ^{37}Ca ground state transition is about 7 times smaller than for the ^{58}Ni to ^{55}Ni transition. Table I is a partial list of the measured cross sections and indicates the typically small magnitude (∿1 μb/ster) for this reaction.

The most striking variation is found in the bombardment of ^{13}C. The 2^+ level of the residual nucleus ^{10}C is excited approximately 40 times more strongly than the 0^+ state of that nucleus. The measured angular distribution for the 2^+ level is shown in Fig. 1 and exhibits some of the characteristics usually associated with a direct reaction mechanism. Part of the large enhancement of the 2^+ excitation relative to the 0^+ can be understood qualitatively on a very simple model, but does not account for the factor of 40 observed. This phenomenon is presently being investigated by G. Bertsch who is carrying out a calculation of the 3n-pickup spectroscopic factors for the reactions using 1p-shell model wave function for the states of ^{13}C, ^{12}C, and ^{10}C.

TABLE I

(^{3}He,^{6}He) Laboratory Cross Section

Target	Residual Nucleus	E_x (MeV)	J^π	dσ/dΩ μb/ster	θ(LAB)
^{12}C(0^+)[a]	^{9}C	0.0	$3/2^-$	2.8 ±0.3	11°
^{13}C($1/2^-$)	^{10}C	0.0	0^+	0.21±0.03	9°
		3.35	2^+	7.7 ±0.2	9°
^{24}Mg(0^+)	^{21}Mg	0.0	$5/2^+$	1.3 ±0.1	8°
		0.21	$1/2^+$	0.05±0.02	8°
		1.08	-	0.42±0.05	8°
^{40}Ca(0^+)	^{37}Ca	0.0	$3/2^+$	0.24±0.03	8°
		1.63	$1/2^+$	0.07±0.02	8°
^{46}Ti(0^+)	^{43}Ti	0.0	$7/2^-$	0.60±0.17	9°
^{54}Fe(0^+)	^{51}Fe	0.27	$7/2^-$	0.70±0.20	9°
^{58}Ni(0^+)	^{55}Ni	0.0	$7/2^-$	1.81±0.20	9°

[a]G.F. Trentelman, B.M. Preedom, and E. Kashy, Phys. Rev. C3, 2205(1971).

Figure 1 →

Search for the Lowest T=2 Level of ^{24}Al

E. Kashy, W. Benenson, and I.D. Proctor

We have measured ^{6}He spectrum from the ^{27}Al(^{3}He,^{6}He)^{24}Al reaction in order to identify the lowest T=2 state in ^{24}Al, i.e. the coulomb analog to ^{24}Ne and ^{24}Si ground states. The level would represent the fourth member of a T=2 isospin multiplet and the first instance of a test of the IMME for T>3/2. The data shows peaks in the region of th spectrum where the level is expected from Coulomb systematics, but there is no enhancement expected (or observed) which would make the state easily identifiable. A better understanding of the reaction mechanism would yield the spin and we are presently investigating that aspect by measuring angular distributions of the (^{3}He,^{6}He) reaction.

The other promising avenue is a comparison of the ^{6}He spectra with spectra from reactions which because of isospin conservation do not populate T=2 levels of ^{24}Al. In this respect, we note that interestingly, the ^{6}He spectra we have measured to levels up to 5 MeV (i.e., T=1 levels) show a very similar excitation of the levels of ^{24}Al as the previously measured spectra of tritons from the ^{24}Mg(^{3}He,t)^{24}Al reaction.[1] If this similarity persists in the region of 6 MeV excitation where the T=2 state is expected, the presence of a peak in the ^{6}He spectrum and not in the triton spectrum would be a good clue for its identification. Since the resolution in the previous (^{3}He,t) data is of ∿85 keV,[1] we are planning to repeat that measurement with special emphasis on the region of excitation around 6 MeV and with improved resolution.

References

1. N. Mangelson, M. Reed, C.C. Lu, and F. Ajzenberg-Selove, Phys. Letters 21, 661(1966).

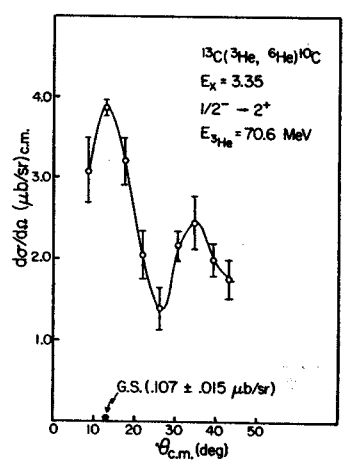

On an ℓ-Forbidden M1 Transition in ^{38}Cl and the Purity of States Whose Energies Obey the Particle-Hole Transformation Rule

S. Maripuu, B.H. Wildenthal, and A.O. Evwaraye*

The analysis of the energies of the low-lying states of ^{38}Cl and ^{40}K was one of the early quantitative successes of nuclear shell model theory.[1,2] If we speak in terms of an ^{16}O core, then the first states of ^{38}Cl should arise in lowest order from the configuration $(\nu d_{5/2})^6$, $(\pi d_{5/2})^6$, $(\nu s_{1/2})^2$, $(\pi s_{1/2})^2$, $(\nu d_{3/2})^4$, $(\pi d_{3/2})^1$, $(\nu f_{7/2})^1$, where ν denotes neutrons and π denotes protons. Similarly, the lowest states of ^{40}K should arise from the configuration formed by adding two more protons to the $d_{3/2}$ orbit. The $d_{5/2}$ and $s_{1/2}$ orbits are thus always filled, as is the $\nu d_{3/2}$ orbit, and we describe ^{38}Cl in terms of $(\pi d^1_{3/2}\text{-}\nu f^1_{7/2})$ couplings and ^{40}K in terms of $(\pi d^{-1}_{3/2}\text{-}\nu f^1_{7/2})$ couplings. In the early shell model predictions of this region, these simple configurations were assumed and it was shown that the observed energies of the 2^-, 3^-, 4^-, and 5^- states in ^{40}K can be obtained almost exactly by applying the appropriate particle-hole transformation rule to the energies of the first 2^-, 3^-, 4^-, and 5^- states of ^{38}Cl.

The accuracy achieved in this transformation was then, and has been since, taken as confirming that the wave functions of the states involved did indeed conform closely to the simple initial assumptions. In addition, subsequent measurements[3,4] have disclosed a higher lying multiplet in each nucleus which can be described in similar fashion as couplings of a $d_{3/2}$ particle (hole) with a $p_{3/2}$ particle, although the transformation of energies is not as accurate as for the lower sets of states.

Recently, however, measurements have revealed some characteristics of ^{38}Cl states which are difficult to reconcile with the simple description just outlined.[5,6] Chief among these data is a strong M1 transition from the 3^- state of the $(d_{3/2}\text{-}p_{3/2})$ multiplet to the 4^- state of the $(d_{3/2}\text{-}f_{7/2})$ multiplet. This transition is, of course, ℓ-forbidden to the extent that the wave functions of the states actually follow the description given heretofore. Other data which cast doubt on the purity of these ^{38}Cl states are the spectroscopic factors for (d,p) stripping on ^{37}Cl.[7] These experiments show some admixing of ℓ=1 into the supposed $(d_{3/2}\text{-}f_{7/2})$ 3^- state.

We have calculated energies and wave functions for ^{38}Cl, ^{39}K, and ^{40}K in a model space which includes active $d_{5/2}$, $s_{1/2}$, $d_{3/2}$, $f_{7/2}$, and $p_{3/2}$ particles, using the codes of French, Halbert, McGrory, and Wong.[8] The two-body matrix elements used in our Hamiltonian were calculated from the Sussex relative oscillator matrix elements[9] with space truncation effects added,[10] and the single-particle energies were chosen to yield calculated spectra for ^{38}Cl, ^{39}K, and ^{40}K in simultaneous best agreement with the experimental spectra. These values for $d_{5/2}$, $s_{1/2}$, $d_{3/2}$, $f_{7/2}$, and $p_{3/2}$ are, respectively, -9.40, -4.90, -2.67, -2.52, and 0.00 MeV. Some of these results for ^{38}Cl and ^{40}K are summarized in Fig. 1 and Table III.

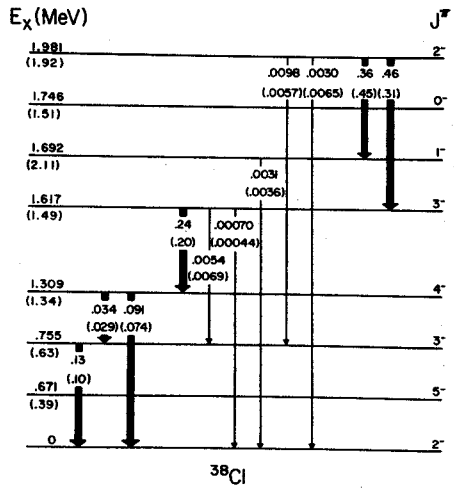

Fig. 1 Experimental and theoretical excitation energies and M1 strengths (in W.U.) of ^{38}Cl. The theoretical values are given in brackets. The experimental numbers refer to the Brookhaven experiment.[4]

The consequences of these wave functions for M1 transitions and S-factors are shown in Tables I and II. Our predictions for these observables (our M1 calculations use operators calculated from the bare-nucleon g-factors) are in uniform good agreement with the observed values. In particular, for ^{38}Cl, the mixing of the ℓ=1 and ℓ=3 strengths for the 3^- states and, most striking, the anomalously large $3^-_2 \to 4^-_1$ M1 transition strength are correctly predicted.

The difficulty of accounting for this M1 transition, enhanced when it should be severely retarded according to simple ideas, has been frequently noted of late.[11,12] No previous calculation seems to have had even qualitative success in reproducing the observed strength. It is thus of interest to see how the correct strength emerges from the present wave functions. The components in the wave functions of the 3^-_2 and 4^-_1 states which are the important contributors to this strength are as follows, with amplitudes preceding the component specification (we now revert to isospin conventions):

$$-.37[(d^5_{3/2})_{3/2,3/2}\ f_{7/2}]+-.87[(d^5_{3/2})_{3/2,3/2}\ f_{7/2}]$$

TABLE I

M1 Transitions in ^{38}Cl and ^{40}K

^{38}Cl				^{40}K			
	M1 Strength (W.U.)				M1 Strength (W.U.)		
$J_i \to J_f$	Argonne[5]	Brookhaven[4]	Theory	$J_i \to J_f$	Argonne[5]	Frankfurt[6]	Theory
$3_1^- \to 2_1^-$	.23	.13	.10	$3_1^- \to 4^-$	.150	.170	.087
$4^- \to 3_1^-$	.062	.034	.029	$2_1^- \to 3_1^-$	.127	.140	.091
$4^- \to 5^-$	.170	.091	.074	$5^- \to 4^-$	.030	.030	.027
$3_2^- \to 4^-$	.38	.24	.20	$2_2^- \to 2_1^-$	.0130	.0100	.0045
$3_2^- \to 3_2^-$	.0084	.0054	.0069	$2_2^- \to 3_2^-$	.0026	.0023	.0016
$3_2^- \to 2_1^-$	.00105	.00070	.00044	$3_2^- \to 2_1^-$	.0033	.0020	.0048
$1^- \to 2_1^-$	.0050	.0031	.0036	$3_2^- \to 3_1^-$	.0046	.0025	.0053
$2_2^- \to 3_1^-$	.0174	.0098	.0057	$3_2^- \to 4^-$	.0030	.0016	.0012
$2_2^- \to 2_1^-$	.0053	.0030	.0065	$1^- \to 2_1^-$	.0076	.0038	.0222
$2_2^- \to 1^-$	.62	.36	.45	$0^- \to 1^-$	.47	.20	.91
$2_2^- \to 3_2^-$	.80	.46	.31				

TABLE II

Spectroscopic Factors of the $^{37}Cl(d,p)^{38}Cl$ Reaction

E_x(MeV)	J^π	Exp [5]		Theory	
		S(ℓ=3)	S(ℓ=1)	S(ℓ=3)	S(ℓ=1)
.0	2^-	.85		.88	.03
.67	5^-	.78		.92	
.76	3^-	.59	.09	.72	.17
1.32	4^-	.70		.81	
1.62	3^-		.40	.15	.46
1.69	1^-		.81		.80
1.75	0^-		1.08		.94
1.98	2^-		.70	.007	.76

$$-.39[s_{1/2}^{-1}(d_{3/2}^6)_{2,1}\ f_{7/2}\ ] \to -.13[s_{1/2}^{-1}(d_{3/2}^6)_{2,1}\ f_{7/2}]$$

and

$$.33[s_{1/2}^{-1}(d_{3/2}^6)_{0,1}\ f_{7/2}\ ] \to .25[s_{1/2}^{-1}(d_{3/2}^6)_{0,1}\ f_{7/2}]$$

Since the weightings of these three pairs of components from the M1 single-particle matrix elements are about 1 to 3 to 3, respectively, we see that the excitations from the $s_{1/2}$ to the $d_{3/2}$ orbit are of comparable importance to the mixing between $f_{7/2}$ and $p_{3/2}$ excitations in contributing allowable paths for the M1 transition. (The $s_{1/2}$ particles, as well as $f_{7/2}$ and $p_{3/2}$, have their spins parallel to the orbital angular momentum, thus producing strong isovector contributions to the M1 strengths.[13]) And, of course, in another sense these $s_{1/2}^{-1}$ components are vital because they provide the fragmentation of the wave functions from which the coherent strength necessary to reproduce the observed enhancement can be built up. The dominating aspect of the coherence of these fragments is pointed up dramatically when we consider that the $3_2^- \to 2_1^-$ transition has individual contributions of equivalent size to those for the $3_2^- \to 4_1^-$ and that those for the $3_2^- \to 3_1^-$ transition are actually considerably larger (as pointed out by Erné[14]). However, in these cases the signs of the individual components are such that the various contributions cancel each other.

The general conclusions from the present calculations are:

1) The $(d_{3/2}\text{-}f_{7/2})$ and $(d_{3/2}\text{-}p_{3/2})$ multiplets in ^{38}Cl are about 80% pure, with considerable $f_{7/2}\text{-}p_{3/2}$ mixing only between the 3^- states.
2) The 5%-20% admixtures of the $s_{1/2}^{-1}$ configuration in these ^{38}Cl states are vital to account for the observed anomalous M1 strength between the 3_2^- and 4_1^- states.
3) The purity of the analogous multiplets in ^{40}K is considerably higher, and, in consequence, no anomalies in M1 strength are predicted, again in accordance with observation.

TABLE III

Configuration Mixing in ^{38}Cl and ^{40}K
(intensities in %)

^{38}Cl E_x(MeV) Exp	Calc	J^π	$d^5_{3/2}f_{7/2}$	$d^5_{3/2}p_{3/2}$	$s^{-1}_{1/2}d^6_{3/2}f_{7/2}$	$s^{-1}_{1/2}d^6_{3/2}p_{3/2}$
0	0	2^-	82	3	7	2
.67	.39	5^-	86		5	
.76	.63	3^-	68	17	7	2
1.31	1.34	4^-	77		8	
1.62	1.49	3^-	14	45	28	1
1.69	2.11	1^-		81	12	3
1.75	1.51	0^-		97		1
1.98	1.92	2^-	1	77	16	1

^{40}K E_x(MeV) Exp	Calc	J^π	$d^{-1}_{3/2}f_{7/2}$	$d^{-1}_{3/2}p_{3/2}$	$s^{-1}_{1/2}f_{7/2}$	$s^{-1}_{1/2}p_{3/2}$
0	0	4^-	96		2	
.03	-.02	3^-	91	5	2	
.80	1.06	2^-	87	7		2
.89	.79	5^-	96			
2.05	1.99	2^-	6	89		
2.07	1.93	3^-	2	76	18	
2.10	2.54	1^-		96		
2.63	2.19	0^-		98		

4) The differences between ^{38}Cl and ^{40}K are consequences of the freedom to excite particles within the sd-shell which exists for ^{38}Cl and which does not exist for ^{40}K. In other words, the differences are consequences of the breakdown of the assumptions upon which the particle-hole transformation are based, e.g. that ^{32}S is a good closed shell nucleus. Since both experiment and the present calculations definitely indicate that these differences exist, the question which remains is why does the energy transformation scheme based on the assumption of pure configurations work so well.

References

1. S. Goldstein and I. Talmi, Phys. Rev. 102, 589(1956).
2. S.P. Pandya, Phys. Rev. 103, 956(1956).
3. R.M. Freeman and A. Gallman, Nucl. Phys. A156, 305(1970).
4. G.A.P. Engelbertink and J.W. Olness, Phys. Rev. C5, 431(1972).
5. R.E. Segel et al., Phys. Rev. Letters 25, 1352(1970).
6. R. Bass and R. Wechsung, Phys. Letters 32B, 602(1970).
7. J. Rapaport and W.W. Buechner, Nucl. Phys. 83, 80(1966).
8. J.B. French, E.C. Halbert, J.C. McGrory, and S.S.M. Wong, Advances in Nuclear Physics, Vol. 2 (Plenum Press, New York, 1970), p. 193.
9. J.P. Elliott et al., Nucl. Phys. A121, 248(1968).
10. S. Maripuu and G.I. Harris, BAPS, 16, 1166(1971) and to be published.
11. D. Kurath and R.L. Lawson, Phys. Rev. C6, 901(1972).
12. P. Goode, BAPS 17, 34(1972).
13. S. Maripuu, Nucl. Phys. A123, 357(1969).
14. F. Erné, W.A.M. Veltman, and J.A.J.M. Wintermans, Nucl. Phys. 88, 1(1966).

* Present Address: Department of Physics, Antioch College, Yellow Springs, Ohio 45387

The $^{39}K(p,t)^{37}K$ and $^{39}K(p,^3He)^{37}Ar$ Reaction

W.A. Lanford, B.H. Wildenthal and J. Johnson

Because of the unexpected outcome of the Davis et al.[1] solar neutrino experiment, there is much interest in the nuclear structure of the mass-37 isobars ^{37}Ca, ^{37}K, ^{37}Ar, and ^{37}Cl. The reaction used to detect neutrinos is $\nu+^{37}Cl\rightarrow^{37}Ar+e^-$, and the calculated cross-section for this process depends on knowing something about the nuclear structure of ^{37}Cl and ^{37}Ar. The wave functions of Wildenthal et al.[2] have been used to calculate the neutrino absorption cross-section on ^{37}Cl.[3]

This study of the $^{39}K(p,t)^{37}K$ and $^{39}K(p,^3He)^{37}Ar$ reaction was undertaken partly to test these calculated wave functions for mass 37 via a type of observable which might sensitive to details which do not affect the results of other kinds of measurements. Conversely, since the calculated wave functions do manage to account for the concensus of present data in this region, another motivation for this pair of experiments was to test our knowledge of the two-nucleon transfer reaction mechanism in a case where we feel relatively confident of our knowledge of the mixed configuration shell-model wave functions.

Shown in Fig. 1 are spectra of the $^{39}K(p,t)^{37}K$ and $^{39}K(p,^3He)^{37}Ar$ reactions observed with a position-sensitive proportional counter in the focal plane of the Enge magnetic spectrograph at a bombarding energy of 40 MeV. The angular distributions of these states are presently being analyzed.

References

1. R. Davis, BAPS 17, 527(1972).

2. B.H. Wildenthal, E.C. Halbert, J.B. McGrory, and T.T.S. Kuo, Phys. Rev. C4, 1266(1971).

3. W.A. Lanford and B.H. Wildenthal, Phys. Rev. Letters 29, 606(1972).

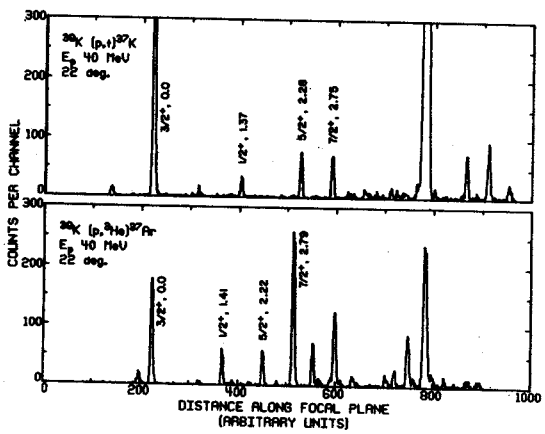

Study of the Germanium Isotopes with the (p,d) Reaction

D.L. Show, J.A. Nolen, W.A. Lanford, and B.H. Wildenthal

We have begun a study of the Germanium isotopes via the (p,d) reaction. While some of the level structure of these nuclei has been established by gamma ray studies,[1,2] and direct reaction work,[3,4] the direct reaction studies have been hindered by the need for a resolution of <20 keV for many of the states. We have used the 35 MeV proton beam from the MSU Cyclotron to study the (p,d) reaction on $^{70,72,74}Ge$ between 6° and 60° in the lab. The deuterons were analyzed in an Enge split-pole magnetic spectrograph and detected in nuclear emulsions. The energy resolution for these spectra vary from 5-9 keV, FWHM. Spectra recorded at 6° are shown in Fig. 1. Scanning of plates exposed at the other angles is in progress.

Preliminary studies using a position-sensitive wire proportional counter in the focal plane of the magnet indicate that at a proton energy of 25 MeV and large scattering angles (90°-120°) the J dependence of ℓ=1 transitions is sufficiently strong to allow unique spin assignments to levels populated with ℓ=1 transfer. Also, work on the $^{60}Ni(p,d)$ reaction indicates that the ℓ=3, forward angle, J-dependence is strong at E_p=35 MeV.

We plan to continue the 35 MeV studies on the other stable Germanium isotopes ($^{73,76}Ge$) and use the data to extract energy levels, ℓ-transfer, and spectroscopic factors. We can also use this data to make spin assignments to the states populated by ℓ=3 transfer because of the J-dependence previously mentioned. We will then repeat the experiment for all the isotopes at 25 MeV and θ_L=90°-120° to get spin assignments for those states populated by the ℓ=1 transfer.

References

1. C. Murray, N.E. Sanderson, J.C. Willmott, Nucl. Phys. A171, 435(1971).

2. S. Muszynski and S.K. Mark, Nucl. Phys. A147, 459(1970).

3. T.H. Hsu, R. Fournier, B. Hird, J. Kroon, G.C. Ball, and F. Ingebretsen, Nuclear Phys. A179, 80(1972).

4. L.H. Goldman, Phys. Rev. 165, 1203(1968).

The Structure of ^{38}K via the $^{39}K(p,d)^{38}K$

J.A. Rice and B.H. Wildenthal

In conjunction with studies of other odd-neutron, odd-proton s-d shell nuclei presently being pursued at the Cyclotron Laboratory, the study of ^{38}K via the $^{39}K(p,d)^{38}K$ reaction has been undertaken at a proton bombarding energy of 35 MeV. The work was motivated by the need for a critical evaluation of recent shell-model predictions[1,2] through the extraction of accurate excitation energies and ℓ=0 and ℓ=2 spectroscopic factors. To this end, (p,d) angular distributions from thin natural potassium targets (93% ^{39}K) were taken utilizing the MSU Cyclotron and split-pole spectrograph. Deuteron spectra were recorded both on nuclear emulsion plates and with a wire proportional counter. The angular distributions were taken between 3° and 55° with special concentration at angles less than 30° to facilitate the unambiguous extraction of ℓ=0 and ℓ=2 spectroscopic factors. The cross-section normalization was performed by comparisons of proton elastic scattering data to optical model calculations.[3] A typical plate spectrum with a resolution of approximately 8 keV FWHM is shown below. Excitation energies, obtained from the plate data only, were extracted by a least-squares fit of energy levels calculated via the spectrograph calibration to corresponding low-lying levels known to $\leq$2 keV from gamma ray studies.[4] Energy levels observed in the present work along with the gamma ray and other single neutron pick-up work are given below in Table I.

DWBA analysis[5] of the deuteron angular distributions is near completion and preliminary results indicate the observation of essentially all of the ℓ=0 and ℓ=2 ($d_{3/2}$) strengths and approximately one-fourth of the ℓ=2 ($d_{5/2}$) strength below 6 MeV of excitation. The distribution of observed spectroscopic strengths favors the 11.0h+ASPE and 12.5p+^{17}O calculations of Wildenthal *et al.*[1] and the Tabakin predictions of Dieperink and Brussaard.[2]

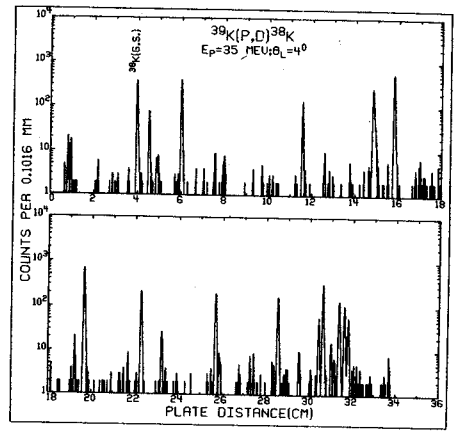

Fig. 1

TABLE I

Energy Levels in ^{38}K

E_x(keV)[a]	E_x(keV)[b]	E_x(keV)[c]
0	0	0
130	131	130
459	460	450
1699	1699	1700
2404	2404	2400
2615	2614	
2649	2649	
2829	2832	
2872	2871	
	2995	
3320	3319	
3343	3347	
3433	3432	
3617		3440
	3670	
3704		
3820		
3860		
3939		
3981		
4177		4000
4218		
4583		
4657		
4698		4670
4982		
5234		
5434		5250
5611		
5723		
5791		
5842		5780
5877		5850
5928		
5961		

[a] Present Work: errors approximately ±2 keV to 2600 keV and an additional ±1 keV/MeV above 2600 keV.

[b] Reference 3: errors ≤±2 keV except the 3347 keV level which is ±3 keV.

[c] G. Ronsin, M. Vergnes, G. Rotbard, J. Kalifa, and I. Lanck, to be published; no errors given.

References

1. B.H. Wildenthal, E.C. Halbert, J.B. McGrory, and T.T.S. Kuo, Phys. Rev. C4, 1266(1971).
2. A.E.L.Dieperink and P.J. Brussaard, Nucl. Phys. A128, 34(1969).
3. Proton parameters of F.D. Becchetti and G.W. Greenlees, Phys. Rev. 182, 1190(1969).
4. W.K. Collins, C.S.C. D.Longo, L. Alexander, E. Berners, and P. Chagnon, University of Notre Dame Progress Report, 1971.
5. Proton channel (Ref. 3) and deuteron parameters of F. Hinterberger, G. Mairle, V. Schmidt-Rohr, G.J. Wagner, and P. Turek, Nucl. Phys. A111, 265(1968) used in computer code DWUCK, P.D. Kunz, University of Colorado.

Study of the Proton Rich Nuclei in the $1f_{7/2}$ Shell

I.D. Proctor, W. Benenson, and E. Kashy

The proton rich nuclei ^{43}Ti, ^{47}Cr, ^{51}Fe, and ^{55}Ni are being studied by the (^{3}He,^{6}He) reaction at 70 MeV. Since the line of nuclear stability in the $1f_{7/2}$ shell is at least two neutrons from the N=Z line, these measurements will extend the three neutron transfer (^{3}He,^{6}He) reaction to its maximal value for study of proton rich T_z=-1/2 nuclei. Mass measurements for ^{43}Ti, ^{47}Cr, ^{51}Fe, and ^{55}Ni have been completed and recently reported.[1] The energy level structure of these Z=N+1 members of the heaviest known mirror pairs are currently under investigation with special emphasis on identification of the $1/2^+$ and $3/2^+$ neutron hole states.

These experiments are performed using the Enge split-pole magnetic spectrograph. Previous measurements[2,3,4] using the (^{3}He,^{6}He) reaction in this laboratory have used silicon position sensitive detectors and photographic emulsions in the focal plane of the spectrograph to detect the ^{6}He particles. These methods were not able to satisfactorily discriminate the ^{6}He particles from the very strong α background encountered in the measurements on the $1f_{7/2}$ shell nuclei. To overcome the particle identification problem, a wire proprotional counter for position information was combined with a plastic scintillator to measure the time-of-flight (TOF) of the particles. Identification of a ^{6}He particle is performed by requiring that the energy losses in the proportional counter and plastic scintillator fall within selected limits, and that the TOF of the particle is the same as that of a triton (tritons have the same TOF as ^{6}He particles of the same rigidity). Using this scheme, we have measured ^{6}He cross sections as low as 20 nb/sr in the presence of an α background of 20 mb/sr.

Spectra obtained for ^{43}Ti, ^{47}Cr, and ^{55}Ni are shown in Figs. 1 to 3 respectively. The energy level and spin-parity assignments shown are preliminary. Spin-parity assignments are from a comparison with the known mirror levels populated in the (p,α) reaction.[5] Further identification of the levels populated in the (^{3}He,^{6}He) reaction in the $1f_{7/2}$ shell nuclei will be obtained by comparing angular distributions with those obtained to states of known spin and parity in the ^{26}Mg(^{3}He,^{6}He) reaction.

References

1. I.D. Proctor, W. Benenson, J. Dreisbach, E. Kashy, G.F. Trentelman; and B.M. Preedom, Phys. Rev. Letters 29, 434(1972).
2. W. Benenson, J. Dreisbach, I.D. Proctor, G.F. Trentelman, and B.M. Preedom, Phys. Rev. C5, 1426(1972).
3. G.F. Trentelman and I.D. Proctor, Phys. Letters 35B, 570(1971).
4. G.F. Trentelman, B.M. Preedom, and E. Kashy, Phys. Rev. Letters 25, 53(1970).
5. J. Nolen, W. Benenson, and E. Kashy, unpublished.

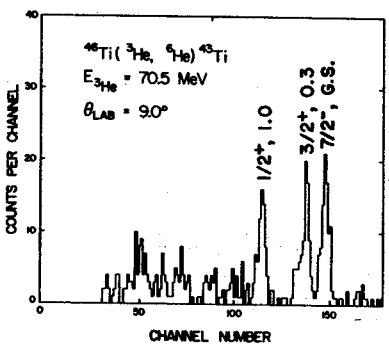

Figure 1

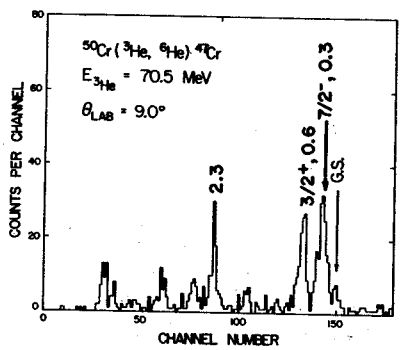

Figure 2

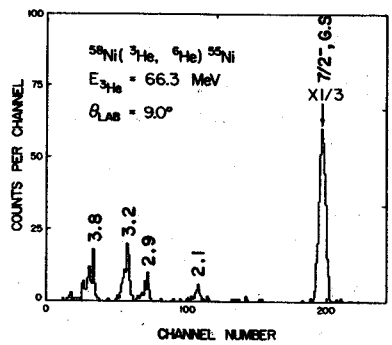

Figure 3

Low-Lying States of ^{48}V from the $^{48}Ti(\underline{p},\underline{n}\gamma)$ and $^{45}Sc(\alpha,\underline{n}\gamma)$ Reactions*

L.E. Samuelson, W.H. Kelly, R.A. Warner, R.R. Todd,** F.M. Bernthal
Wm.C. McHarris, E.M. Bernstein,** and R. Shamu**

The $^{48}Ti(\underline{p},\underline{n}\gamma)^{48}V$ reaction was used to study the states of ^{48}V below 3.34 MeV of excitation. Proton beams of 4.81 to 7.03 MeV in 50 keV steps were furnished for the excitation function measurements by the WMU Tandem Van de Graaff. Proton beams at four different energies for the γ-γ coincidence measurements and at six different energies for the γ-ray angular distribution measurements were furnished by the MSU Cyclotron. The excitation functions and γ-ray angular distributions were measured by detecting deexciting γ rays in a 2.5%-efficient Ge(Li) detector while the γ-γ coincidences were measured using the Ge(Li)-Ge(Li) spectrometer described in the article on ^{56}Co in this same publication. The target was a 99.36% isotopically enriched ^{48}Ti foil of 0.66 mg/cm^2 thickness (approximately 30 keV thick at the beam energies used). A typical γ-ray singles spectrum is shown in Fig. 1, while an integral coincidence spectrum and a typical gated coincidence spectrum is shown in Fig. 2. Typical excitation functions for excited states below 2 MeV in ^{48}V are shown in Fig. 3.

Some examples of the analyses of the γ-ray angular distributions are shown in Fig. 4. A least squares fit to the experimental γ-ray angular distributions using the computer code GADFIT[1] was made to the equation

$$W(\theta) = A_0[1+A_2^*P_2(\cos\theta)+A_4^*P_4(\cos\theta)].$$

Absolute cross sections and the γ-ray mixing-ratio dependent parameters $A_2^*=A_2/A_0$ and $A_4^*=A_4/A_0$ (i.e. δ-ellipses) were calculated using the statistical CN computer code MANDY.[2] For these calculations, nine proton channels and all known open neutron channels were included as "extra" open exit channels. Comparisons of relative cross sections for the population of each state, and of the γ-ray angular distributions with the predictions of the statistical CN theory has then led to the spin assignments shown on the ^{48}V excited-state level scheme in Fig. 5, and to the γ-ray multiple mixing ratios listed in Table I.

The WMU Tandem Van de Graaff was used to provide alpha beams of 6.8, 7.8, 9.8, and 12.0 MeV for the $^{45}Sc(\alpha,\underline{n}\gamma)^{48}V$ γ-ray singles experiments. The γ-ray spectrum taken at 12.0 MeV is shown in Fig. 1. Since alpha particles are expected to preferentially excite high spin states in the residual ^{48}V nucleus, this experiment is expected to give qualitative confirmation of high spin assignments made in the $(\underline{p},\underline{n}\gamma)$ work and to allow identification of other high spin states not identified therein. Since the analyses of these data are not yet complete, only the confirmations of high spin assignments are indicated in Fig. 1.

References

1. GADFIT, computer code written by R. Warner, unpublished.

2. E. Sheldon and R.M. Strang, Computer Physics Communication 1, 35(1969); and references cited therein.

* Supported by the USAEC and the NSF.

** Department of Physics, Western Michigan University, Kalamazoo, Michigan 49001

TABLE I

γ-ray Energies and Mixing Ratios of ^{48}V Measured Using the $^{48}Ti(\underline{p},\underline{n}\gamma)^{48}V$ Reaction

Energies (keV)	Mixing Ratio[a]	Transition Assumed[b]
308.3±0.1	E2	$2^+\rightarrow4^+$
112.5±0.1	$-0.14<\delta<-0.02$	$1^+\rightarrow2^+$
427.9±0.1	$-0.15\leq\delta\leq-0.12$	$5^+\rightarrow4^+$
98.0±0.1	$-0.08\leq\delta\leq+0.37$	$1^-\rightarrow1^+$
210.4±0.1	$+0.01\leq\delta\leq+0.07$	$1^-\rightarrow2^+$
185.5±0.1	$-0.02\leq\delta\leq+0.07$	$4^+\rightarrow5^+$
613.4±0.1	$-0.21\leq\delta\leq-0.17$	$4^+\rightarrow4^+$
199.3±0.2	$-0.23\leq\delta\leq+0.03$	$6^+\rightarrow5^+$
627.3±0.2	E2	$6^+\rightarrow4^+$
226.3±0.1	$-0.08<\delta<-0.06$	$2^-\rightarrow1^-$
324.2±0.1	$-0.21\leq\delta\leq 0.16$	$2^-\rightarrow1^+$
436.8±0.1	$-0.21\leq\delta\leq 0.14$	$2^-\rightarrow2^+$
151.7±0.2	-	$3^+\rightarrow4^+$
456.7±0.1	$-0.03<\delta<-0.01$	$3^+\rightarrow2^+$
746.9±0.1	$-0.05\leq\delta\leq+0.00$	$3^+\rightarrow4^+$
310.8±0.1	-	$3^-\rightarrow2^-$
537.2±0.2	E2	$3^+\rightarrow2^+$
1099.3±0.2	$-0.21<\delta<+0.22$	$4^\pm\rightarrow4^+$
637.3±0.2	-	$5^+\rightarrow6^+$
651.2±0.2	$-0.26<\delta<-0.03$	$5^+\rightarrow4^+$
756.4±0.1	$-0.02\leq\delta\leq+0.13$	$2^+\rightarrow3^+$
1101.0±0.2	$-0.05\leq\delta\leq+0.03$	$2^+\rightarrow1^+$
1212.9±0.2	$+0.14\leq\delta\leq+0.28$	$2^+\rightarrow2^+$
501.8±0.1	$-0.11\leq\delta\leq-0.06$	$4^-\rightarrow3^-$
812.2±0.3	E2	$4^-\rightarrow2^-$
586.3±0.2	-	$5^\pm\rightarrow4^\pm$
1167.8±0.2	$-0.20<\delta<+0.07$	$3^+\rightarrow4^+$
1472.5±0.2	$-0.12\leq\delta\leq+0.07$	$3^+\rightarrow2^+$
1780.9±0.3	-	$3^+\rightarrow4^+$
899.4±0.2	-	$3^-\rightarrow4^\pm$
1253.3±0.2	-	$3^-\rightarrow2^-$

[a] Missing mixing ratios could not be measured because of insufficient peak statistics. An exception is the 310.8-keV γ ray where a systematic analysis error makes the results dubious.

[b] The mixing ratios shown were calculated for the indicated spin and parity sequences. It should be noted that the parities were not measured in the present experiments and therefore have been assumed.

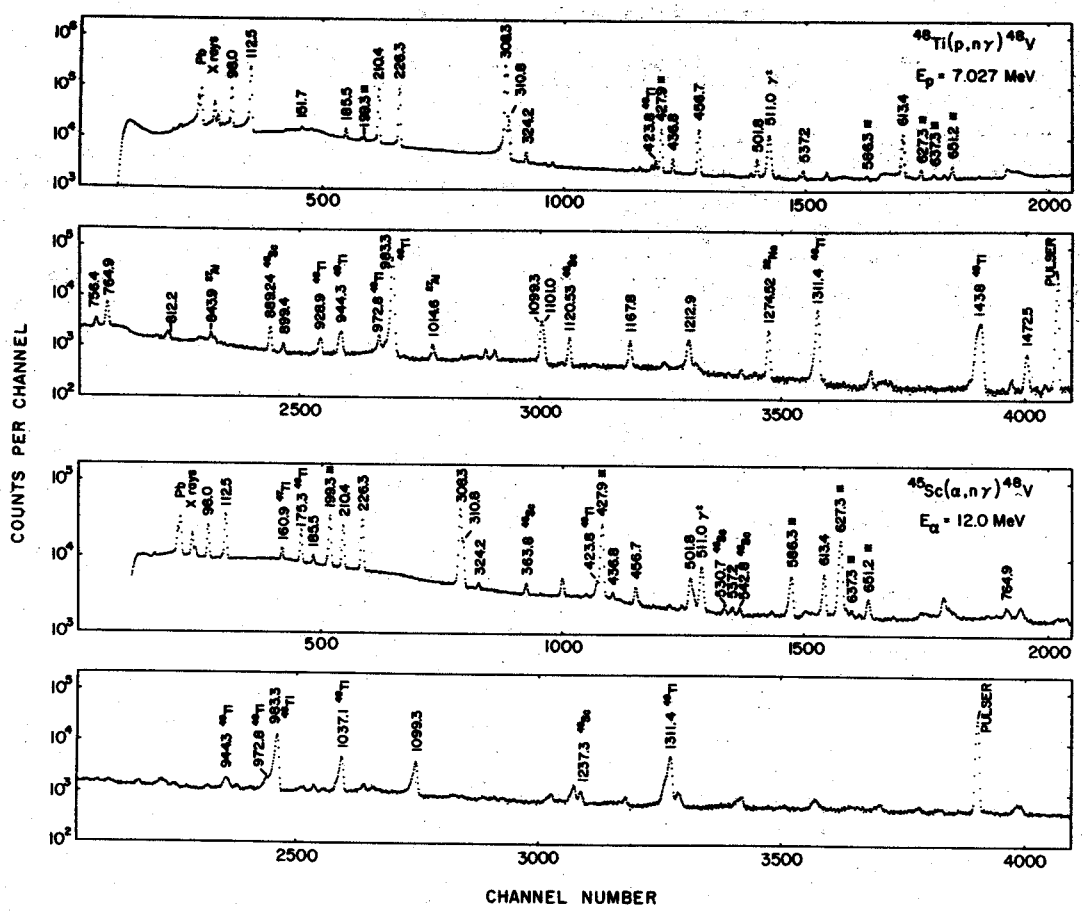

Fig. 1 Singles γ-ray spectra of the ^{48}Ti(p,nγ)^{48}V reaction at E_p=7.027 MeV and the ^{45}Sc(α,nγ)^{48}V reaction at E_α=12.0 MeV. In both spectra γ-rays believed to deexcite "high" spin states are indicated with an asterisk.

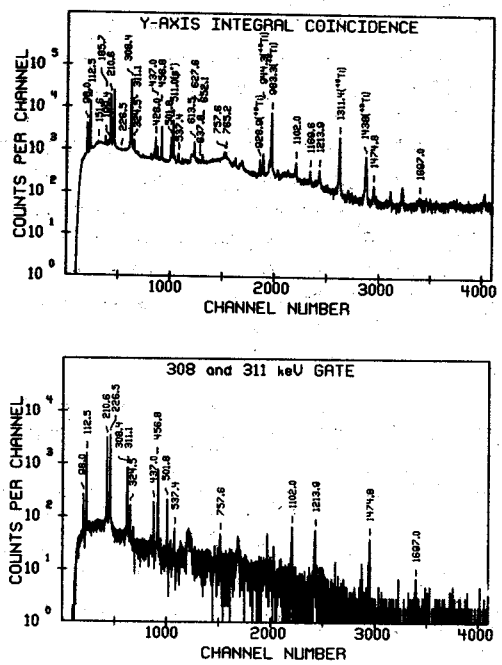

Fig. 2 Integral coincidence spectrum and the 308-311 keV doublet gated spectrum at E_p=7.03 MeV taken with the 7.4%-efficient Ge(Li) detector. The gate was set on the opposite axis which was taken with the 2.5%-efficient Ge(Li) detector. Careful background subtraction using adjacent continuum has been included. The final energies are slightly different from those values labeling the peaks.

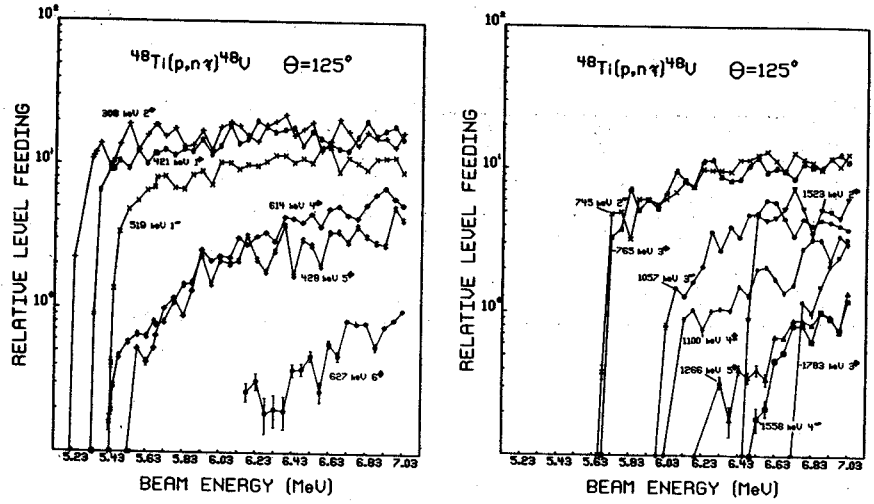

Fig. 3 Excitation functions for fourteen excited states of ^{48}V lying below 1.8 MeV of excitation. The data were taken at θ=125°, a zero of $P_2(\cos\theta)$. The appropriate intensities of de-exciting and feeding γ rays have been added and subtracted to obtain the relative cross sections. The thresholds were calculated using Q=-4.803 MeV for the ground state.

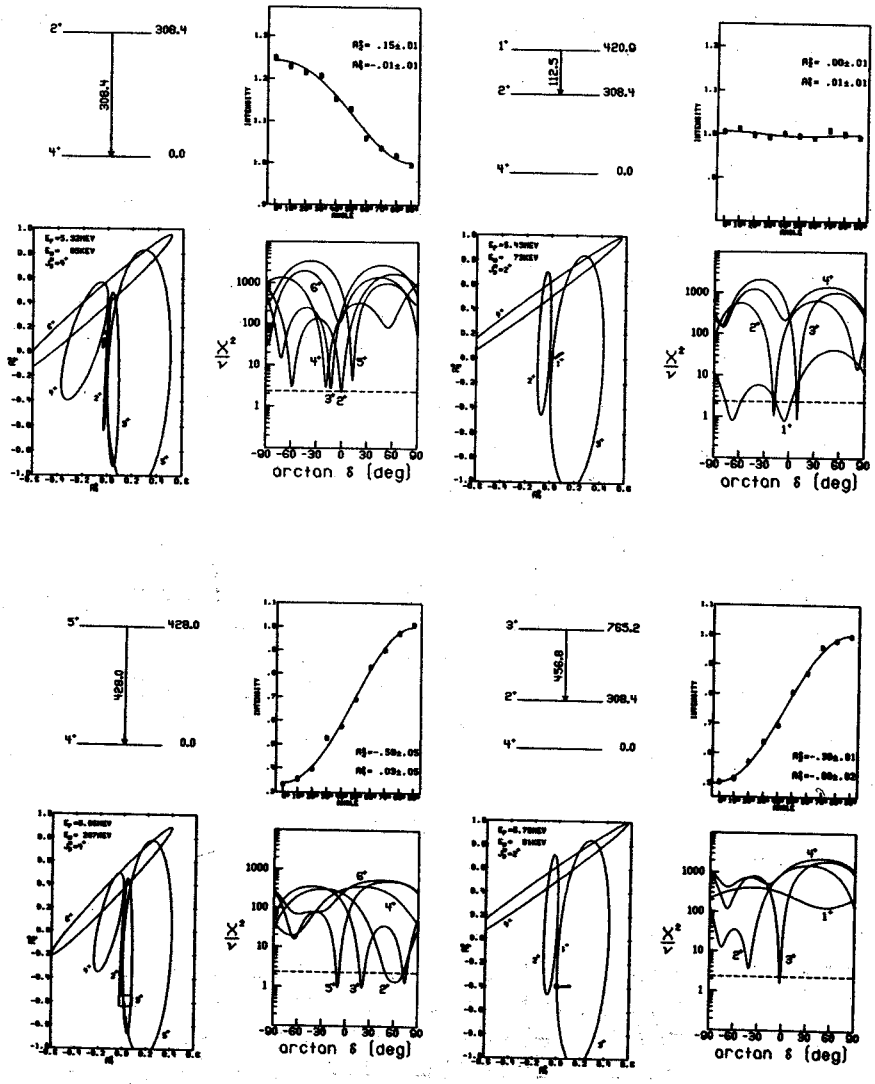

Fig. 4 Analyses of several γ-ray angular distributions from the ^{48}Ti(p,nγ)^{48}V reaction. Shown for the γ-ray transition in question are its angular distribution, the theoretical δ-ellipse plots with the experimental values of A_2^* and A_4^* drawn in as a rectangle (initial spin values labeling their appropriate ellipses), and a plot of chi-square per degree of freedom (reduced chi-square) versus arc tangent δ. The γ ray energies shown are slightly different from their final values.

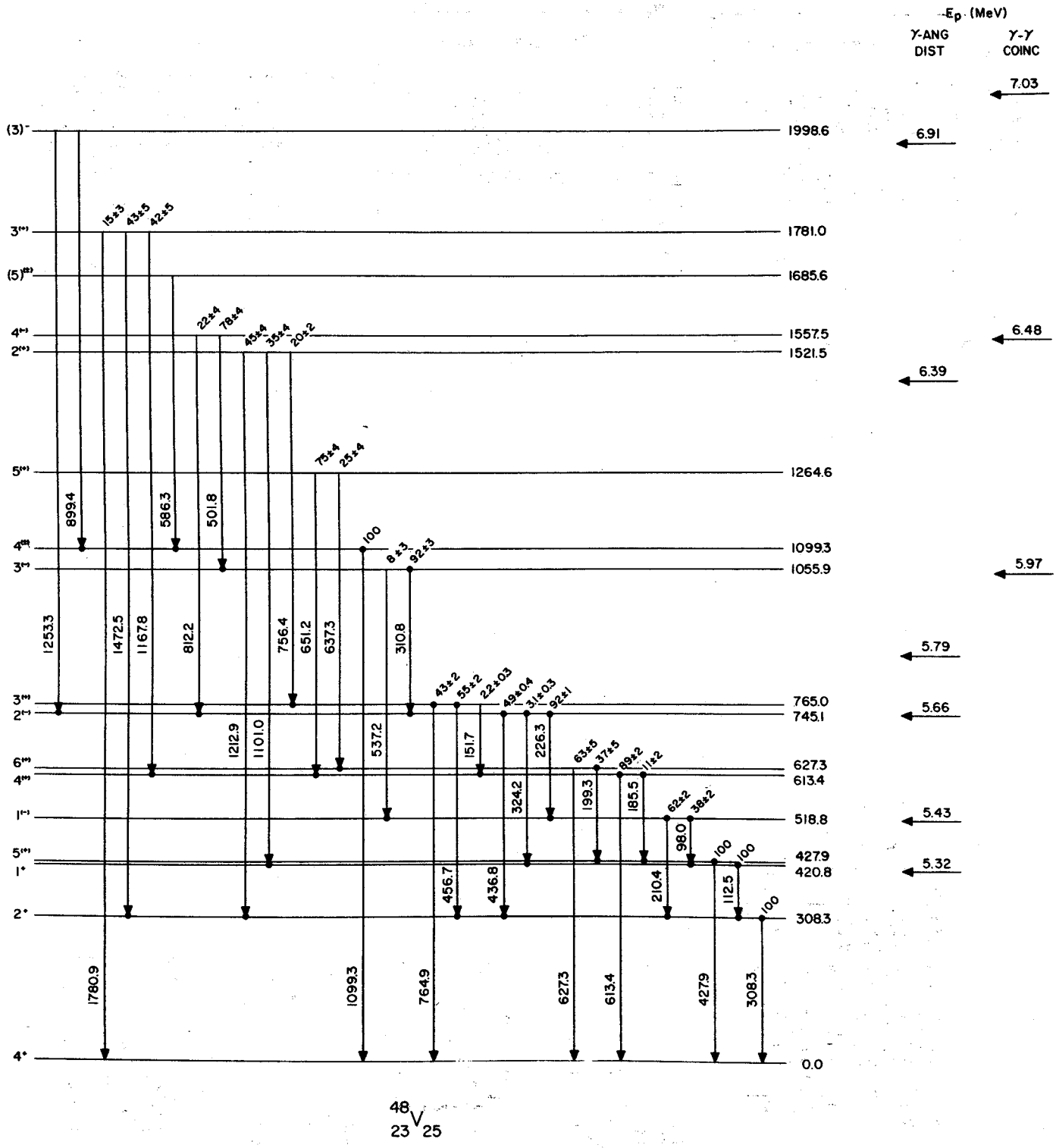

Fig. 5 The excited-state level scheme of ^{48}V. The arrows on the right indicate the maximum possible excitation for the labeled incident proton energy. The spin assignments on the left (except for the ground state) are all from this work. The γ-ray and level energies shown are the final values.

70 MeV ^{3}He Scattering

R.R. Doering, A.I. Galonsky, and R.A. Hinrichs

In the preceding annual report we presented preliminary angular distributions and optical-model parameters for 70 MeV ^{3}He elastic scattering from ^{50}Ti and ^{51}V. During the past year we have refined both the data and its theoretical analysis. In particular, we found it necessary to modify the optical-model search code GIBELUMP in order to obtain sufficient numerical accuracy for the small, back-angle cross sections observed in ^{3}He elastic scattering at 70 MeV.[1] Figure 1 illustrates the inadequacy of a few commonly used codes. The solid reference curve has been computed with our modified version of GIBELUMP (SGIB) and is considered accurate to better than one percent at all angles. The discrepancies between the back-angle oscillations of the less accurate calculations result from insufficient numbers of terms and losses of significance in the partial-wave sums. SGIB allows the user to employ enough partial waves and integration steps to overcome these difficulties.

The fits to our data were generated with 60 partial waves, a 22 F matching radius, and a 0.05 F integration step size. The optical-model parameters were fairly well determined except for a continuous ambiguity related to the strength of the spin-orbit potential. The table lists best-fit parameters from grid searches on V_{SO}. Fits to the ^{51}V data for the V_{SO}=0.0 and 3.0 MeV cases are shown in Fig. 2. The smooth drop in the angular distribution at large angles is particularly sensitive to the optical-model parameters. Our preliminary calculations with GIBELUMP required a spin-orbit potential of a few MeV to damp out the erroneous back-angle oscillations (see Fig. 1). The more accurate SGIB results indicate little preference for any particular V_{SO} less than about 3 MeV. Other recent analyses of ^{3}He elastic scattering tend to either agree with this result[2,3] or prefer a spin-orbit potential of about 2-4 MeV.[4,5] In all cases the parameters of the real, central potential appear correlated with the spin-orbit strength. Current polarization and spin-flip data suggest that the ^{3}He spin-orbit potential is around 2-5 MeV. In an effort to further restrict this continuous ambiguity, we are currently comparing our empirical ^{3}He optical-model potentials with "theoretically realistic" nucleon-nucleus folding-model predictions based on refinements of calculations by Abul-Magd and El-Nadi.[6] We are also in the process of extracting deformation parameters from macroscopic DWBA analyses of inelastic ^{3}He scattering to low-lying 2^+ and 4^+ states in ^{50}Ti and $3/2^-$, $5/2^-$, $9/2^-$, and $11/2^-$ states in ^{51}V.

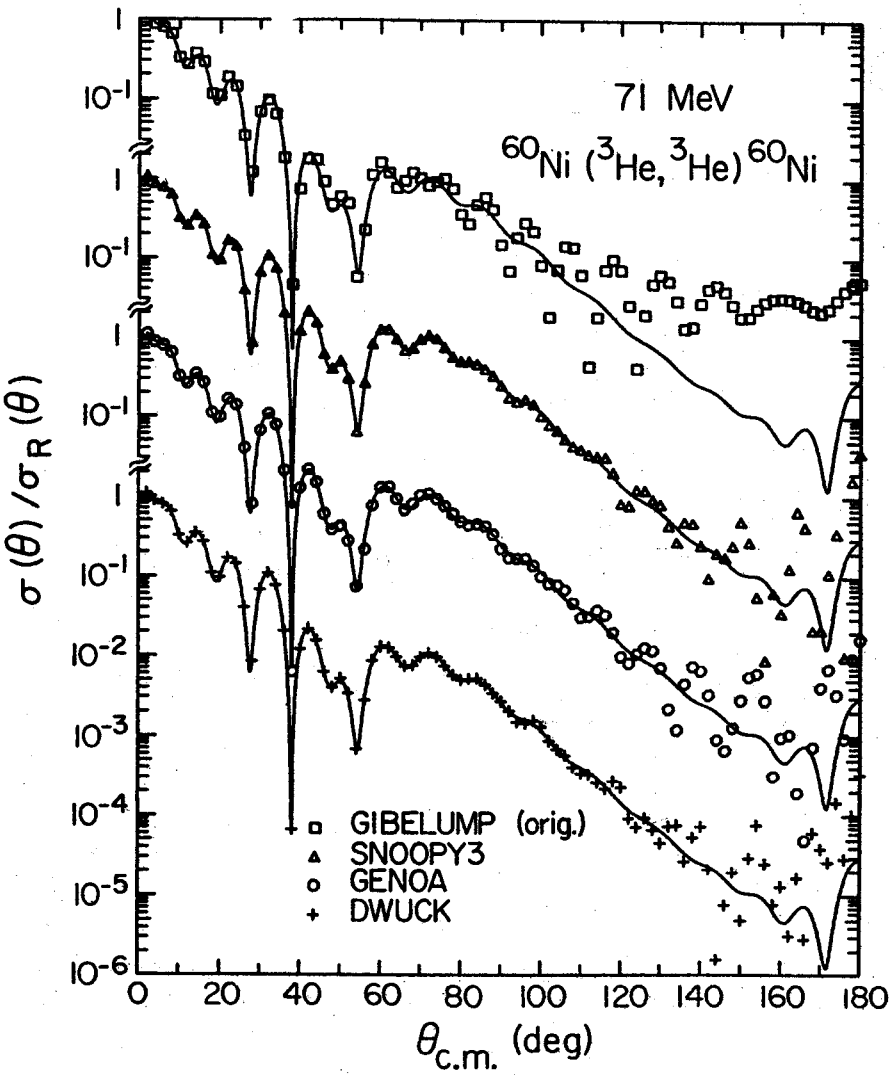

Fig. 1 Comparison of elastic scattering calculated with 4 codes from the same potential. The reference lines are from a more accurate calculation with a modified version of GIBELUMP (SGIB)

References –

1. R.R. Doering, BAPS 17, 590(1972).
2. P.P. Urone, et al., Nucl. Phys. A167, 383(1971).
3. P.B. Woollam, et al., Nucl. Phys. A189, 321(1972).
4. C.B. Fulmer and J.C. Hafele, Phys. Rev. C5, 1969(1972).
5. H.P. Morsch and R. Santo, Nucl. Phys. A179, 401(1972).
6. A.Y. Abul-Magd and M. El-Nadi, Prog. Theor. Phys. 35, 798(1965).

TABLE I

70 MeV ^{3}He Optical-Model Parameters

	V_R	r_R	a_R	W_D	r_I	a_I	V_{SO}	χ^2/N
^{50}Ti	103.6	1.24	.747	19.9	1.25	.795	0.0	6.7
	113.4	1.17	.794	19.1	1.27	.799	3.0	8.7
^{51}V	106.5	1.22	.768	19.3	1.24	.825	0.0	8.6
	123.2	1.11	.842	18.4	1.27	.820	3.0	17

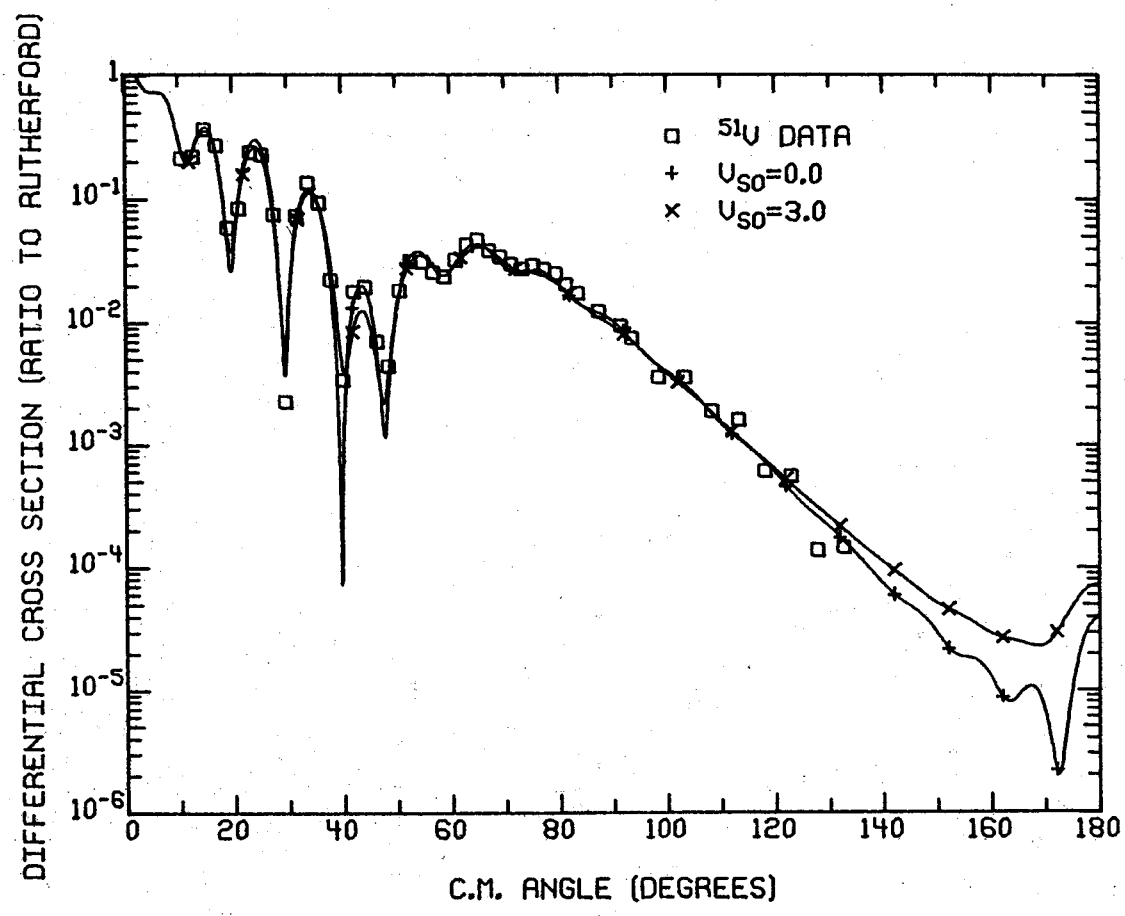

Fig. 2 Best fits to 70 MeV ^{3}He elastic scattering from ^{51}V with the spin-orbit potential fixed at 0.0 and 3.0 MeV. Corresponding optical-model parameters are listed in the table.

Electromagnetic Transitions in ^{56}Co Below 2.85 MeV of Excitation from the ^{56}Fe(p,nγ)^{56}Co Reaction

L.E. Samuelson, W.H. Kelly, R.A. Warner, R.R. Todd,* Wm.C. McHarris
F.M. Bernthal, E.M. Bernstein,* and R. Shamu*

As a continuation of our study of ^{56}Co using ^{56}Fe(p,nγ)^{56}Co, we have recently performed two-dimensional γ-γ coincidence experiments using proton beams with energies of 7.38 and 8.36 MeV (corresponding to excitations in ^{56}Co of 1.89 and 2.85 MeV, respectively) supplied by the MSU cyclotron. The purposes of these experiments were to confirm the decay scheme[1,2] previously proposed from γ-ray thresholds that were obtained from excitation functions up to 1.8 MeV of excitation, and to search for those electromagnetic transitions deexciting higher lying states.

The target was an iron foil enriched to 99.4% ^{56}Fe having a thickness of 0.90 mg/cm^2. A Ge(Li)-Ge(Li) spectrometer positioned in the geometry shown in Fig. 1 was used to detect the coincident γ rays. The lead block placed between the detectors served as a beam dump as well as an attenuator for coincident Compton events scattering from one detector into the other. A typical fast-slow coincidence circuit utilizing constant-fraction timing discrimination ($2\tau \simeq 50$ nsec) was used. The coincidence events were stored on magnetic tape and later sorted off-line using background subtraction. The 7.38-MeV spectrum accumulated 1 million coincidence events in 12 hours of counting, while the 8.36-MeV spectrum accumulated close to 7 million coincidence events in 31 hours. Typical singles counting rates for both runs were 7000 cts/sec in the 2.5%-efficient detector and 20,000 cts/sec in the 7.4%-efficient detector. Typical beam currents were about 7 nA.

The two integral spectra, as well as some representative gated spectra from the run with E_p=8.36 MeV, are shown in Fig. 2. (A complete set of the gated spectra are given in Ref. 3.) In all, some 35 definite and 7 possible γ rays were identified to be from ^{56}Co. These include 21 γ rays previously reported to be in coincidence with neutrons by Del Vecchio et al.[4] using the same reaction. The excited-state decay scheme for ^{56}Co, which is consistent with the γ-γ coincidence data, is shown in Fig. 3. The spin assignments for states below and including the 1720.3-keV state are based upon excitation function and γ-ray angular distribution work previously reported by us,[1,2] while the remaining spin assignments are those of Schneider and Daehnik.[5] The parity assignments are based upon shell-model considerations as well as experimental ℓ-transfers in particle transfer work. (See Ref. 5 and references cited therein.) The γ-ray energies (and, hence, level energies) were determined using the well-known energies[6] of the simultaneously present ^{56}Fe γ rays (arising from the ^{56}Fe(p,p'γ) reaction) and by counting in the presence of γ-ray energy standards of ^{75}Se, ^{88}Y, ^{113}Sn, ^{137}Cs, and ^{22}Na.

The γ-ray properties resulting from the work done on ^{56}Co[1-3] have been compared with shell-model predictions calculated by McGrory.[7] In McGrory's calculations, ^{56}Co was represented as a ^{40}Ca core plus 14 or 15 nucleons in the $f_{7/2}$ orbit and the remainder in the $p_{3/2}$, $f_{5/2}$, or $p_{1/2}$ orbits. He used Kuo-Brown matrix elements for the effective two-body Hamiltonian and single particle energies which best reproduced the ^{57}Ni spectrum. The resulting ^{56}Co wave functions were used to calculate the reduced transition probabilites, B(M1) and B(E2), from which γ-ray multipole mixing ratios and γ-ray branching ratios were determined. In general, the agreement between theory and experiment was quite good. The results will be presented in the Physical Review.

References

1. L.E. Samuelson, R.A. Warner, W.H. Kelly, R.R. Todd, and W.C. McHarris, BAPS 16, 12(1971).

2. L.E. Samuelson, Michigan State University Cyclotron Laboratory Annual Report 1970-71, p. 65.

3. L.E. Samuelson, Ph.D. Thesis, Michigan State University, (1972).

4. R. Del Vecchio, R.F. Gibson, and W.W. Daehnik, Phys. Rev. C5, 446(1972).

5. M.J. Schneider and W.W. Daehnik, Phys. Rev. C4, 1649(1971).

6. D.C. Camp and G.L. Meredith, Nucl. Phys. A166, 349(1971).

7. J.B. McGrory, private communication.

* Present Address: Department of Physics, Western Michigan University, Kalamazoo, Michigan.

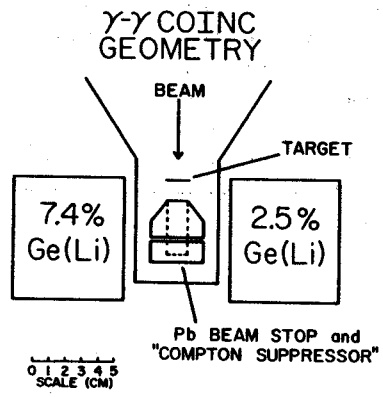

Fig. 1. Geometry for the γ-γ coincidence experiment. The squares represent the position of the Ge(Li) detectors' cryostat caps.

High Resolution Studies of the ^{59}Co and ^{60}Ni(p,d) Reactions

J. Nolen, R.G.H. Robertson, and S. Ewald

The low-lying energy levels of the odd-odd nucleus ^{58}Co are predominantly of the configuration $(\pi f_{7/2}^{-1})$ coupled to mixtures of neutrons in the $p_{3/2}$, $f_{5/2}$, and $p_{1/2}$ shells.[1,2] However, it is also known that the main $(\pi f_{7/2}^{-1})(\nu f_{7/2}^{-1})$ multiplet strength is in the excitation energy region near 2.7 MeV. The degree to which this $f_{7/2}$ neutron hole strength mixes with the low-lying levels is not known. We are studying the ^{59}Co(p,d) reaction to shed light on this question and to determine more accurately the detailed wave functions of the low-lying levels of ^{58}Co.

It is necessary in this work to determine accurately the relative amounts of ℓ=3 and ℓ=1 strength in the transition to each level. Since transitions to levels of spin $2 \leq J \leq 5$ are possibly of such a mixture it is very important to resolve as many energy levels as possible in this experiment. If members of unresolved doublets were individually single ℓ-value transitions the DWBA could be used to extract the relative yields and good resolution would not be as critical.

Data have been recorded on photographic emulsions at proton bombarding energies of 30 MeV and 35 MeV. The MSU cyclotron-magnetic spectrograph combination were used in the dispersion matching mode to achieve an energy resolution of 5 keV FWHM corresponding to line widths 0.2 mm FWHM. With this resolution the 8 keV doublet at 365.6 keV and 373.7 keV was clearly resolved thereby permitting separate DWBA analysis of each level.

The scanning of the Co plates is nearly complete, but only a preliminary DWBA analysis has been done. A sample ^{58}Co spectrum is shown in the figure. To check or verify the DWBA prediction we are also studying the transitions from the ^{60}Ni(p,d) reaction which, for angular momentum reasons, have unique ℓ-values. It would not be possible to use the DWBA to extract reliable spectroscopic strength from the mixed transitions in Co if good fits were not obtained for the pure transitions in the nearby even-even Ni target. Since ^{59}Co and ^{60}Ni both have four neutrons outside the closed N=28 subshell it will also be interesting to see the effect of the change in proton number on the neutron configurations in these targets.

The ^{60}Ni(p,d) angular distributions were measured at 35 MeV over the angular range 3°-90° with a resistive wire proportional counter in the focal plane of the Enge split-pole spectrograph. In order to verify that certain of the transitions, in regions of unresolved states, are dominated by single levels high resolution data were also recorded on photographic emulsions at a few angles.

This 35 MeV Ni data also extends to higher bombarding energies previous studies in this mass region of (p,d) and (d,p) j-dependence.[3,4] At this bombarding energy the $3/2^-$, $1/2^-$, ℓ=1 j-dependence seems to be almost completely washed out. At scattering angles less than 90° there is very little effect as indicated in the figure. At angles between 90° and 120° there seems to be only a weak indication of what was a characteristic dip in the $1/2^-$ curves at lower energies. The $5/2^-$, $7/2^-$, ℓ=3 j-dependence, also shown in the figure, is more pronounced at this energy than it was at the lower energies. The effects are qualitatively the same as in the earlier work: A shift of the primary maximum of the $5/2^-$ curve 4° towards smaller scattering angles relative to the $7/2^-$ curve and the conventional DWBA prediction; and a washing-out of structure in the $7/2^-$ angular distribution relative to the $5/2^-$ curve and the DWBA prediction. Published calculations[5,6] indicate that this qualitative structure difference may be due to the D-state component of the deuteron wave function. However, quantitative calculations at this energy have not been done.

References

1. R.G.H. Robertson and R.G. Summers-Gill, Can. J. Phys. 49, 1186(1971).

2. M.J. Schneider and W.W. Daehnick, Phys. Rev. C5, 1330(1972).

3. C. Glashausser and M.E. Rickey, Phys. Rev. 154, 1033(1967).

4. J.L. Yntema and H. Ohnuma, Phys. Rev. Letters 19, 1341(1967).

5. R.C. Johnson and P.D. Santos, Particles and Nuclei, 2, 285(1971).

6. G. Delic and B.A. Robson, Nucl. Phys. A193, 510(1972).

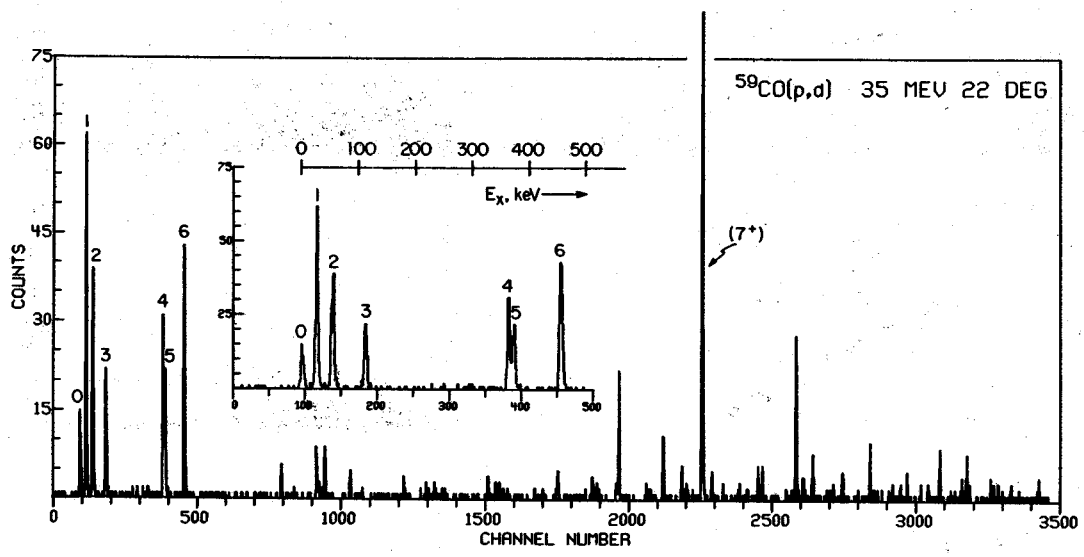
^{59}CO(p,d) 35 MEV 22 DEG
COUNTS
CHANNEL NUMBER
E_x, keV
(7⁺)
0
1
2
3
4
5
6

Fig. 1

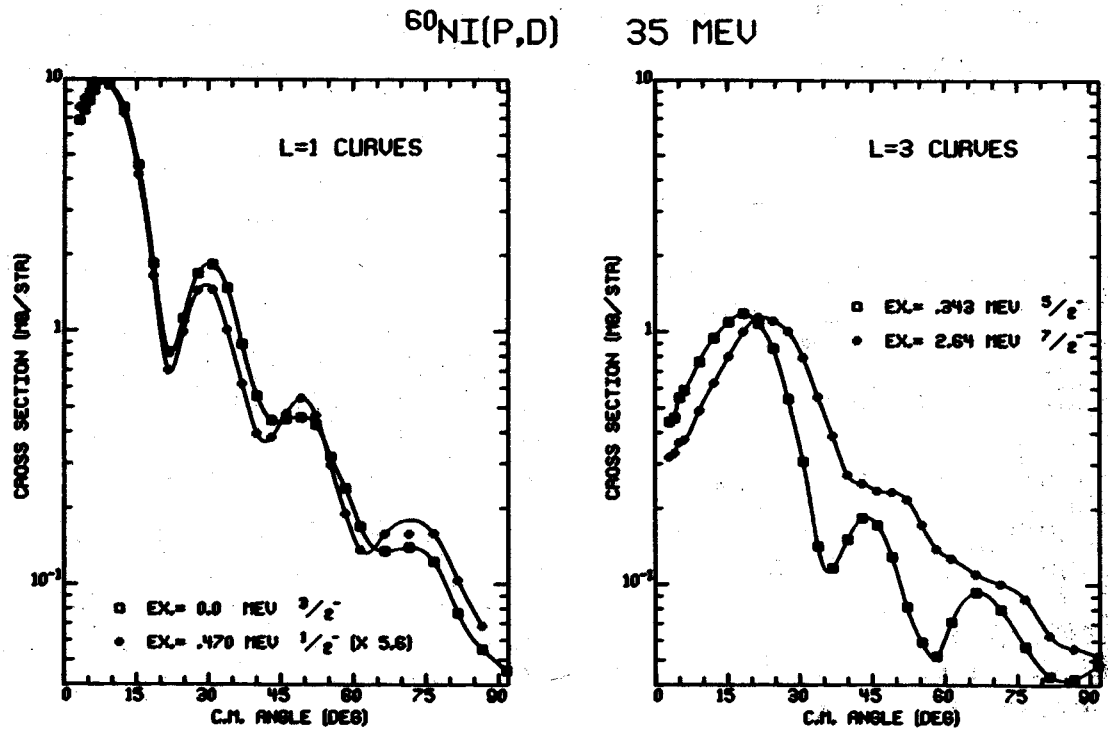
^{60}NI(P,D) 35 MEV
L=1 CURVES
L=3 CURVES
CROSS SECTION (MB/STR)
C.M. ANGLE (DEG)
EX.= 0.0 MEV 3/2⁻
EX.= .470 MEV 1/2⁻ (X 5.6)
EX.= .343 MEV 5/2⁻
EX.= 2.64 MEV 7/2⁻

Fig. 2

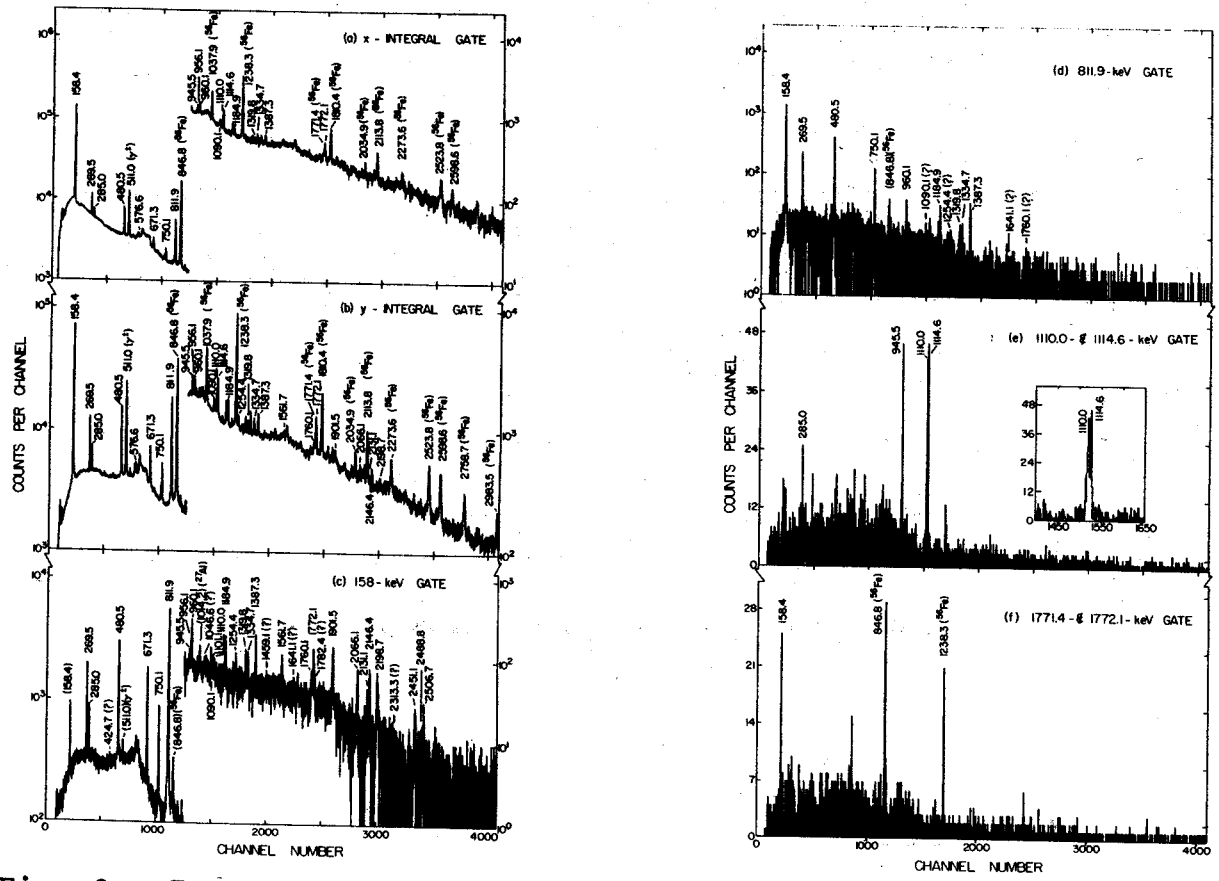

Fig. 2 Integral and representative gated spectra from the $^{56}Fe(\underline{p},n\ \gamma\text{-}\gamma)^{56}Co$ γ-γ coincidence experiment with $E_{\underline{p}}$=8.36 MeV.

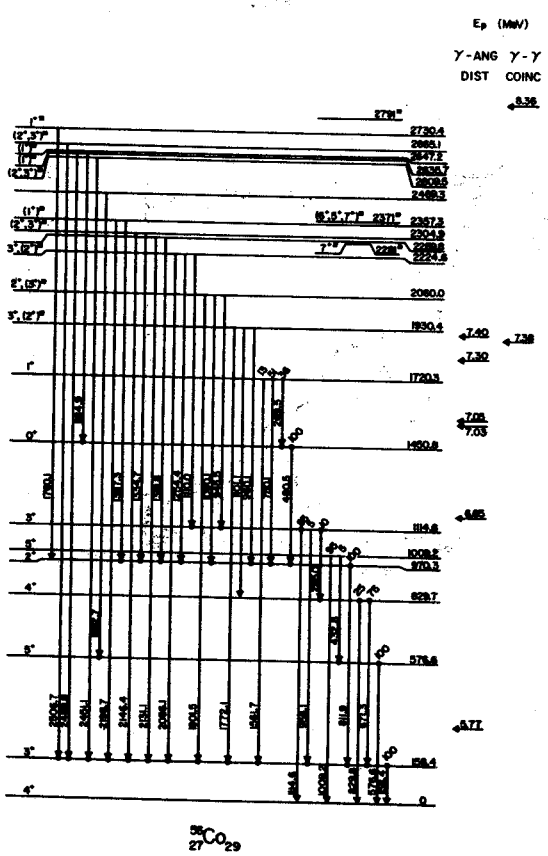

Fig. 3 Excited state decay scheme of ^{56}Co from the $^{56}Fe(\underline{p},n\gamma)^{56}Co$ reaction. Dots denote definite coincidence relationships between γ-ray transitions entering and γ-ray transitions leaving a given state. The beam energies (and the corresponding maximum possible ^{56}Co excitations) at which the γ-γ coincidences and previous γ-ray angular distributions were taken are shown on the right side. Spin and parity assignments are briefly described in the text. Asterisked values are not from the present experiment but are from Ref. 4.

The Isospin Interaction-(p,n) to Analog States

A. Galonsky, R. Hinrichs, T. Amos, J. Branson,
R. Doering and D. Patterson

In (p,n) transitions between isobaric analog states (IAS) the isospin interaction may be the main, in many cases the total, interaction causing the transition. Consequently, the most direct manner of studying the isospin interaction is through these transitions.

Excitation of the IAS by (p,n) was studied with targets of ^{27}Al, ^{51}V, and ^{90}Zr at proton energies of 22, 30, and 40 MeV. A typical time-of-flight spectrum is shown in Fig. 1 for the Zr target with E_p=30 MeV. The ground state (unresolved) of ^{90}Nb is near channel 860 (and 360) and the IAS, the only prominent single state, is near channel 820 (and 320). Angular distributions of the IAS at the three bombarding energies are shown in Fig. 2 for ^{27}Al(p,n)^{27}Si, in Fig. 3 for ^{51}V(p,n)^{51}Cr, and in Fig. 4 for ^{90}Zr(p,n)^{90}Nb. In each of these figures there are three sets of data plotted twice each for comparison with various DWBA calculations. On the right side comparison is made with a pure volume interaction and on the left side with a pure surface interaction for the $\vec{t}\cdot\vec{T}$ term of the generalized optical model. The volume interaction has the same geometry as the real well in the optical-model potential, and the surface interaction has the geometry of the derivative of that well. As noted on the figures, three different sets of optical-model parameters were used.

Figure 2 demonstrates that a surface interaction is to be favored over a volume interaction for ^{27}Al. A look at the ^{51}V and ^{90}Zr results in Figs. 3 and 4, however, shows that the isospin form factor is more complicated. For these two targets the surface interaction fits better at 22 and 30 MeV but not at 40 MeV. A mixture of surface and volume is indicated.

We used a complex mixture, $-Vf(X_R)+i4W\frac{d}{dx}f(X_I)$. The Becchetti and Greenlees best-fit parameters were used for generating the distorted waves and for the geometries of the interaction. The results of the calculation, the dotted curves in Fig. 5, lack the structure contained in some of the data. Variations of the interaction were made in which V/W and r_I were separately changed; the distorted waves were unchanged. The results for V/W=2/3 are given by the solid curves in Fig. 5. To obtain the dashed curves we let V/W=2, as in the Becchetti-Greenlees potential, but we increased r_I to 1.35 F. It is seen that a reasonable fit is obtained in most cases.

The isospin strengths obtained from both the real and the complex analyses diminished with increasing proton energy for all three targets. Most of the decrease occurs between 22 and 30 MeV, perhaps indicating a surprising persistence of compound-nucleus effects.

It is clear that there are enough parameters in the analysis to allow a variety of solutions that fit some of the data very well and all of the data reasonably well. If the ambiguities are to be removed, and underlying simplicities or systematics in the interaction discovered, there will have to be more and better data. We hope to provide some of this.

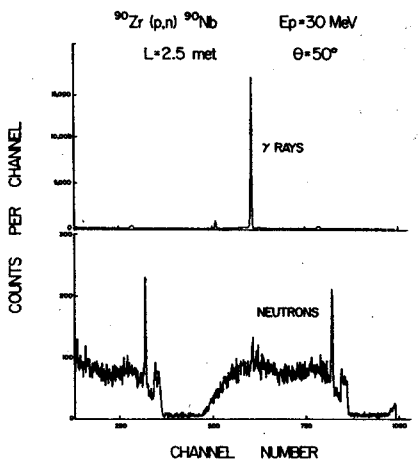

Fig. 1

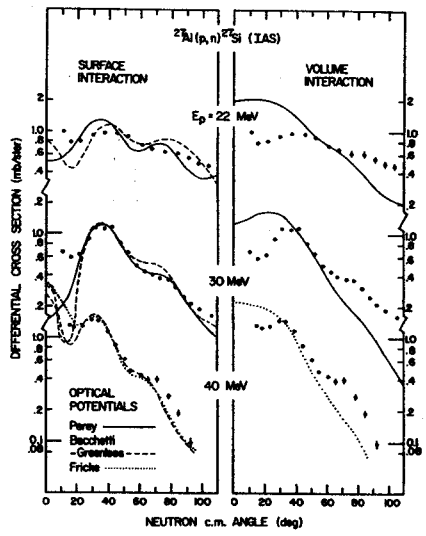

Fig. 2

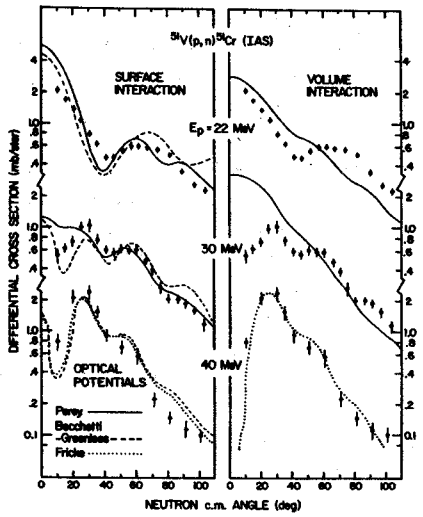

Fig. 3

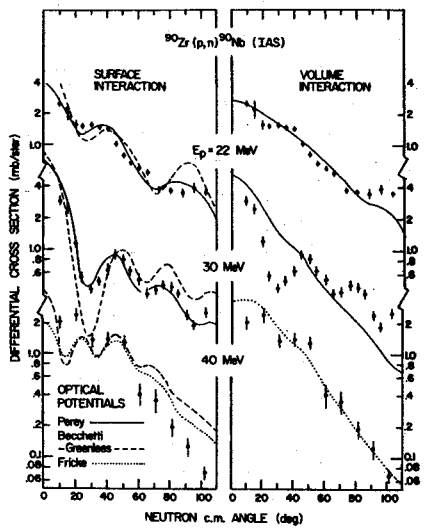

Fig. 4

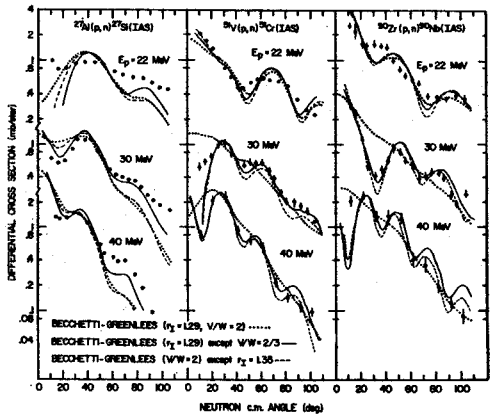

Fig. 5

Measurement of β^+ Endpoint of ^{63}Ga*

R.B. Firestone, K. Kosanke, Wm.C. McHarris, and W.H. Kelly

The decay of 32.4-sec ^{63}Ga has been studied in great detail by Giesler, McHarris, et al. at this laboratory.[1] An important missing piece of data at this point is the β^+ endpoint energy for decay to the ground state of ^{63}Zn. From the systematics of this region, the β^+ endpoint has been predicted to be 4.6 MeV.

In order to measure this endpoint, a pilot B plastic scintillator was constructed 4.5 cm in diameter and 9 cm deep. This scintillator was mounted on an EMI 95308 photomultiplier tube. The tube was operated at 1000 V and the resolution for 662-keV conversion electrons was 20% (FWHM). This was acceptable because the detector was designed primarily for high energy particles and even then only to measure endpoints. All sources were measured both with and without absorbers in front of the detector such that correction could be made for the contribution of γ-ray Compton electrons to the spectra.

Sources of ^{63}Ga were produced using 30-MeV protons from the Michigan State University sector focussed cyclotron on a natural Zn target. Because of the short half-life (32.4-sec) of ^{63}Ga, recoils from the target were collected by a He-thermalizer jet transport system and deposited in front of the detector on a moving tape transport so as not to allow a build up of longer lived activities. The energy calibration of the system was performed using ^{64}Ga and ^{144}Pr standards.

A modified Fermi-Kurie plot (2) for ^{63}Ga decay is shown in Fig. 1. A tentative endpoint of 4.5 ± 0.1 MeV is measured, although it was necessary to strip out higher energy betas from the ^{64}Ga decay which are also produced. This is in good agreement with the prediction. Transitions to excited states were not resolvable, and in future experiments β-γ coincidence data will be taken to determine these.

References

1. G.C. Gielser, Ph.D. Thesis, Michigan State University, COO-1779-55,(1971); G.C. Gielser, MSU Cyclotron Laboratory Annual Report for 1970-71, p. 67.

2. J.G. Kramer, B.J. Farmer, and C.M. Class, Nucl. Instr. and Methods 16, 289(1962).

* Supported by the USAEC and the NSF.

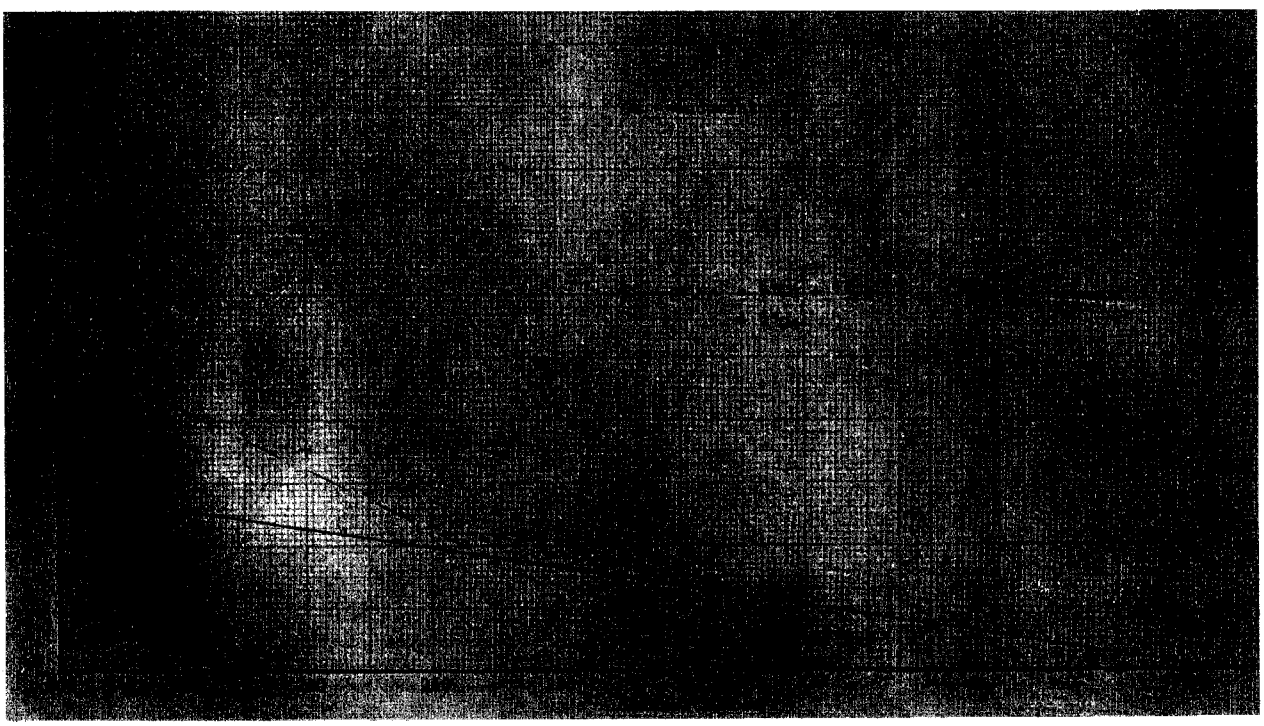

Fig. 1 Adjusted Kurie plot of betas from ^{63}Ga and ^{64}Ga decay measured with a large Pilot B plastic scintillator detector. Non-linearity at lower energies is due to lower energy beta branches which were not resolvable in a Kurie plot.

The Odd-Odd Nucleus $^{116}_{51}Sb_{65}$*

C.B. Morgan, Jean Guile, R.A. Warner, W.B. Chaffee, W.C. McHarris, W.H. Kelly, E.M. Bernstein,** and R. Shamu**

Experimental investigations are underway of the states of both odd- and even-mass antimony isotopes. Radioactive decay, particle transfer and (p,nγ) reactions are being used in a coordinated way to determine the low-lying states and their properties. These studies are motivated by an interest in the systematic behavior of the excited states and in the residual p-n interaction in this region of the periodic table. We have already studied extensively the radioactive decays of the odd-mass telluriums to the antimonies. Most recently we have begun experiments on ^{116}Sb.

Previous experiments[1] with a Ge(Li)-NaI(Tl) coincidence spectrometer on the decay of the 2.5-hour ^{116}Te have suggested excited states at 93.5 and 723.5 keV with another state tenatively placed at 196.5 keV. Internal conversion experiments[2] have shown the 93.5-keV transition to be an E2 and a 103.2-keV transition an E1.

To date, we have performed only a few in-beam gamma-ray experiments using the $^{116}Sn(p,n\gamma)^{116}Sb$ reaction: namely, excitation functions and γ-γ [Ge(Li)-Ge(Li)] coincidence measurements.

Figure 1 is the Ge(Li) gamma-ray spectrum obtained at approximately 1.0 MeV of excitation. Figure 2 contains integral and typical gated coincidence spectra. Table 1 summarizes the coincidence relationships that have been observed. Figure 3 is a preliminary decay scheme suggested by these data.

Since the 93.5 keV transition is an E2,[2] one expects this transition to be delayed. No prompt coincidences have been seen with this gamma ray. Conflicting coincidence data indicate that some of the transitions maybe doublets.

Additional gamma-ray experiments will be performed at higher resolution as well as timing ans coincidence experiments at a low excitation energy. Gamma-ray angular distributions combined with particle transfer experiments will be performed as well.

References

1. O. Rahmouni, Le Journal de Physique 29, 550(1968).

2. R.W. Fink, G. Anderson and J. Katele, Arkiv Fysik 19, 323(1961).

* Supported in part by the USAEC and the NSF.

** Department of Physics, Western Michigan University, Kalamazoo, Michigan.

TABLE I

Summary of Prompt γ-γ Coincidence Results and the Excitation Energies at Which Each Transition was First Observed

Gated γ-Ray (keV)	Excitation (keV)	Coincident γ-Ray (keV)
103	155	108,158,308,353,364, 551, 712
108	380	103,364
158		103,353,481
308	680	103
353	580	103,158
364	580	103,108
367	1180	103,551
395	1280	629
404	980	411
411	480	404,471
424	580	481,706
455	680	158
471	780	103,411
481	680	158,364,424,518
518	680	481,706
551	680	103,367
629	880	103,364,395
706	1480	424,518
712	980	103

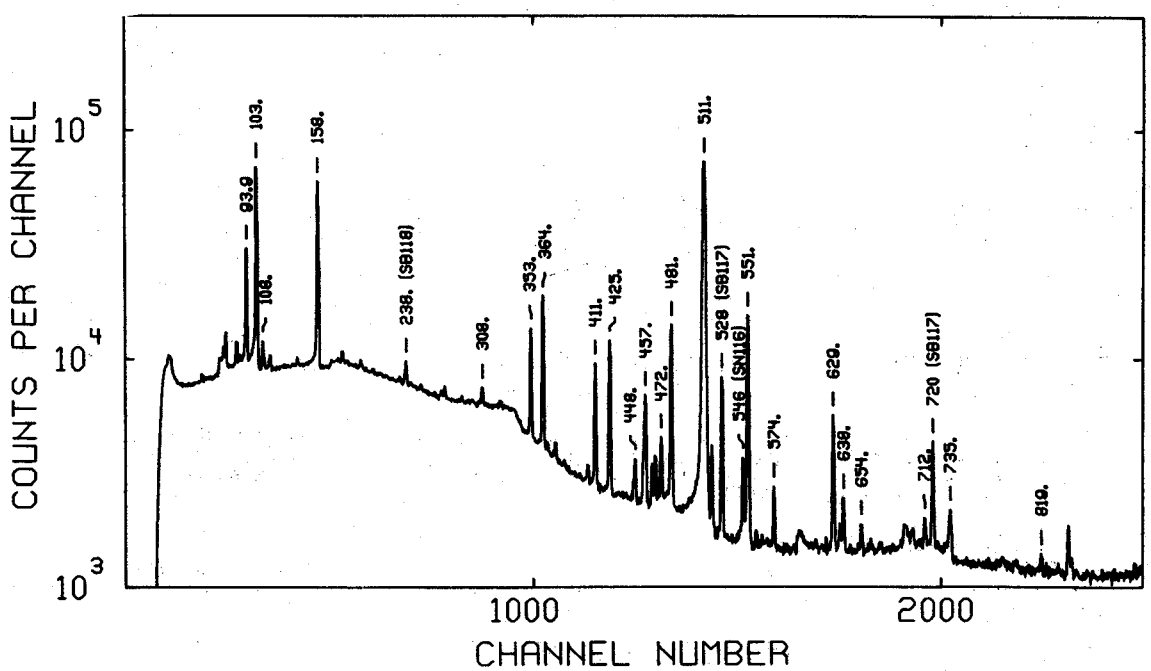

Fig. 1 Typical ^{116}Sb singles spectrum taken at approximately 1.0 MeV of excitation via the (p,nγ) reaction.

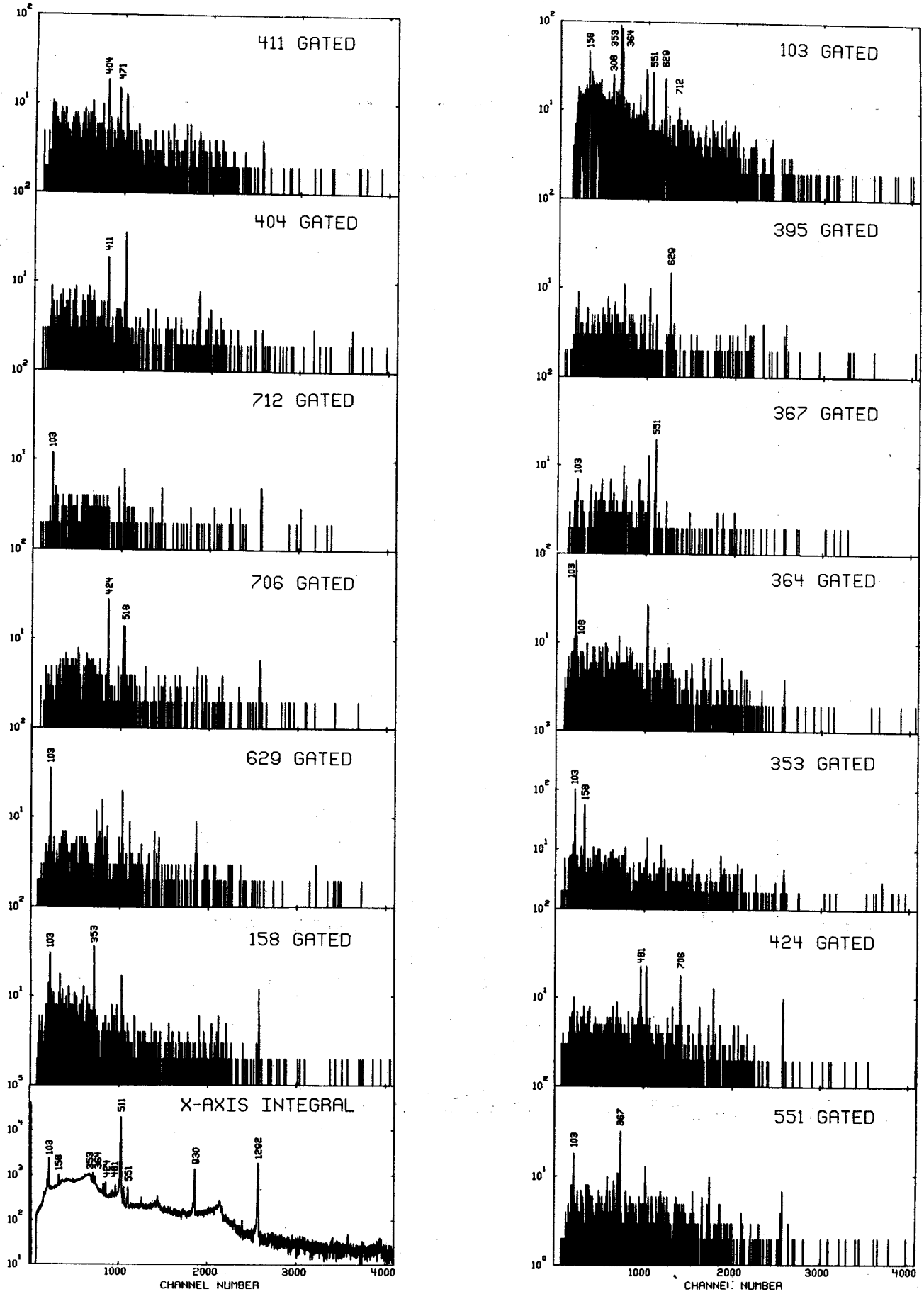

Fig. 2 Integral and gated spectra of ^{116}Sb γ-γ coincidence.

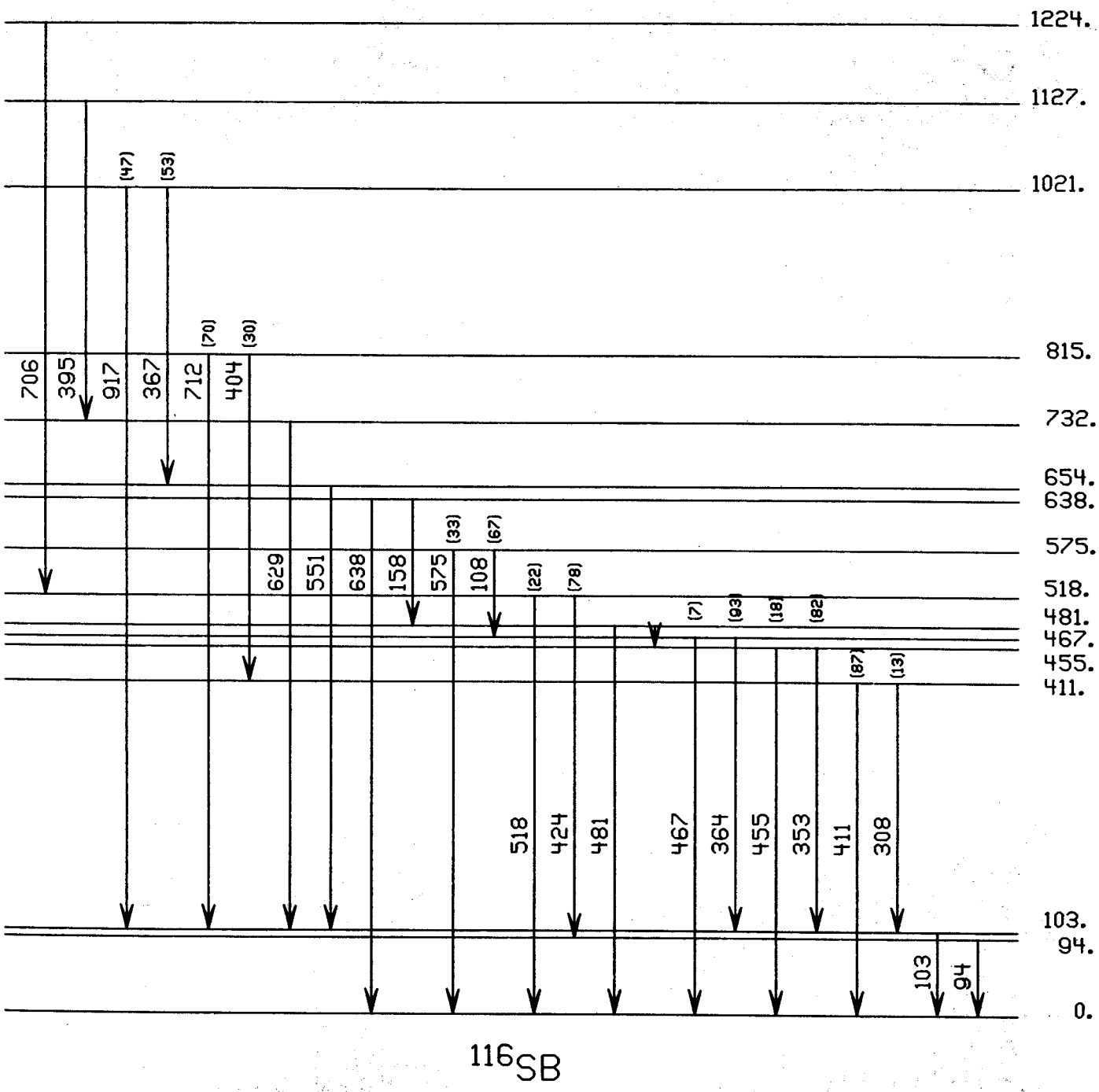

Fig. 3 A preliminary level scheme for ^{116}Sb.

The Low-Lying Levels of ^{118}Sb*

W.B. Chaffee, C.B. Morgan, R.A. Warner, Wm.C. McHarris,
W.H. Kelly, E.M. Berntein,** and R. Shamu**

A systematic investigation of the energy levels of the odd-odd nucleus $^{118}_{51}$Sb has been undertaken using gamma-ray spectroscopy with the reaction $^{118}_{50}$Sb(p,nγ)$^{118}_{51}$Sb, and also by using charged particle spectroscopy with the reactions ^{118}Sn(^{3}He,t)^{118}Sb, ^{117}Sn(^{3}He,d)^{118}Sb, and ^{117}Sn(^{4}He,t)^{118}Sb.

Very little has been known about the excited states of this nuclide. The ground state ($J^{\pi}=1^{+}$) with half-life of 3.5 minutes, an isomeric state (8^{-}) with half-life of 5.1 hour and an isomeric state with half-life of 0.87 seconds are all that have been reported.[1] The two spin assignments are well documented,[2,3] although the energy of the 8^{-} level at 190 keV is ambiguous.

For the (p,nγ) experiments, enriched metallic ^{118}Sn targets were bombarded with protons from the MSU sector-focused cyclotron and from the Western Michigan University tandem-Van de Graaff accelerator. A series of excitation functions were obtained using beam energies from 4.45 MeV to 6.30 MeV. These energies provided excitation from 70 keV below threshold to 1800 keV above. Gamma rays resulting from the reaction were detected by one of several Ge(Li) detectors, processed by standard state-of-the art electronics and Northern Scientific ADC's. Data were stored for later analysis on the Cyclotron Laboratory's Sigma 7 computer.

By raising the energy of the proton beams in slow stages and counting the emitted gamma radiation it was possible to identify, by the rapid increase in intensity, those gamma's which were due to the de-excitation of states in ^{118}Sb and the threshold energies for these states. The accompanying ^{118}Sn(p,γ)^{119}Sb* whose Q-value is +5.12 MeV, contains intense gamma transitions at 270.3 and 644.1 keV. Since the change of excitation for these gammas over the bombardment energy range was small, the intensity of these transitions provided a convenient normalization, with the relative intensity of these two providing a check on the data reduction techniques. Subsequent analyses of the spectral data were made using the peak fitting program SAMPO.[4] Two such spectra are shown in Fig. 1. The upper spectrum was taken with a proton beam energy of 5.40 MeV, corresponding to an excitation of 880 keV. The lower spectrum, taken with a proton beam of 4.45 MeV, was below threshold for the ^{118}Sn(p,nγ)^{118}Sb Reaction.

A series of gamma-gamma prompt coincidence experiments were also performed. A pair of Ge(Li) detectors in 180° geometry bracketed the beam line. A wedge shaped block of lead with an axial hole drilled partially through it was placed directly behind the target and between the two detectors. This acted as a beam stop, and reduced Compton scattering between the two detectors. The coincidence output from each detector, timed to <40 n seconds with a TPHC, was stored as two halves of a word on magnetic tape for processing later. Setting gates on selected peaks and recovering the data from the tape using background subtraction made the observation of the gamma cascades possible. An "any-coincidence" spectrum and two selected gated coincidence spectra are illustrated in Fig. 2. This run was at a bombardment energy of 5.54 MeV which corresponds to an excitation of 1000 keV.

A study of the levels of ^{118}Sb by charged particle transfer reactions was also carried out in order to aid in the placement of the excited states. These used beams of ^{4}He and ^{3}He particles at energies from 32 MeV to 40 MeV. Evaporated enriched (96.6%, for ^{118}Sn, 78.8%, for ^{117}Sn) targets were mounted in the scattering chamber of the Enge split-pole spectrometer and the reaction particles were focussed on NTB 25μ plates. All of these data have not yet been analyzed so only preliminary findings are included in the decay scheme. The lowest energy levels of ^{118}Sb, as seen on four of the plates, is illustrated in Fig. 3.

A total of 86 gamma rays have been identified as probably belonging to the de-excitation of the levels of ^{118}Sb below 1300 keV. Of these, 52 have been identified as being in coincidence with one or more other transitions. With these coincident gammas, the threshold values from the excitation curves and the levels obtained from the plate data, a preliminary decay scheme has been obtained and is shown in Fig. 4.

Experiments attempting to find the threshold of any gammas which might be feeding the 8^{-} state were of limited success. These experiments indicate that the 8^{-} state lies at an excitation <200 keV. No gamma-rays feeding this state have been identified.

No evidence of the reported isomeric state with lifetime of 0.875 sec. has been found.

References

1. C.M. Lederer, J.M. Hollander, and I. Perlman, Table of Isotopes, 6th Ed., 1967, p. 261 and references cited therein.

2. H.H. Bolotin, A.C. Li, and A. Schwarzschild, Phys. Rev. 124, 213(1961).

3. A.D. Jackson, Jr., E.H. Rogers, Jr., and G.J. Garrett, Phys. Rev. 175, 65(1968).

4. J.T. Routti, S.G. Prussin, Nucl. Instr. and Methods 72, 125(1969).

* Supported by the USAEC and the NSF.

** Dept. of Physics, WMU, Kalamazoo, Michigan.

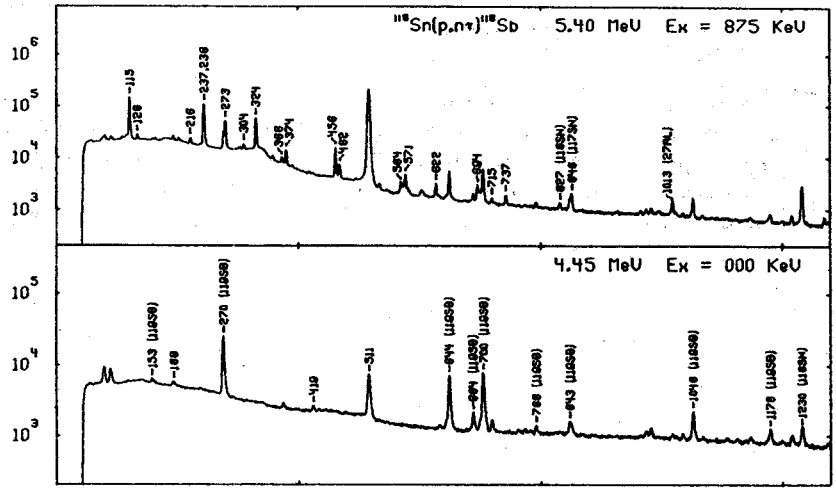

FIGURE 1

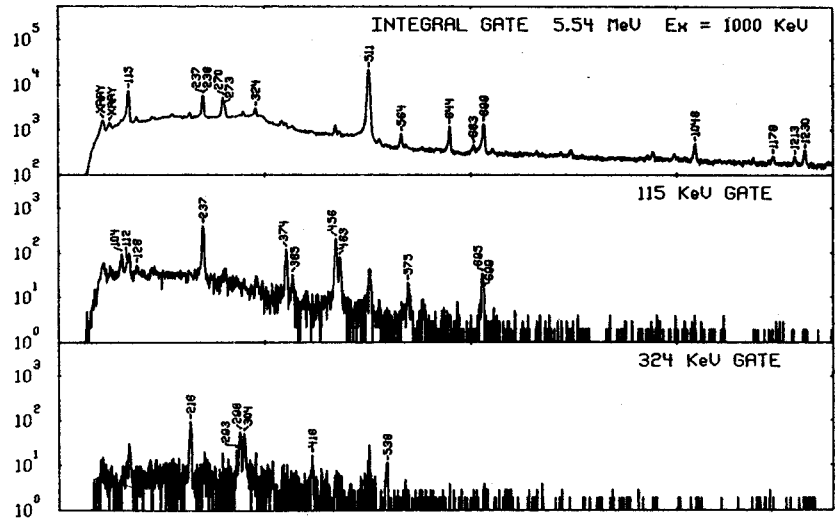

FIGURE 2

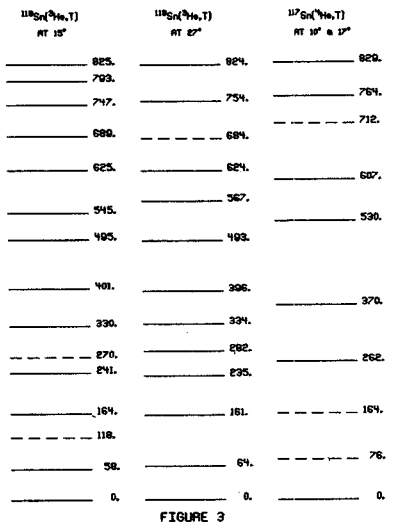

FIGURE 3

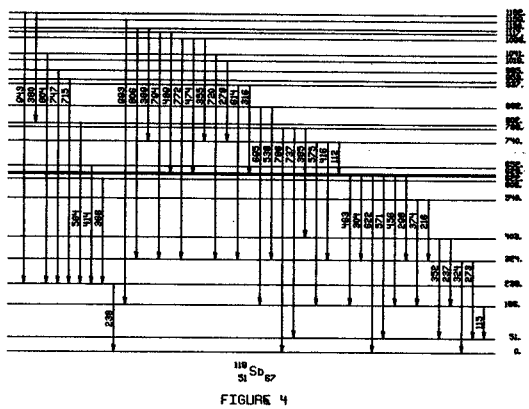

FIGURE 4

Electromagnetic Transitions for N=82 Nuclei

D. Larson and B.H. Wildenthal

Recently there has become available a large amount of experimental information on the N=82 nuclei. Proton and neutron transfer reactions, inelastic proton, neutron and alpha scattering, and electromagnetic transitions have all been studied in an attempt to understand the structure of these nuclei. Experimental evidence indicates that Z=50, N=82 forms a good doubly closed core, and the N=82 nuclei are then formed by adding from 1-14 protons in the next major proton shell.

Two different theoretical approaches have been applied to these nuclei. The approach used by Waroquier and Heyde,[1] Freed and Miles,[2] and Rho[3] is based on BCS quasiparticle theory which works quite well for single closed shell nuclei such as the N=82 nuclei. This theory is quite easy to calculate with—for example the energy matrices are generally less than 40x40.

The calculation we report here was done in the standard shell model formalism using the Oak Ridge-Rochester shell model codes.[4] The basis space for the calculation included the $1g_{7/2}$, $2d_{5/2}$, $2d_{3/2}$, and $3s_{1/2}$ single particle orbitals—the $h_{11/2}$ orbital was not included and hence no negative parity states were calculated. However, this basis space must be truncated in order to keep the dimensionality of the energy matrices to such a size that they can be diagonalized.

The shell model calculations of Wildenthal were actually done by distributing active protons over the $1g_{7/2}$-$2d_{5/2}$ orbitals in all Pauli allowed ways, and in addition including those configurations which allowed one particle in either the $3s_{1/2}$ or $2d_{3/2}$ orbitals and distributed the remaining (n-1) protons over the $1g_{7/2}$-$2d_{5/2}$ space. This led to energy matrices which were 290x290 for the $7/2^+$ states in ^{139}La.

The two-body interaction was parameterized in terms of the modified surface delta interaction. The 2 parameters of the interaction, as well as the 4 single particle energies—a total of 6 parameters—were obtained by a fitting technique which required an rms minimum between calculated and experimental level energies.

Two sets of calculations were done. The parameters for the first Hamiltonian were obtained by fitting to nuclei from ^{136}Xe to ^{145}Eu. (A=136-145 Hamiltonian) The second set of calculations was done using parameters obtained from fitting to nuclei from ^{136}Xe to ^{140}Ce. (A=136-140 Hamiltonian) The basis space was the same for both sets of calculations, only the parameters of the Hamiltonian differed. The basic difference between the two Hamiltonians is the $g_{7/2}$-$d_{5/2}$ single particle splitting, which increases from 500 keV for A=136-145 Hamiltonian to 900 keV for the A=136-140 interaction. Good agreement is obtained between the calculated energies and their experimental counterparts with both Hamiltonians for nuclei around A=138-140.[5,6]

We present here the results for the B(E2) transition rates for ^{138}Ba and the B(M1) and B(E2) rates for ^{139}La. An effective proton charge of 1.5 was used, consistent with that found for the s-d shell and the lead region. We also increased g_ℓ^p from the free particle value of 1.0 to 1.1, based on recent results by Nagamiya and Yamazaki.[7]

Table I shows a comparison between experiment and theory for ^{138}Ba. We also show the results of the quasi-particle calculations of Waroquier and Heyde. For the $2_1^+ \to 0^+_{g.s.}$ transition, the A=136-145 interaction predicts a B(E2) 10% too low, A=136-140 predicts a B(E2) 30% low, while if a value of e_p=1.5 is used in the WH calculation, their B(E2) is 50% low. The $6^+ \to 4^+$ transition in the N=82 nuclei is an isomeric transition, and thus has a small B(E2). The quadrupole moment of the first excited 2^+ state in ^{138}Ba is predicted oblate, but too large by the shell model.

Tables 2-5 shows the results for ^{139}La. Freed and Miles used the free particle values for g_p^ℓ and g_p^s, while WH fit to the known magnetic dipole moments to get g_s^p. The B(M1) from $7/2^+ \to 5/2^+$ is forbidden in the single quasiparticle picture since the initial and final states differ in the orbital angular momentum quantum number, so the B(M1) is due solely to admixtures in the wave functions. The two shell model calculations are consistent with experiment.

References

1. M. Waroquier and K. Heyde, Nucl. Phys. A164, 113(1971).
2. N. Freed and W. Miles, Nucl. Phys. A158, 230(1970).
3. M. Rho, Nucl. Phys. 65, 497(1965).
4. J.B. French, E.C. Halbert, J.B. McGrory, and S.S.M. Wong, Advances in Nuclear Physics, Vol. III, eds. M. Baranger and E. Vogt, (Plenum Press, New York, 1969).
5. B.H. Wildenthal, Phys. Rev. Letters 22, 1118(1969).
6. B.H. Wildenthal and D. Larson, Phys. Letters 37B, 266(1971).
7. S. Nagamiya and T. Yamazaki, Phys. Rev. C4, 1961(1971).

^{138}Ba Electromagnetic Properties

Observables	Interaction A=136-145	Interaction A=136-140	Waroquier & Heyde	Experiment
B(E2) $2_1^+ \to 0^+$ g.s.	392 e^2f^4 e_p=1.5	308 e^2f^4 e_p=1.5	426 e^2f^4 e_p=2	442 e^2f^4
B(E2) $4_1^+ \to 2_1^+$	5.2 e^2f^4 e_p=1.5	27.4 e^2f^4 e_p=1.5	2.19 e^2f^4	12 e^2f^4
B(E2) $6_1^+ \to 4_1^+$	17.1 e^2f^4 e_p=1.5	0.47 e^2f^4 e_p=1.5	1.48 e^2f^4	2.3 e^2f^4
Quadrupole Moment of 2_1^+	-27.3 ef^2 e_p=1.5	-30.4 ef^2 e_p=1.5	-8 ef^2	-11 ± 15 ef^2

Table 1

^{139}La Electromagnetic Properties

Observables	Interaction A=136-145	Interaction A=136-140	Freed & Miles	Heyde & Waroquier	Experiment
Magnetic Moment Of Ground State	2.21 n.m. g_ℓ=1.1	2.15 n.m. g_ℓ=1.1	1.70 n.m.	2.80 n.m. g_ℓ=1 g_s=2.66	2.78 n.m.
Quadrupole Moment of Ground State	19.4 ef^2 e_p=1.5	27.3 ef^2 e_p=1.5	-0.6 ef^2 e_p=1.0	+24.8 ef^2 e_p=2.0	+23 ef^2
$5/2^+ \to 7/2^+$ g.s. B(E2)	1.26 e^2f^4 e_p=1.5	0.22 e^2f^4 e_p=1.5	0.10 e^2f^4	0.27 e^2f^4	4.8 e^2f^4
$5/2^+ \to 7/2^+$ g.s. B(M1)	.00384 n.m.^{2}	.00136 n.m.^{2}	.00042 n.m.^{2}	.0000057 n.m.^{2}	.0046 n.m.^{2}
Magnetic Moment of $5/2^+$ 1st Excited State	4.80 n.m. g_ℓ=1.1	4.86 n.m. g_ℓ=1.1			
Quadrupole Moment of $5/2^+$ 1st Excited State	-9.94 ef^2 e_p=1.5	-21.0 ef^2 e_p=1.5			

Table 2

Single particle values
g_ℓ=1.0 g_s=5.585

B(M1)'s in ^{139}La (g_ℓ=1.1]

2*Initial State	2*Final State	Interaction A=136-140	Interaction A=136-145	2*Initial State	2*Final State	Interaction A=136-140	Interaction A=136-145
5_1	7_1	.00136 n.m.^{2}	.00384 n.m.^{2}	3_1	5_1	.887 n.m.^{2}	.117 n.m.^{2}
5_2	7_1	.00127	.000839	3_2	5_1	.455	.222
5_3	7_1	.00127	.00385	3_3	5_1	.179	.258
5_4	7_1	.000756	.00225	3_4	5_1	.500	1.19
7_2	7_1	.00842	.00961	5_2	5_1	.0115	.00486
7_3	7_1	.0000167	.000169	5_3	5_1	.00375	.00971
7_4	7_1	.00253	.00791	5_4	5_1	.000316	.00818
9_1	7_1	.0571	.0490	7_1	5_1	.00102	.00288
9_2	7_1	.00350	.00293	7_2	5_1	.00149	.00453
9_3	7_1	.0000522	.00219	7_3	5_1	.000106	.000118
9_4	7_1	.0104	.00147	7_4	5_1	.000384	.00389

Table 3

B(E2)'s in ^{139}La (e_p=1.5)

2⁺Initial State	2⁺Final State	Interaction A=136-140	Interaction A=136-145	2⁺Initial State	2⁺Final State	Interaction A=136-140	Interaction A=136-145
3_1	7_1	3.7 e^2f^4	47.5 e^2f^4	5_2	5_1	50.4 e^2f^4	54.2 e^2f^4
3_2	7_1	<0.01	104	5_3	5_1	167	252
5_1	7_1	0.2	1.3	7_2	5_1	116	218
5_2	7_1	322	491	7_3	5_1	65.2	0.3
7_2	7_1	6.0	0.1	3_1	5_1	338	500
7_3	7_1	48.4	182	3_2	5_1	72.2	50
9_1	7_1	5.7	61.0	1_1	5_1	682	-
9_2	7_1	222	224	1_2	5_1	115	207
11_1	7_1	197	311	9_1	5_1	232	196
11_2	7_1	2.9	0.01	9_2	5_1	21.6	109

Table 4

Characteristics of Low-Lying Levels in ^{139}La

J^π_ν	E_{calc}	E_{expt}	Interaction	Model Wave Function (Largest Components)[c]		
$7/2^+$ g.s.	0.0	0.0	I[a]	$.74(g_7)^5_{J=7}(d_5)^{2,0}_{J=0}$	$+.46(g_7)^3_{J=7}(d_5)^{4,0}_{J=0}$	$+.43(g_7)^7_{J=7}$
$7/2^+$ g.s.	0.0	0.0	II[b]	$.66(g_7)^5_{J=7}(d_5)^{2,0}_{J=0}$	$+.65(g_7)^7_{J=7}$	$+.28(g_7)^3_{J=7}(d_5)^{4,0}_{J=0}$
$5/2^+_1$	0.084	0.166	I	$.70(g_7)^{4,0}_{J=0}(d_5)^3_{J=5}$	$+.65(g_7)^{6,0}_{J=0}(d_5)^1_{J=5}$	$-.26(g_7)^{2,0}_{J=0}(d_5)^5_{J=5}$
$5/2^+_1$	0.193	0.166	II	$.79(g_7)^{6,0}_{J=0}(d_5)^1_{J=5}$	$+.56(g_7)^{4,0}_{J=0}(d_5)^3_{J=5}$	$-.15(g_7)^{2,0}_{J=0}(d_5)^5_{J=5}$

[a] A=136-145 interaction.

[b] A=136-140 interaction.

[c] Half-integral spins are given as two times their value, i.e. 7/2=7. The additional quantum numbers labeling a few components are the seniorities, e.g. $(g_7)[4,2]$ refers to the seniority 2, coupling of four 7/2 particles coupled to total angular momentum J.

Table 5

Low-Lying States of ^{140}Pr from a Study of the ^{140}Ce(p,nγ)^{140}Pr and ^{141}Pr(p,d)^{140}Pr Reactions*

Jean Guile, R.W. Goles, C.B. Morgan, R.A. Warner, Wm.C. McHarris, W.H. Kelly, E.M. Bernstein,** and R. Shamu**

In the past year we have undertaken an investigation of the energy levels in yet another odd-odd nucleus, $^{140}_{59}Pr_{81}$. Three other studies of this nuclide have been conducted. The first was that done by Fulmer and coworkers[1] in 1962. From a study using the (d,t) reaction on ^{141}Pr with 60-keV resolution, this group proposed a level scheme. Two years later Krehbiel[2] irradiated ^{141}Pr with 22 MeV bremstrahlung and observed two coincident γ-rays of 644±15 keV and 98±5 keV. He also noted that the 98 keV transition was delayed with respect to the 644 keV transition. Taking this information as our starting point, we are examining the excited states of ^{140}Pr using both the ^{140}Ce(p,nγ)^{140}Pr and ^{141}Pr(p,d)^{140}Pr reactions. Just recently it has come to our attention that a related ^{141}Pr(p,d)^{140}Pr study has been conducted with 30 MeV protons at Texas A&M by Helton and Hiebert.[3] With an achieved resolution of 14 keV on an Enge split-pole spectrograph, they obtained excitation energies up to 430 keV via the (d,t) reaction using 20 MeV deuterons. Their angular distribution measurements were performed with a thin window Ge(Li) detector. Unfortunately, we have not had the opportunity to compare their data with ours.

In our ^{140}Ce(p,nγ)^{140}Pr work both oxide (enriched) and evaporated metal (natural) targets have been used. By incrementing the bombarding energy in small steps from just below that energy required to produce the ^{140}Pr ground state to approximately 2 MeV of excitation, we have been able to single out those γ-rays of interest. This technique also enables us to place upper limits on the energy of the level deexcited by a particular γ-ray. The energies and relative intensities of the observed γ-rays at 2 MeV of excitation are given in Table I. A γ-γ coincidence experiment has also been performed to help us place these γ-rays in a consistent decay scheme. Although the data resulting from this experiment need a great deal more study, our preliminary results indicate a decay scheme similar to the skeleton shown in Fig. 1. One should note the absence of the previously reported 640 keV transition. Coincidence measurements indicate a strong 140.4 keV-241.2 keV-640.6 keV cascade. This is not displayed in the present decay scheme due to some apparently conflicting evidence concerning its placement. Some of the data indicate that the first excited state may actually be a doublet with a 1.4 keV spacing. The evidence is not yet conclusive and thus the first excited state in our preliminary decay scheme is displayed without any doublet character.

In our ^{141}Pr(p,d)^{140}Pr study we bombarded evaporated metal targets with 35 MeV protons. One of the resulting spectra is displayed beside our decay scheme for easy comparison of the populated levels. The 9 keV resolution attained in this experiment with the Michigan State University magnetic spectrograph has allowed us to resolve several doublets and to place more precise energy values on the deuteron groups. An angular distribution experiment has been performed and the data are now being analyzed.

Although all our results are preliminary at this stage, thus far we are much encouraged by the agreement of this two-sided attack on ^{140}Pr.

References

1. R.H. Fulmer, A.L. McCarthy, and B.L. Cohen, Phys. Rev. 128, 1302(1962).

2. H. Krehbiel, Phys. Letters 13, 65(1964).

3. V.D. Helton and J.C. Hiebert, Final Report on Research at the Texas A&M University Cyclotron for the period June 1, 1970-December 31, 1971. ORO-3398-45 (March, 1972).

TABLE I

Energies and Relative Intensities of γ-rays Observed in ^{140}Pr at 2 MeV of Excitation

Energy (keV)	Relative γ-ray Intensity
98.0±0.3	12.0±0.9
126.9±0.4	5.5±0.7
132.9±0.3	41.4±1.9
140.4±0.3	17.4±0.9
162.0±0.3	43.0±3.1
164.1±0.3	41.2±2.0
212.9±0.5	1.5±0.3
227.3±0.5	1.1±0.9
241.2±0.5	49.2±2.1
243.0±0.5	38.7±2.5
257.2±0.2	78.4±4.3
263.3±0.2	10.3±1.2
270.9±0.2	17.3±1.4
286.7±0.4	3.1±0.4
361.1±0.4	2.3±0.2
368.5±0.4	2.8±0.2
384.6±0.4	5.1±0.3
390.9±0.4	3.1±0.3
393.0±0.4	5.5±0.3
412.4±0.4	5.9±0.2
419.6±0.4	8.5±0.3
546.7±0.4	6.5±0.3
574.4±0.4	7.6±0.4
612.6±0.4	4.6±0.3
633.0±0.4	6.1±0.8
640.6±0.2	≡100
669.5±0.4	14.7±0.8
762.5±0.4	8.6±0.4
876.5±0.3	13.8±0.5
888.0±0.5	5.5±0.3
903.9±0.3	16.4±0.5
939.1±0.4	8.2±0.4
966.9±0.4	2.5±0.3
1035.6±0.4	3.8±0.5
1053.5±0.4	5.8±0.4
1182.9±0.4	4.9±0.4
1201.3±0.4	7.3±0.5

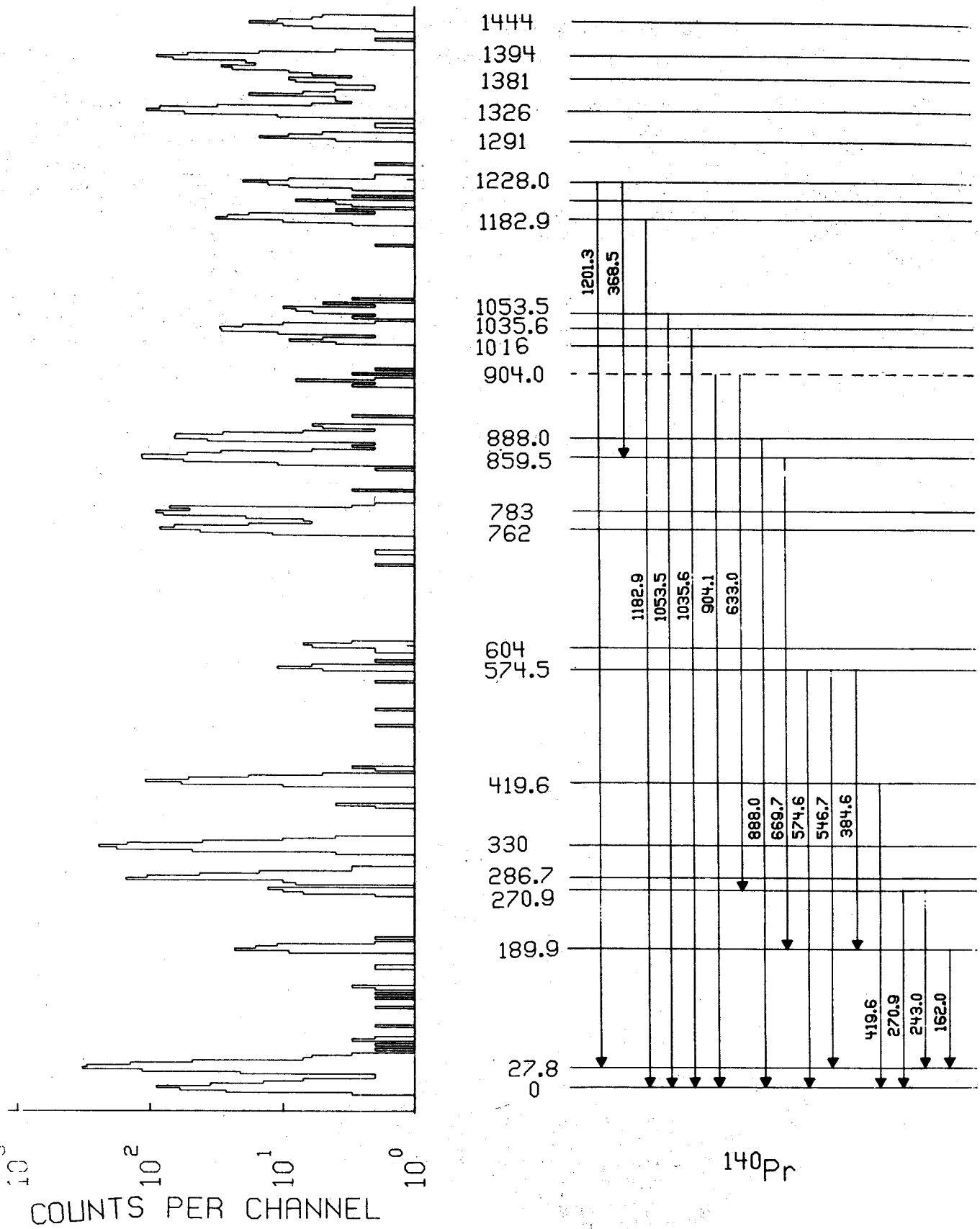

Fig. 1 A preliminary level scheme for ^{140}Pr incorporating the current (p,d) and (p,nγ) results. The (p,d) spectrum shown was taken at 45° using 35-MeV protons.

Lifetime of the 629-keV 11/2$^-$ State in ^{141}Pm*

R.A. Warner, R.R. Todd, R.E. Eppley,** W.H. Kelly, and Wm.C. McHarris

In a recently published study[1] of the decay of ^{141m}Sm, the level at 628.7 keV excitation in ^{141}Pm was determined to have $J^\pi = 11/2^-$. Transitions to and from this state had been identified in simple one-parameter delayed coincidence experiments. The half-life of this level is now measured to be 0.70 ± 0.02 μsec.

The parent activity was produced by the (^{3}He,4n) reaction at 40 MeV on separated ^{142}Nd. This reaction strongly populates 22.1-min ^{141m}Sm. The source was not counted until about 10 min after the activation, in order to reduce interference from the 11.3-min ^{141g}Sm activity. The detectors used in the experiment were a Ge(Li) coaxial crystal with 10.4% efficiency (at 1332 keV and 25 cm, relative to the efficiency of a 7.6x7.6 cm NaI(Tl) crystal), and one-half of a 20x20 cm NaI(Tl) annulus. The signals from these detectors were processed essentially as indicated in Fig. 1. The timing signals from the annulus were derived from that portion of the γ-ray spectrum above the annihilation peak, as 97% of the γ-ray intensity feeding the 629-keV state lies in transitions with energy greater than 538 keV. These transitions depopulate a 3 quasiparticle multiplet centered at about 2 MeV and fed strongly in the ^{141m}Sm decay.

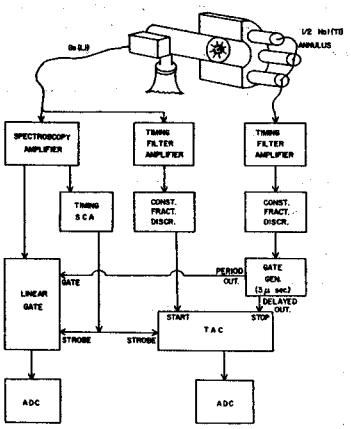

Fig. 1 Diagram of the experimental electronics.

The 2 ADC's scaled addresses corresponding to the energy deposited in the Ge(Li) counter and the time interval between the pulses from the 2 detectors. These addresses were then recorded in pairs on magnetic tape by EVENT,[2] a task of the JANUS II timesharing system. A isomeric view of the spectrum is displayed

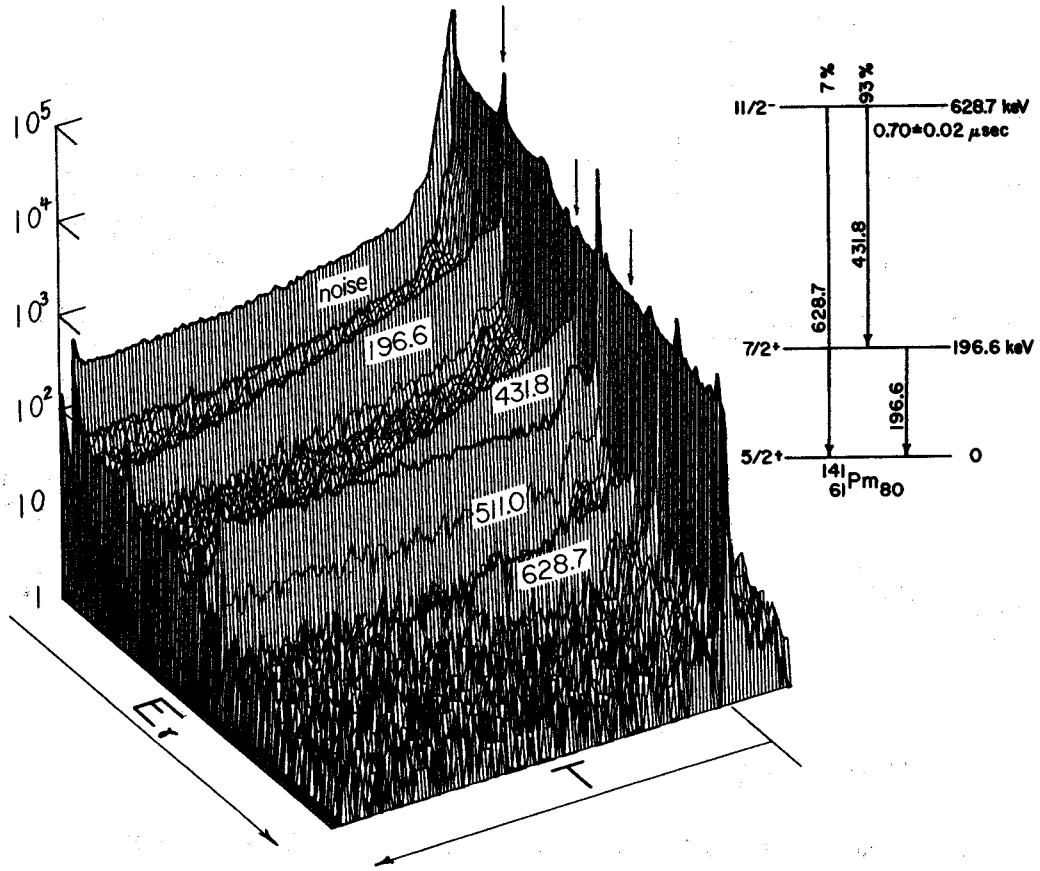

Fig. 2 Isometric view of the 2-parameter data compressed into a 128x128 channel array. The levels and transition relevant to the measurement are shown in the inset.

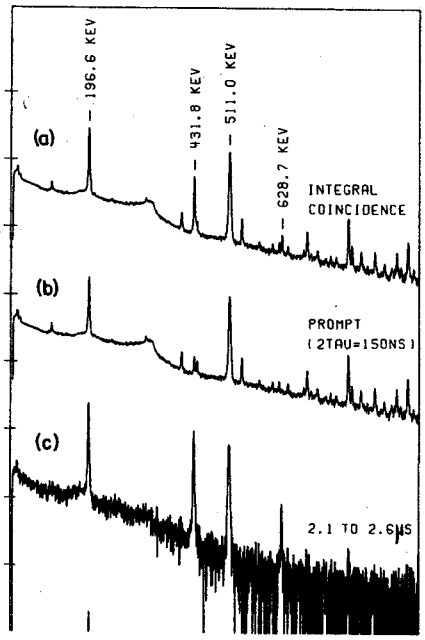

Fig. 3 The Ge(Li) energy spectrum, showing (a) all events, (b) pulses in prompt coincidence with the NaI pulses, and (c) pulses following the NaI pulses by from 2.1 to 2.6 μsec.

in Fig. 2 along with a diagram including only those levels and transitions of interest here.

Figure 3 contains the Ge(Li) energy spectrum separated into prompt and delayed components, while Fig. 4 shows the distribution in time for different peaks in the energy spectrum. Background subtraction was used in the sorting program[3] to remove from the spectra those events in the continuum under the gated peak. The bump just to the left of the prompt peak in the time distribution is the result of an instrumental problem which has little effect on most of the data. The 196.6-, 431.8-, and 628.7-keV transitions all have components decaying with the same half-life, which, when computed from the combined data, is 0.70 ± 0.02 μsec. From the known[1] 628.7-keV to 431.8-keV branching ratio, the E3 transition is found to be enhanced by 40% and the M2 transition to be retarded by a factor of 6 when compared with the Moszkowski single-particle estimates.

References

1. R.E. Eppley, R.R. Todd, R.A. Warner, Wm.C. McHarris, and W.H. Kelly, Phys. Rev. C5, 1084(1972).

2. D.L. Bayer, Programs 8 and 13 in MSU Sigma-7 Users Manual.

3. G. Giesler, Program 35 in MSU Sigma-7 Users Manual.

* Supported by the USAEC and the NSF.

** Present Address: Bldg. 70A Lawrence Berkeley Radiation Laboratory, Berkeley, California 94720

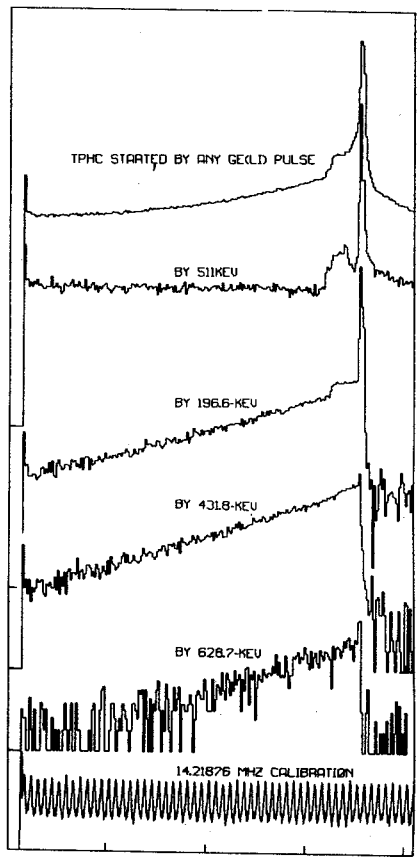

Fig. 4 Distributions in time with respect to the NaI pulses for events in various parts of the Ge(Li) spectrum.

γ-Rays in ^{141}Pm from the Decay of ^{141g}Sm*

R.R. Todd,** R.E. Eppley,*** R.A. Warner,
Wm.C. McHarris, and W.H. Kelly

As a part of a series of gamma-ray spectroscopic studies of nuclei near the N=82 closed shell we have recently reported on the decay of ^{141m}Sm[1] and its subsequent population of a three-quasiparticle multiplet in the daughter ^{141}Pm. Here, we briefly report on an investigation of the ^{141g}Sm decay scheme which completes our studies on this isotope.

The ^{141g}Sm activity has been produced by two methods: the ^{142}Nd(^{3}He,4n)$^{141m+g}$Sm (Q=-27.3 MeV) reaction, and indirectly by the ^{144}Sm(p,4n)^{141}Eu $\xrightarrow{EC}$ ^{141}Sm reaction (Q=-36.8 MeV). The second method was used to check the results of the first and was an attempt to enhance the relative production of ^{141g}Sm in order to distinguish it better from ^{141m}Sm which is abundantly produced in the first reaction. The results using this second reaction were only partially successful because of other strong competing reactions.

We have measured the half-life to be 11.3±0.3 min and the γ-rays associated with the ^{141g}Sm decay have been identified by following the decay through several half-lives. The decay scheme has been constructed using various experimental configurations which include two-dimensional γ-γ coincidence, anticoincidence and γ-511-511-keV triple coincidence experiments.

The study of ^{141g}Sm is complicated by the presence of the longer-lived and more intense ^{141m}Sm activity in the same spectra, and by the additional difficulty that almost 90% of the ^{141g}Sm decay is directly to the ground state of ^{141}Pm. The strong interference masks many weaker transitions that might be expected.

The energies and relative intensities of the γ-rays observed are presented in Table I. The γ-γ two-dimensional coincidence results [Ge(Li)-Ge(Li)] are presented in Table II. In Fig. 1 we present the decay scheme we have deduced from the current data. The transition and excited state energies are given in keV and the disintegration energy Q_ε is a calculated value.[2] The log(ft) values shown on the decay scheme have been calculated by assuming the total EC plus β^+ feeding to the ^{141}Pm ground state by ^{141g}Sm to be 86.2%.[3]

On the basis of log(ft) values and relative gamma-ray intensities, the spins and parities of the excited states shown in Fig. 1 (excepting the questionable state of 728.0 keV) are expected to be $1/2^+$, $3/2^+$, or $5/2^+$. Since the beta

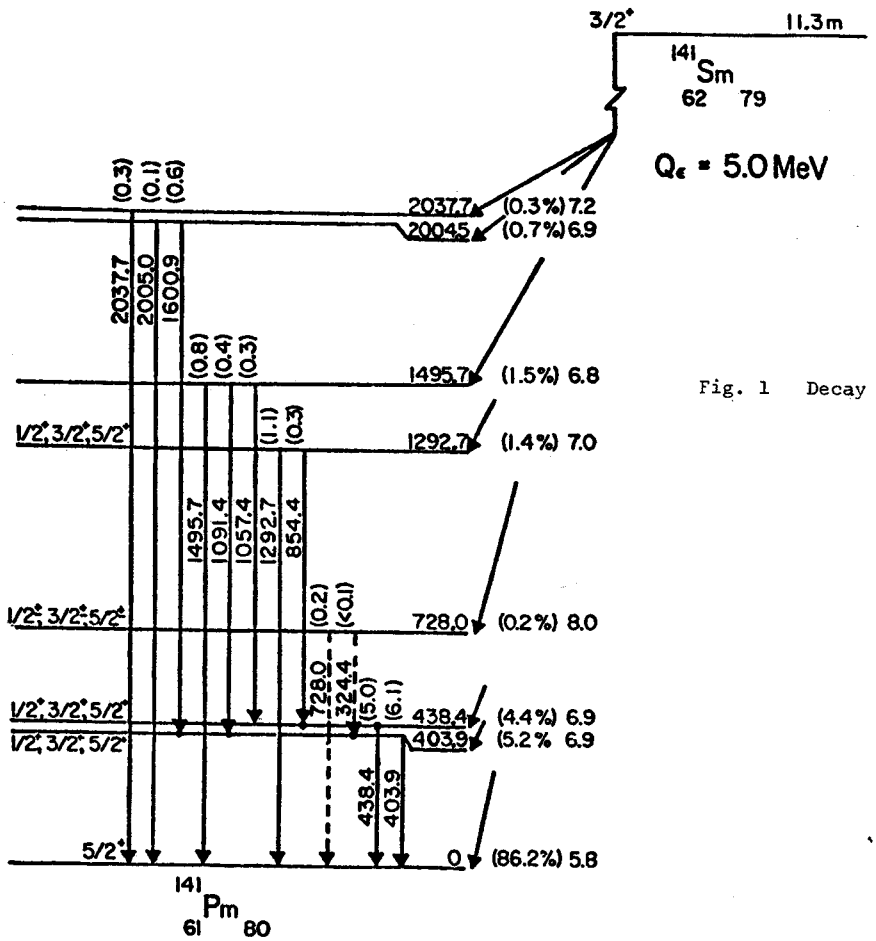

Fig. 1 Decay Scheme of ^{141g}Sm.

transition to the 728.0-keV state has a log(ft)=8.0, this transition may be either allowed or first-forbidden. Thus the spin of this state is also expected to be 1/2, 3/2, or 5/2.

References

1. R.E. Eppley, R.R. Todd, R.A. Warner, Wm.C. McHarris, and W.H. Kelly, Phys. Rev. C5, 1084(1972).

2. William D. Myers, and Wladyslaw J. Susatchki, UCRL 11980(1965).

3. R.R. Todd, Ph.D. Thesis (1972) unpublished.

* Supported by the USAEC and the NSF.

** Now at the Department of Physics, Western Michigan University, Kalamazoo, Michigan.

*** Now at the Lawrence Berkeley Laboratory, Berkeley, California.

TABLE I

^{141g}Sm Summary of γ-Ray Energies and Relative Intensities

Energy (keV)	Singles Intensities
324.4±0.2	≤1
403.9±0.1	≡100
438.4±0.1	82.6±3
728.0±0.2	7.9±0.5
854.4±0.2	3.7±0.3
1057.4±0.1	5.5±0.4
1091.9±0.2	6.1±0.4
1292.7±0.1	16.9±0.5
1495.7±0.2	12.3±0.4
1600.9±0.3	10.3±0.5
2000.5±0.5	1.2±0.2
2037.9±0.5	5.4±0.4

TABLE II

Summary of γ-γ Coincidence Results for ^{141g}Sm

Gate Energy (keV)	γ-Rays Seen in Coincidence (keV)
324.4	196.6, 403.8, 511.0, 777.4
403.9	324.4, 511.0, 1091.9, 1600.9
438.4	854.4, 1057.7 (very weak)
854.4	511.0
1091.9	403.9, 511.0
1292.7	511.0
1600.9	403.9

Some New Transitions in the Decay of ^{142}Eu*

M.F. Slaughter,** R.R. Todd, R.A. Warner and W.H. Kelly

Four previously unreported γ-ray transitions belonging to the decay of 1.2-min ^{142}Eu have been discovered in the course of a search for the decay of ^{141}Eu. In this study, ^{144}Sm oxide was bombarded with 40-MeV and 45-MeV protons, and γ-ray activities were counted with a Ge(Li) detector during several consecutive intervals; the first intervals started 1 min. after each few second activation.

Figures 1a and 1b contain the spectra from activation at 40 MeV and 45 MeV respectively, accumulated during the 5-min periods following each bombardment by 3.5 min. An energy of 40 MeV should be about optimum for the ^{144}Sm(p,3n)^{142}Eu reaction.

Six γ-ray peaks, two of which were previously reported,[1] were assigned to the decay of ^{142}Eu because of their observed common half-life and their relative strengths from the activations at the two beam energies. These transitions and their relative intensities are listed in Table I. There is not yet sufficient data to place these transitions in a decay scheme.

TABLE I

Gamma Rays from the Decay of ^{142}Eu

Energy	Relative Intensity
556.8	70
565.0	5
754.5	13
768.2[a]	≡100
1015.9	13
1023.5[a]	68

[a]Previously reported in Ref. 1.

References

1. H.P. Malan, H. Munzel, and G. Pfenning, Radiochemica Acta 5, 24(1966).

* Supported by the USAEC and the NSF.

** NSF Undergraduate Research Participant.

Fig. 1 Spectra of γ-rays counted during the 5-min periods following by 3.5 min the bombardment of Sm_2O_3 enriched to 95.1% in ^{144}Sm by (a) 40-MeV and (b) 45-MeV protons.

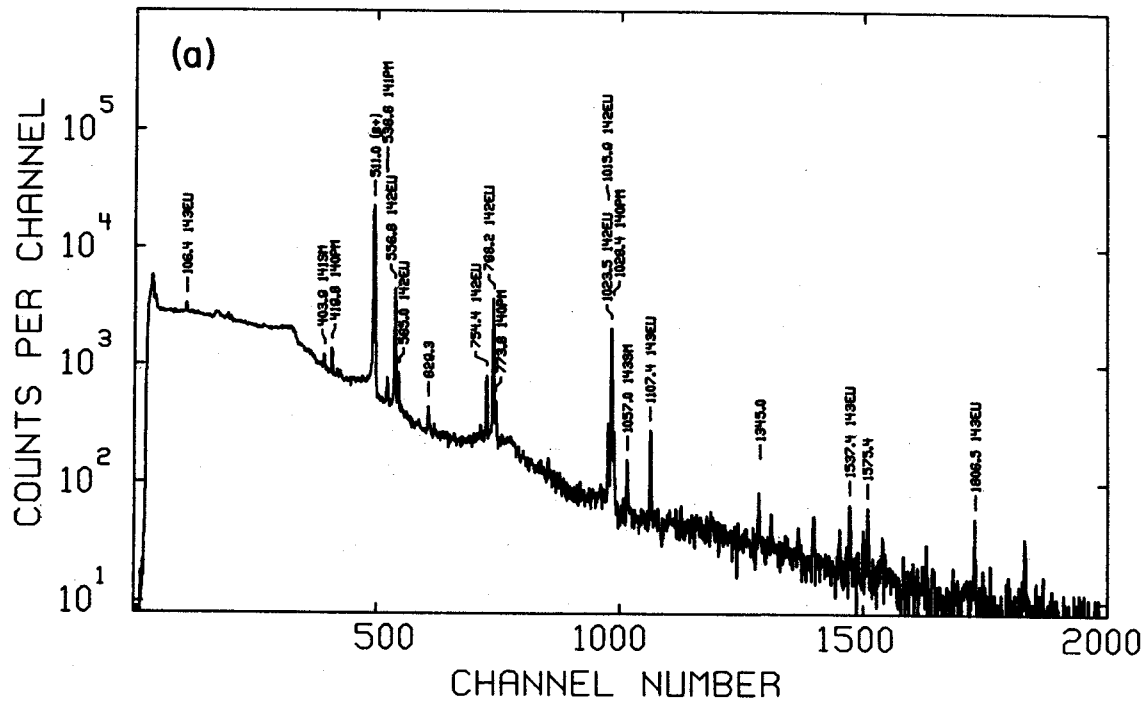

Fig. 1b

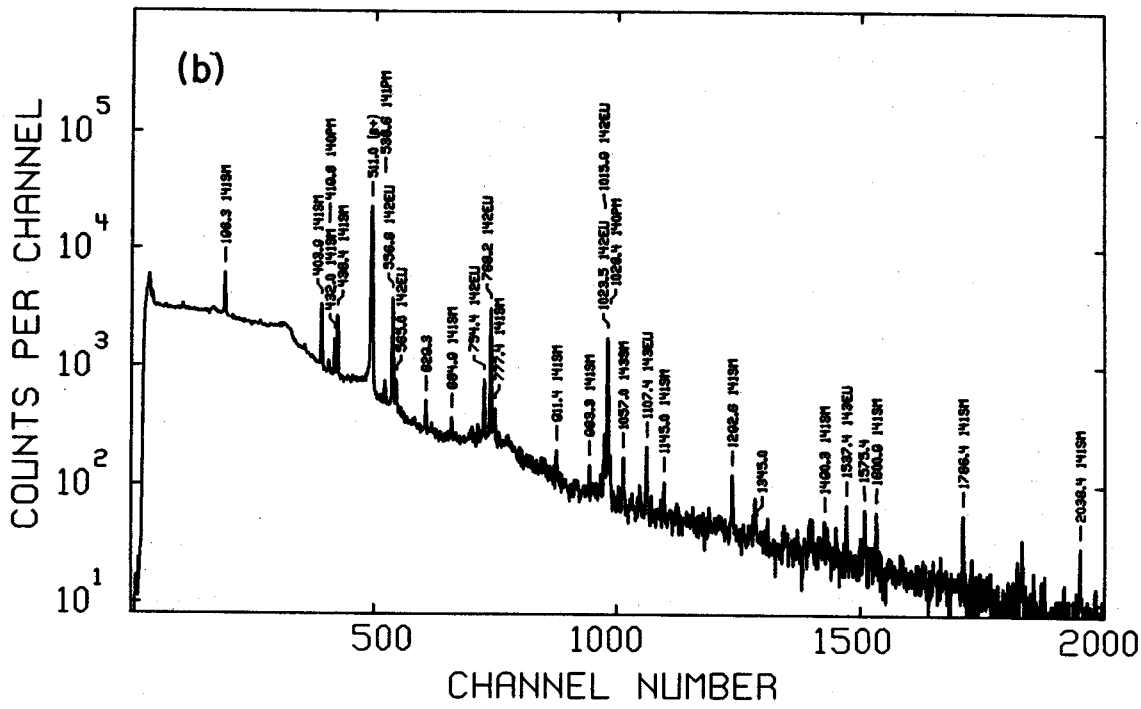
(b)
COUNTS PER CHANNEL
10^5
10^4
10^3
10^2
10^1
500
1000
1500
2000
CHANNEL NUMBER

^{142}Nd(p,p')

Duane Larson, S.M. Austin, and B.H. Wildenthal

As part of our study of inelastic proton scattering on the N=82 isotones, we have studied the ^{142}Nd(p,p') reaction at a proton energy of 30 MeV. The targets were fabricated by vacuum evaporation of isotopically enriched (97.5%) Nd_2O_3 onto a 20 μg/cm^2 carbon foil. Target thickness was estimated to be approximately 100 μg/cm^2.

Use of the high resolution system developed by Blosser et al.[1] enabled us to obtain an energy resolution of 7-9 keV FWHM for the inelastically scattered peaks.

A spectrum taken at 40° in the lab is shown in Fig. 1, along with the excitation energies of the labeled peaks. The calibration energies were taken from Raman et al.[2] and are noted in Table 1.

From systematics in the N=82 nuclei, the 3^- collective state is expected to be the strongest state in the (p,p') spectra, and this should correspond to the state we observe at 2084 keV in ^{142}Nd. Table 1 shows a comparison of the states we observe with the previously known states in ^{142}Nd. These results are preliminary, as the emulsions exposed at other angles are still in the process of being scanned.

TABLE I

Energies of States in ^{142}Nd

E_x (present)	E_x (Raman et al.)	J^π (previous)
0.000	0.000	0^+
1.576	1.576	2^+
2.084	2.084	(3^-)
2.101	2.101	(4^+)
2.210	2.209	(6^+)
	2.217	0^+
2.384	2.385	$(1,2)^+$
2.438		
2.582	2.583	$(1,2)^+$
2.738		
2.847	2.846	(2^+)
2.937	... *	
2.977		
3.081	3.080	
3.244		
3.319		
3.366		
3.414		
3.578		
3.708		
3.782		
3.833		
3.976		
4.007		
4.034		

*Many levels observed above this excitation.

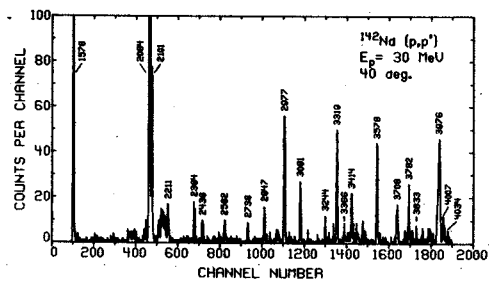

Fig. 1 Spectrum of (p,p') on ^{142}Nd.

References

1. H.G. Blosser et al., Nucl. Instr. and Methods 91, 61(1971).

2. S. Raman, et al., submitted to Nucl. Phys., 1972.

The β^+/ε Decay of ^{143}Sm*

R.B. Firestone, Wm.C. McHarris, and W.H. Kelly

The decay of ^{143}Sm has been studied most thoroughly by Frenne and Heyde, et al.[1,2] They produced ^{143}Sm by the (α,n) reaction on natural Sm_2O_3 (3.09% ^{144}Sm). A decay scheme was presented along with several log(ft) values.

The study of ^{143}Sm decay is of considerable interest in the light of previous work[3,4] on the neighboring odd-Z, N=81 isotones, ^{141}Nd and ^{145}Gd. All three isotones have $11/2^-$ metastable states at 720-756 keV with 60- to 85-sec half-lives. The ^{143}Sm and ^{145}Gd metastable states were found to have small β-branches in their decays.[5,6]

Of further interest are the $7/2^+$ first excited states in the daughters of all three isobars. These appear to be the $1g_{7/2}$ quasiparticle states predicted for N=82 nuclei by Kisslinger and Sorenson.[7] These states occur at 145.4, 271.9, and 329.5 keV in ^{141}Pr, ^{143}Pm, and ^{145}Eu respectively. The log(ft) values given for the decay to the $7/2^+$ states in ^{141}Pr and ^{145}Eu were 8.8 and 7.5. Prior to this study, no value was reported for the log(ft) to the corresponding state in ^{143}Pm, but since the transition to this state is from the $3/2^+$ ground state of ^{143}Sm, the second-forbidden transition might be expected to be in the range $10 \leq \log(ft) \leq 14$. The transition in ^{141}Nd is also second-forbidden, suggesting that the ^{143}Sm decay to the $7/2^+$ state may also show an abnormally low log(ft) value.

In an attempt to measure this log(ft) and to determine more precisely other properties of the decay scheme for ^{143}Sm, the reaction ^{142}Nd(τ,2n)^{143}Sm was first tried. This reaction proved unsatisfactory, as the rather loosely bound α-particles in this region make the (τ,αn) reaction more probable. The problem is compounded by the fact that ^{143}Sm decay goes overwhelmingly to the ground state of ^{143}Pm.

The reaction ^{144}Sm(p,2n)^{143}Eu, in which the 2.6-min ^{143}Eu, quickly decays to its ^{143}Sm daughter, has been used with more success. [The ^{143}Eu decay is discussed in another section.] Singles γ-ray spectra have been taken using a 10.4% Ge(Li) detector with 2.1-keV (FWHM) resolution and a peak-to-Compton ratio of 38:1 at 1332 keV. A series of singles spectra were taken at 9-min intervals to identify transitions corresponding to the 8.8-min ^{143}Sm, and weak transitions were verified through several experiments. A singles spectrum is shown in Fig. 1.

Additional coincidence experiments were performed to determine the ^{143}Sm decay scheme. Coincidences between 10.4% Ge(Li) and 7.0% Ge(Li) detectors were recorded on magnetic tape. Coincidence gates on the 271.9-keV and 458.8-keV transitions are shown in Fig. 2. Direct ground-state transitions were indicated by their absence in coincidence data and their intensity in β-γ coincidence experiments. A decay scheme for ^{143}Sm is given in Fig. 3, based on the above

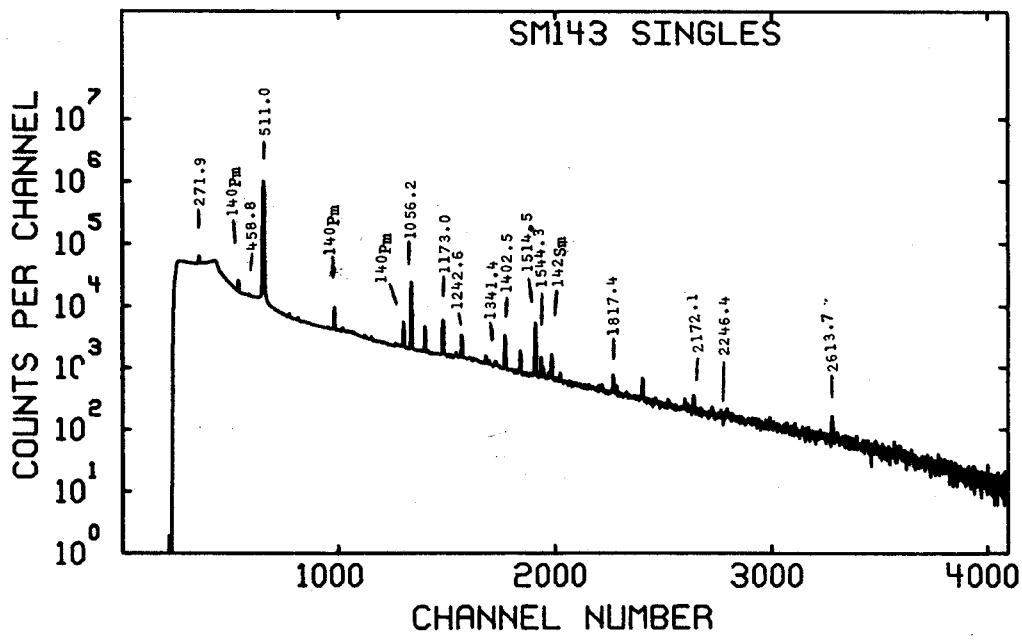

Fig. 1 ^{143}Sm singles spectrum taken with 10.4% Ge(Li) detector.

results and ^{142}Nd(τ,d) reaction studies of Wildenthal et al.[8]

The log(ft) for the second forbidden decay to the 271.9 keV level is seen to be 8.1, much lower than usual, but similar to those for the corresponding decays of ^{145}Gd and ^{141}Nd.

References

1. D. deFrenne, K. Heyde, L. Dorikens-Vanpraet, M. Dorikens, and J. Demuynk, Nucl. Phys. A110, 273(1968).

2. D. deFrenne, E. Jacobs, and J. Demuynk, Z. Phys. 237, 327(1970).

3. D.B. Beery, W.H. Kelly, and Wm.C. McHarris, Phys. Rev. 171, 1283(1968).

4. R.E. Eppley, Wm.C. McHarris, and W.H. Kelly, Phys. Rev. C3, 282(1971).

5. J. Felsteiner and B. Rosner, Phys. Letters 31B, 12(1972).

6. R.E. Eppley, Wm.C. McHarris, and W.H. Kelly, Phys. Rev. C2, 1929(1970).

7. K.S. Kisslinger and R.A. Sorenson, Rev. Mod. Phys. 35, 853(1963).

8. B.H. Wildenthal, E. Newman, and R.L. Auble, Phys. Rev. C3, 1199(1971).

* Supported by the USAEC and the NSF.

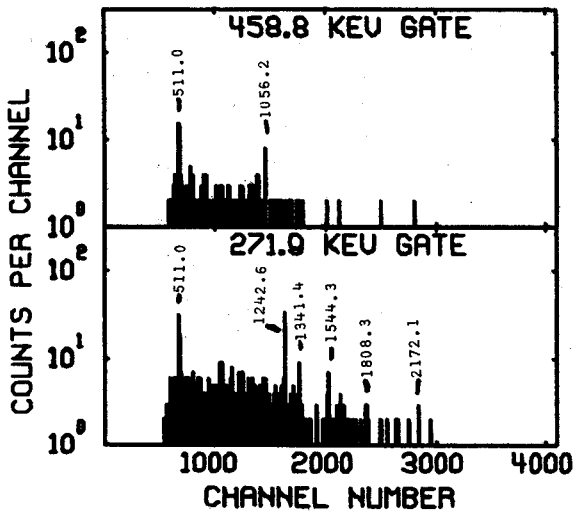

Fig. 2 ^{143}Sm 10.4% Ge(Li)-7.0% Ge(Li) coincidence spectra (2τ=80 nsec).

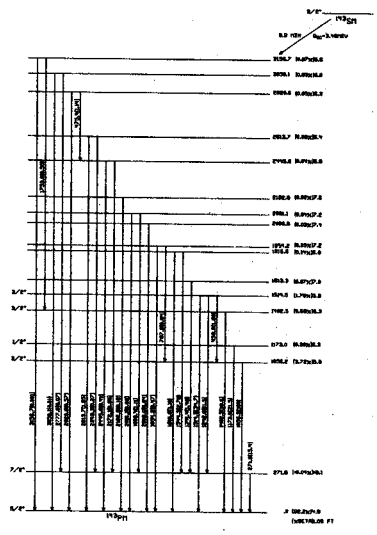

Fig. 3 ^{143}Sm decay scheme. Levels below 2 MeV placed from coincidence data. Spins determined from ^{142}Nd(τ,d) studies.[8]

The β^+/ε Decay of ^{143}Eu*

R.B. Firestone, Wm.C. McHarris, and W.H. Kelly

The decay of ^{143}Eu was first studied by Kotajima and Malan,[1,2] who measured its half-life (2.6 min) and β-endpoint energy (4.0 MeV). No γ-ray decay schemes were reported, presumably because of the weak transitions and the interference of the short lived ^{143}Sm daughter decay. ^{143}Sm decay has been part of a continuing study of N=81 isotones by the Nuclear Spectroscopy Group at Michigan State University, and the ^{143}Eu decay scheme is a welcome by-product of this study.

^{143}Eu was prepared by the reaction ^{144}Sm(p,2n)^{143}Eu on a separated isotope target (95.10% ^{144}Sm), using 28-MeV protons from the Michigan State University Sector-Focussed Cyclotron. As the ^{143}Sm daughter has an 8.8-min half-life, a series of 9-min spectra were taken to so that transitions arising from varying decays could be separated by half-life. Additional singles spectra have been taken to confirm the weaker ^{143}Eu transitions. One such spectrum is shown in Fig. 1. This spectrum was taken with a 10.4% Ge(Li) detector of 2.1 keV (FWHM) resolution at 1332 keV.

In addition to the singles spectra, coincidence information was collected. Figure 2 shows coincidence spectra for gates set on the 107.6-keV and 1106.6-keV γ's. In this experiment coincidences between 10.4% Ge(Li) and 7.0% Ge(Li) detectors within a resolving time of 80 nsec were recorded in pairs on magnetic tape. Direct ground state transitions were determined by their intensities in γ-γ coincidence experiments as well as their failure to appear in coincidence work.

From the ^{144}Sm(p,d)^{143}Sm reaction data of Jolly and Kashy,[3] levels in ^{143}Sm were found at 0.110 MeV ($1/2^+$), 0.76 MeV ($11/2^-$), 1.11 MeV ($5/2^+$), 1.36 MeV ($7/2^+$), 1.53 MeV ($5/2^+$), 1.72 MeV ($5/2^+$), 1.95 MeV ($1/2^+$), 2.06 MeV ($5/2^+$), 2.16 MeV ($7/2^+$), and 2.29 MeV ($7/2^+$).

Combining the above information, a decay scheme for ^{143}Eu has been prepared, and is shown in Fig. 3. Some of the higher lying levels were strongly suggested by the data but are only tentatively placed at this time. Approximately 98% of the observed γ-ray intensity is placed in this level scheme and log(ft) values have been calculated from the measured intensities.

References

1. K. Kotajima, K.W. Brockman, Jr., and G. Wolzak, Nucl. Phys. 65, 109(1965).

2. H.P. Molon, H. Munzel, and G. Pfenning, Radiochem Acte 5, 24(1966).

3. R.K. Jolly and E. Kashy, MSUCL-28, 1970.

* Supported by the USAEC and the NSF.

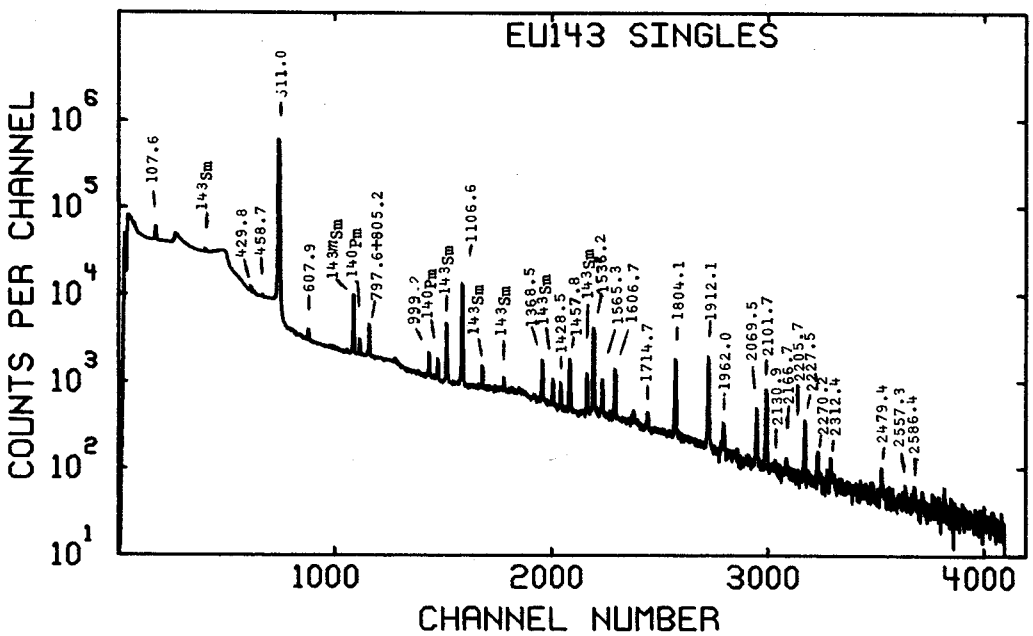

Fig. 1 ^{143}Eu singles taken with a 10.4% Ge(Li) detector.

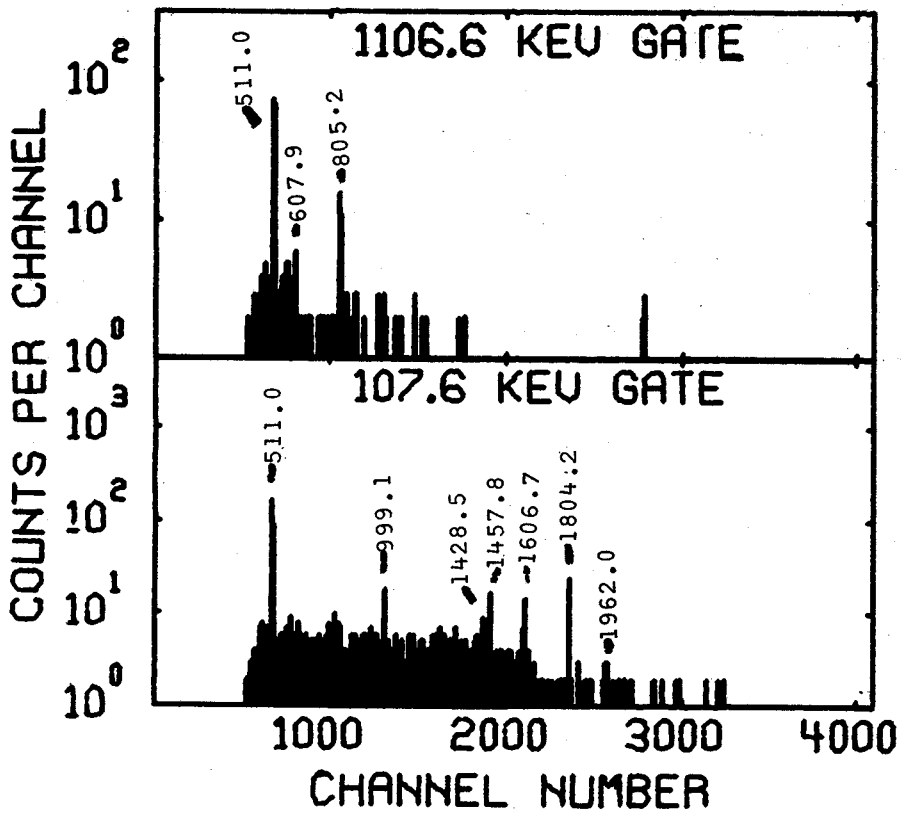

Fig. 2 ^{143}Eu 10.4% Ge(Li)=7.0% Ge(Li) coincidence spectra (2τ-80 nsec).

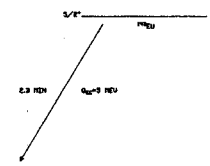

Fig. 3 ^{143}Eu decay scheme. Levels below 2 MeV placed from coincidence data. Spins determinded from ^{144}Sm(p,d) studies.[3]

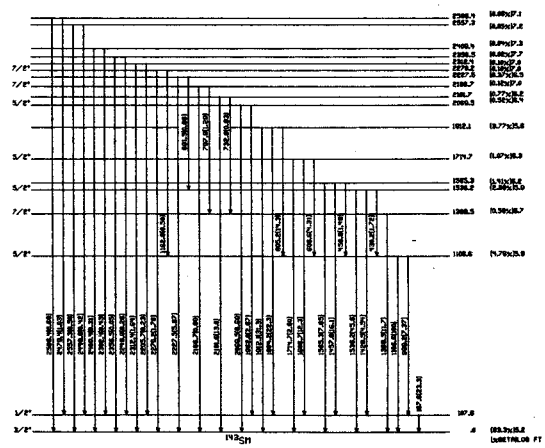

Anomolous ε/β^+ Decay Branching Ratios

R.B. Firestone and Wm.C. McHarris

The β decay of proton-rich nuclei can involve two competing processes, electron capture and positron decay, if sufficient decay energy (W_o=1022 keV) is available. These processes may be abbreviated as

Electron capture (ε): $p^+ + e^- \rightarrow n + \nu$
Positron decay (β^+): $p^+ \rightarrow n + e^+ + \nu$

where the protons and neutrons are assumed to be bound particles.

Theoretical predictions of these ε/β^+ branching ratios have been made,[1-2] and several experimental verifications of these predictions have been shown.[3-10] Nevertheless, such measurements have been difficult, and a few[7-8] have indicated significant disagreement with theory. Inherent to the theoretical predictions lies the assumption of the vector-axial vector form of the beta-interaction. This, in turn, forms the basis of the two-component neutrino theory. Thus, it is clear that measurements of ε/β^+ branching ratios are important to an understanding of the beta-decay process.

Such measurements have been done at the Michigan State University Cyclotron Laboratory using a highly accurate method. Nuclei near the N=81 closed shell were chosen such that several beta decays to various excited daughter states could be studied simultaneously. β-γ coincidence measurements were done to yield relative β^+ feedings to daughter states, and these values were normalized to a "good" transition to determine ε/β^+ branching ratios. Theoretically it should not be significant which transition was chosen, but here a "good" transition was taken as a fast transition in which good statistics were obtainable. Instead of measuring the positrons directly, sufficient absorber material was placed around the radioactive material to annihilate all of the positrons, and the annihilation quanta $\gamma^{\pm}$ were measured in an 8x8-in. NaI split annulus. Coincidence between 511-keV γ's in each half of the annulus was considered a positron event, and a third γ-ray coincidence in a large Ge(Li) detector (10.4% relative to 3x3-in NaI) labeled the daughter state coincident to the positron. A resolving time for all three events of 2τ=50 nsec. and the use of only direct ground state γ-ray transitions to identify the daughter state made the results quite unambiguous, and the chance rate was virtually negligible. A spectrum for ^{145}Gd is shown in Fig. 1. The measurements made so far for ^{145}Gd, ^{143}Eu, and ^{143}Sm decays are given in Table I. Although most of the experimental data fit the predictions quite well, there is considerable deviation in the transitions to the 808.5- and 1041.9-keV levels of ^{145}Eu, the 1173.8-keV level in ^{143}Pm, and the 1566.3-keV level in ^{143}Sm. The last case indicates strong hindrance of the electron capture decay, while it is the positron decay that is hindered for the others.

TABLE I

Comparison of Experimental and Theoretical ε/β^+ Ratios

Decay	Daughter Level	ε/β^+ (Experimental)	ε/β^+ (Theory)	log(ft)
^{145}Gd→^{145}Eu	808.5	>10	0.44	6.9
	953.4	2.2 ±0.7	0.53	8.2
	1041.9	0.94±0.1	0.55	6.5
	1757.8	≡1.2 ±0.1	1.2	5.6
	1880.6	1.4 ±0.1	1.4	5.6
	2494.8	3.7 ±0.4	4.0	6.7
	2642.2	4.9 ±0.5	4.3	6.4
^{143}Sm→^{143}Pm	1056.7	≡6.4 ±0.5	6.4	6.2
	1173.8	30±6.3	7.9	6.6
	1403.9	24±5.2	15.	6.6
	1515.5	34±7	19.	6.0
^{143}Eu→^{143}Sm	1107.4	≡0.73±0.11	0.73	5.4
	1537.1	1.2 ±0.2	1.1	5.5
	1566.3	0.51±0.12	1.3	6.1
	1715.7	3.6 ±3.0	1.5	5.8
	1912.9	1.7 ±0.3	1.8	5.2
	2070.5	1.4 ±0.5	2.5	6.0
	2102.8	3.1 ±1.7	2.6	6.9

It is notable that the deviant transitions involve hindered decays with large log(ft) values. This suggests that allowed beta-decay theory may breakdown for hindered decay. The inhibition of positron decay could be evidence of Fierz interference terms in the beta-decay matrix element or, more precisely, scalar and tensor forces participating in the interaction. If this is indeed the case, an overhauling of beta-decay theory is needed to accommodate these new facts. Additional work is now in progress to measure x-ray—γ-ray coincidences to obtain electron capture feedings directly. Such data will be used to obtain even less ambiguous ε/β^+ ratios.

References

1. A.H. Wapstra, G.J. Nijgh, R. van Lieshout, Nuclear Spectroscopy Tables, North-Holland Publishing Co., Amsterdam (1959).

2. P.F. Zweifel, Phys. Rev. 96, 1572(1954); 107, 329(1957).

3. M.L. Perlman, J.P. Welker, and M. Wolfsburg, Phys. Rev. 110, 381(1958).

4. B.L. Robinson, R.W. Fink, Rev. Mod. Phys. 32, 117(1960).

5. D. Berenyi, Nucl. Phys. 48, 121(1963).

6. E.J. Ronopinski, The Theory of Beta Radioactivity, Oxford University Press, New York (1966).

7. I. Adam, K.S. Toth, and M.F. Roche, Nucl. Phys. A121, 289(1968).

8. R.E. Eppley, Wm.C. McHarris, and W.H. Kelly, Phys. Rev. C3, 282(1971).

9. J.B. Gerhoit, Phys. Rev. 109, 897(1958).

10. R. Sherr and R.H. Miller, Phys. Rev. 93, 1076(1954).

* Supported by the USAEC and the NSF.

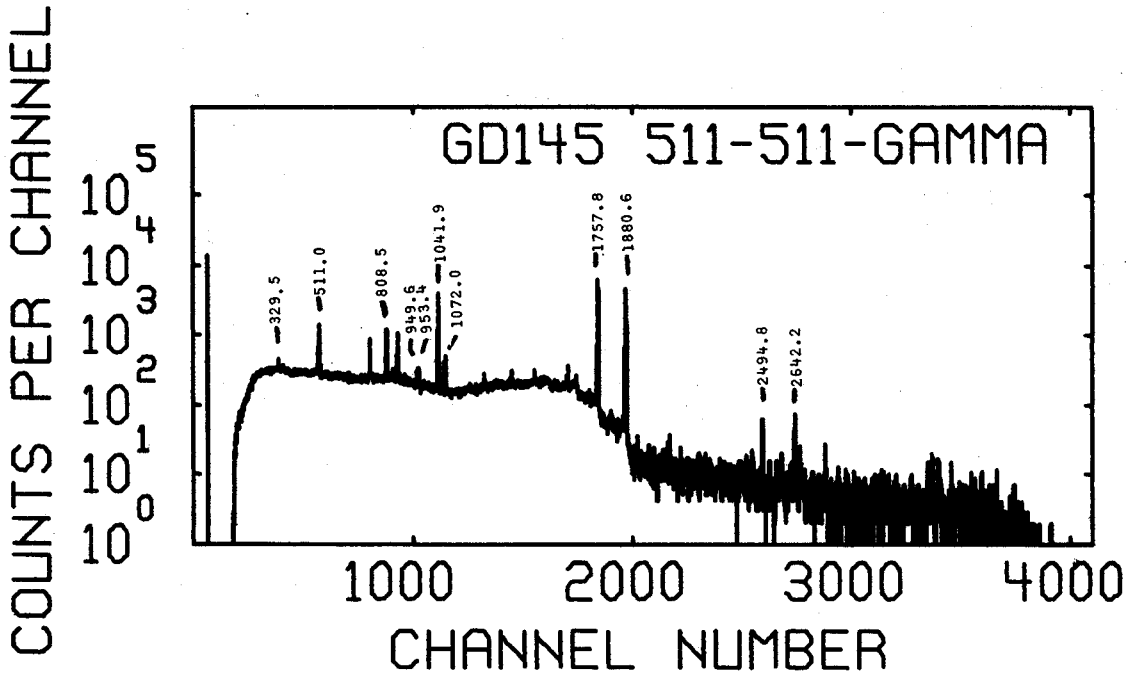

Fig. 1 Pair coincidence spectrum showing β^+ feedings from ^{145g}Gd decay.

The (p,t) Reaction on ^{165}Ho, ^{163}Dy, and ^{161}Dy*

R.W. Goles, R.A. Warner, and Wm.C. McHarris

The (p,t) reaction on ^{165}Ho, ^{163}Dy, and ^{161}Dy has been conducted as part of a continuing investigation of this reaction on rare earth nuclei. Previous work involving the (p,t) reaction on the spherical ^{141}Pr nucleus[1] and the strongly deformed ^{159}Tb nucleus[2] has show this reaction to be a very powerful tool for probing the collective characteristics of these nuclei. In particular, the study of the deformed ^{159}Tb(p,t) reaction[2] revealed large cross sections associated with the population of β- and γ-vibrational and ground state rotational band members.

In the present study ≃300 μg/cm^2 metallic targets of the rare earth elements, of 95% or greater isotopic purity, were bombarded with 30 MeV protons accelerated by the Michigan State University sector focussed cyclotron. The scattered tritons were analyzed with an Enge split-pole magnetic spectrometer and collected on nuclear emulsions. Overall experimental resolution determined in these studies was ≃12 keV.

^{165}Ho Results

The characteristics of the triton spectrum obtained from ^{165}Ho are very much like those exhibited by the previously discussed ^{159}Tb(p,t) spectra[2] and are illustrated in Fig. 1. In this spectrum, one finds a strong population of the $K^\pi=7/2^-[523]$ ground state rotational band with level spacings similar to those occurring in the same band in the ^{165}Ho nucleus.

From Coulomb excitation experiments conducted on ^{165}Ho by Seaman *et al.*,[3] one would expect from systematics to observe the $K^\pi=3/2^-$ and $11/2^-$ γ-vibrational bands at ≃500 keV and ≃700 keV, respectively, and indeed one does observe a set of states originating at 562 keV of excitation which appear to have some intensity interrelationships. Furthermore, the lowest three energy states of this set exhibit spacing which are characteristic of a K=3/2 rotational band if the simple first order rotational energy expression is assumed. If one parameterizes this simple rotational energy expression, one finds convincing evidence for the presence of additional band members up to a spin of 15/2. However, no evidence for the presence of a K=11/2 γ-vibrational band could be found in our spectrum. The results of the ^{165}Ho(p,t) spectrum are summarized in Table 1.

As in the case of ^{159}Tb, the (p,t) reaction on ^{165}Ho is found to strongly populate rotational as well as vibrational states in the residual nucleus. The present study has identified six members of the K=7/2 ground state rotational band and seven members of the K=3/2 γ-vibrational band. Moreover, with the single exception of the 755 keV peak, these states completely exhaust all significant (p,t) reaction strength occurring below the pairing gap.

Experimental angular distributions of the previously discussed states appear in Fig. 2 along with appropriate distorted wave predictions. The finite-range, two-neutron pickup predictions for various ℓ-transfers were calculated using the distorted wave code DWUCK.

As in the two previous (p,t) angular distribution studies involving ^{141}Pr,[1] and ^{159}Tb,[2] the ^{165}Ho(p,t) ground state transition proceeds through a strong dominant ℓ=0 transfer as is evidenced by the very good agreement between the experimental points and theory. The first two excited ground state band members, the $9/2^-$ and $11/2^-$ states, exhibit very similar angular distributions. The position of the relative maxima occurring in these curves are reiniscent of ℓ=2 angular shapes which are referenced with the data for comparison; however, the deep minimum occurring at 30°, along with the unusual strength of the observed diffraction proton makes simple ℓ=2 assignments for these states extremely uncertain. This phenomenon has its analog in the ^{159}Tb(p,t) angular distribution study where a completely similar situation exists for the first two excited member of the ^{157}Tb ground state band. The remaining members of the ^{163}Ho ground state band exhibit angular distributions which cannot be explained in terms of any single dominant angular momentum transfer.

The angular distribution exhibited by the first two members of the γ-vibrational band are very much like those exhibited by the $7/2^-$ and $11/2^-$ members of the ground state rotational band. Again, the positions of the maxima and minima occurring in these curves can be and are compared with ℓ=2 predicted shapes. The remaining states in this band exhibit complex angular shapes which do not appear to have any single dominating angular momentum components.

Angular distributions of five additional states of unknown origin were also determined in this study and appear in Fig. 2 under the heading "Other States". The 755 keV state appearing in this group is a relatively strong state which exhibits no apparent relationship to any other peaks appearing in the ^{165}Ho(p,t) spectra. Its angular distribution is flat and unstructured and is in no way related to any single dominant angular momentum transfer. Being below the pairing gap, this state must certainly be a collective excitation, but of what particular type is not clear from our data alone.

The 1.19 MeV, 1.30 MeV, and 1.45 MeV states exhibit distributions which are similar to each other as well as to all previously discussed states exhibiting some $\ell=2$ characteristics. Again the $\ell=2$ character is suggested solely on the basis of the positions of the relative maxima in these distributions.

The 1.38 MeV state appears to be populated by a pure $\ell=0$ wave; however, the positions of the experimental maxima and minima appear to be systematically shifted form values they assumed in the experimental ground state distribution—an effect that has been previously observed and discussed in Ref. 2. Nevertheless, the overall shape and underlying strength of this experimental curve undoubtedly expresses its dominant $\ell=0$ character and further suggests a β or pairing vibrational origin for this state.

The remaining states in this category exhibit complex angular shapes which at present cannot be understood.

^{161}Dy and ^{163}Dy Results

Unlike all previous odd-mass, rare earth isotopes studied in this program, these isotopes are odd neutron nuclei. Thus one would expect to observe a very high density of low energy states in the (p,t) spectra of these nuclei. This expectation was born out as is illustrated in Figs. 3 and 4 which contain (p,t) spectra of ^{161}Dy and ^{163}Dy, respectively. As one can see from these figures, most triton peaks have a multiple composite nature making interpretation of these spectra extremely difficult.

Compounding this problem is the fact that one would not expect a strong population of the ground state in either (dysprosium) isotope. And, indeed, one is hard pressed to find a consistent set of states which would establish a position for the ground state or would otherwise tie down the relative energy peak of either spectra. Only in the ^{161}Dy(p,t) results does one find those states which are sufficiently resolved from their surroundings to suggest a common origin. Located at the low excitation end of the ^{161}Dy(p,t) spectra, the three prominent peaks exhibit a spacing similar to the first three members of the previously determined[4] $K^{\pi}=5/2^{+}[642]$ rotational band. The presence of additional members of this proposed band cannot be determined because of the composite nature of most of the higher lying peaks. Furthermore, a ground state cannot be found whose position is consistent with the known excitation energy of the band. This by no means eliminates the possibility of the suggested band origin of these states but adds no credit to it. On the other hand, one would expect a strong population of this band to occur since it can be populated directly by a one step pickup of a pair of coupled neutrons from the highest filled orbital below the $K^{\pi}=5/2^{+}[642]$ orbit which characterizes the ground state of ^{161}Dy and contains the lone "optical" neutron in this nucleus. However in order to make a conclusive statement as to the nature of these and other states occurring in the ^{161}Dy and ^{163}Dy(p,t) spectra much higher resolution experiments (FWHM <5 keV) must be conducted.

References

1. R.W. Goles, R.A. Warner, Wm.C. McHarris, and W.H. Kelly, Phys. Rev. C6, 587(1972).
2. R.W. Goles, R.A. Warner, Wm.C. McHarris, and W.H. Kelly, Phys. Rev. Letters 24, 802(1972).
3. G.G. Seaman, E.M. Bernstein, and J.M. Palms, Phys. Rev. 161, 1223(1967).
4. K.G. Rensflet, S.A. Hjorth, and W. Klemra, Stockholm Annual Report (1971).

* Supported by the USAEC and the NSF.

TABLE 1

States Populated Through the ^{165}Ho(p,t)^{163}Ho Reaction

Energy[a] (keV)	Theory (keV)	Assignment[b] J^{π}
0	---	$7/2^{-}$
100	---	$9/2^{-}$
224	222	$11/2^{-}$
369	367	$13/2^{-}$
533	533	$15/2^{-}$
560	---	$3/2^{-'}$
618	---	$5/2^{-'}$
695	699	$7/2^{-'}$
720	722	$17/2^{-}$
755	---	---
791	---	---
807	804	$9/2^{-'}$
826	---	---
898	---	---
912	---	---
926	931	$11/2^{-'}$
1060	---	---
1075	1082	$13/2^{-'}$
1117	---	---
1156	---	---
1175	---	---
1194	---	---
1232±5	---	---
1245±5	---	---
1259±5	1256	$15/2^{-'}$
1286±5	---	---
1308±5	---	---
1345±5	---	---
1373±5	---	---
1419±5	---	---
1441±5	---	---
1457±5	---	---
1513±5	---	---

[a] All energy uncertainties are ±3 keV unless otherwise specified.

[b] I = member of ground state rotational band; I' = member of $K=K_{o}-2$ γ-vibrational band.

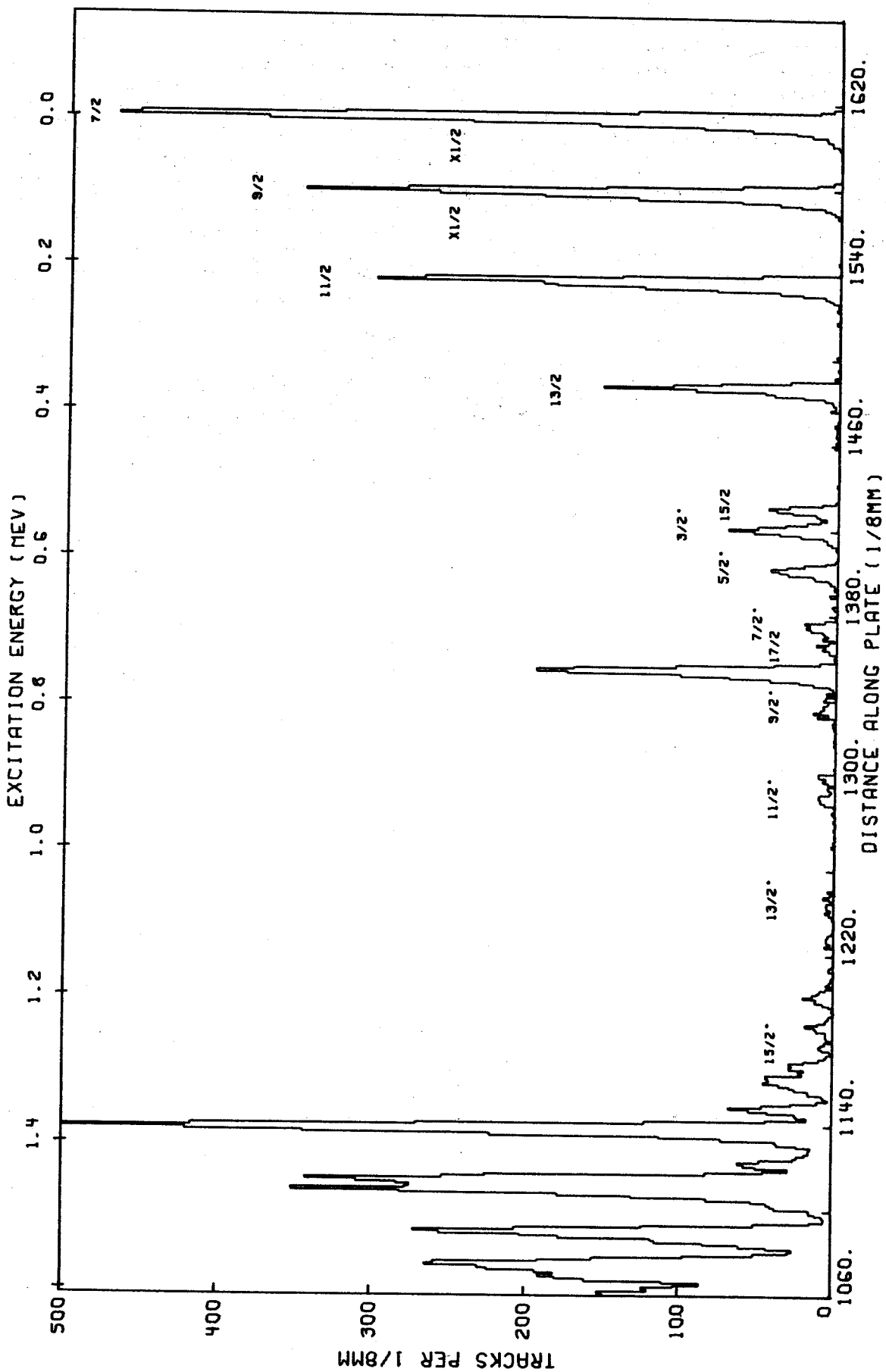

Fig. 1 ^{165}Ho(p,t) spectrum taken at the laboratory angle of 20°.

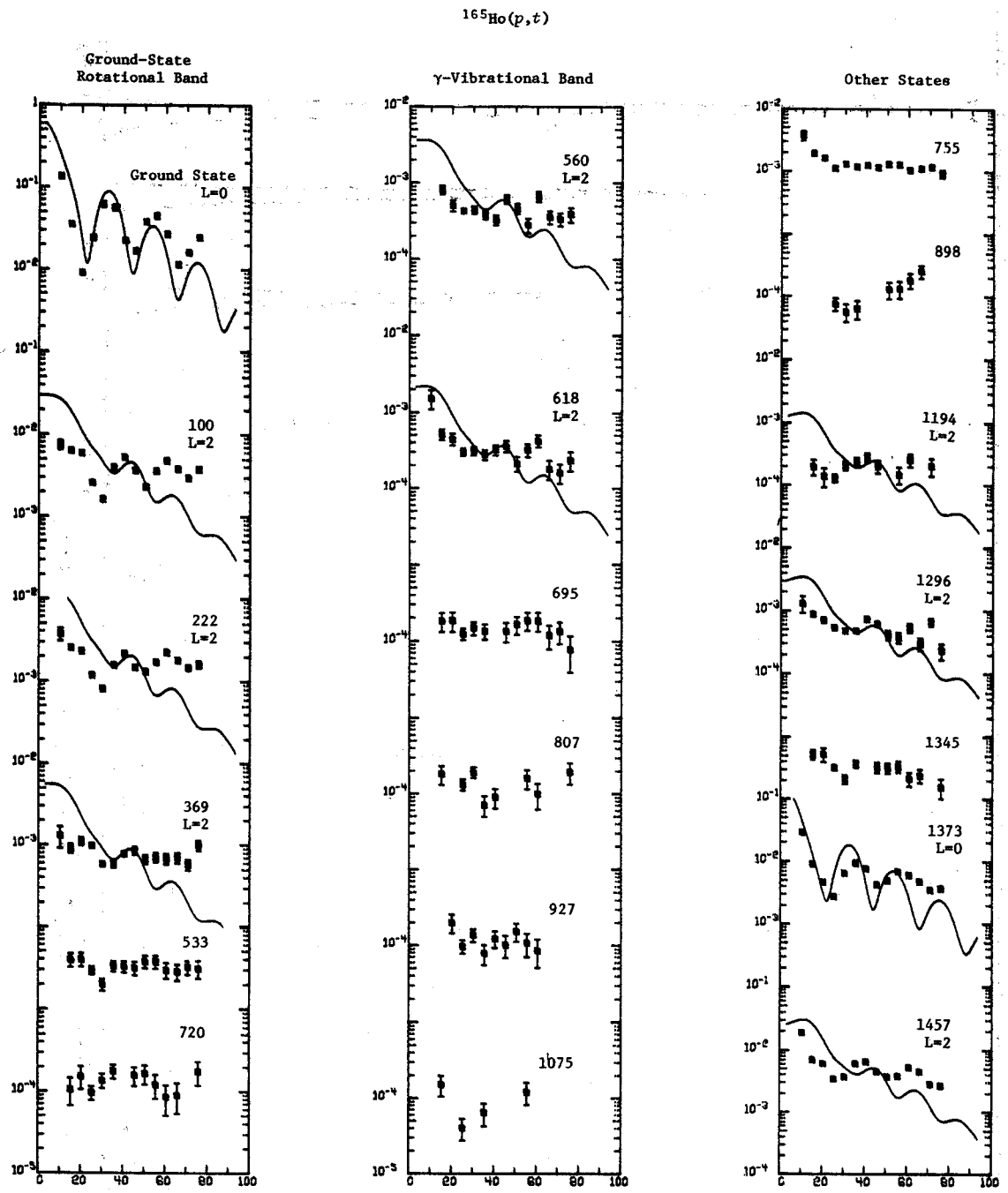

Fig. 2 Relative angular distributions of states populated through the ^{165}Ho(p,t) reaction. Relative cross sections have been normalized to reflect measured absolute values.

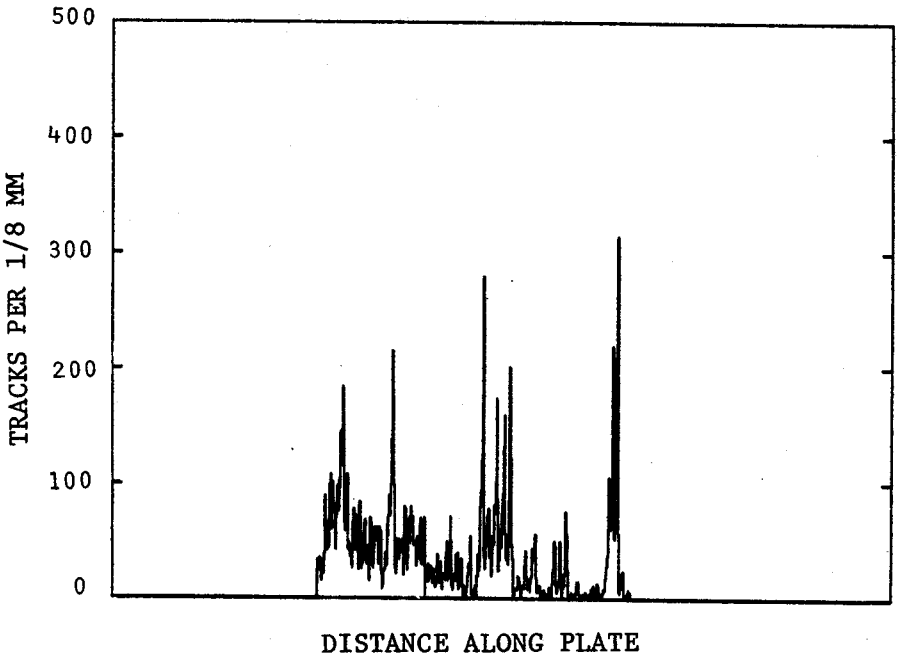

Fig. 3 ^{161}Dy(p,t) spectrum taken at the laboratory angle of 20°.

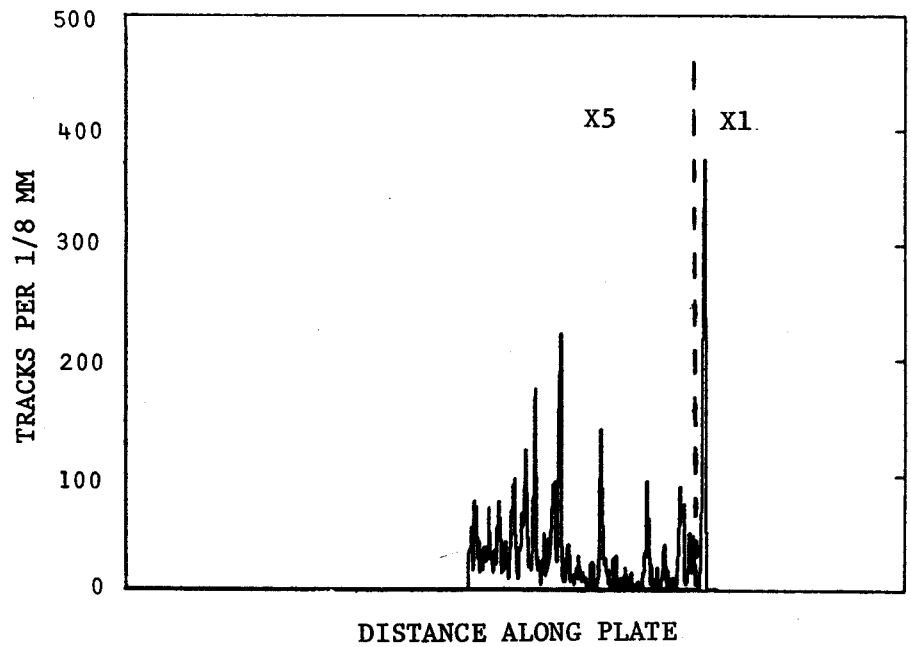

Fig. 4 ^{163}Dy(p,t) spectrum taken at the laboratory angle of 30°.

Study of ^{173}Hf Levels Populated in the Decay of ^{173}Ta*

I. Rezanka,** I.M. Ladenbauer-Bellis,** F.M. Bernthal,
T. Tamura,** and W.B. Jones**

In collaboration with the group at the Yale Heavy Ion Accelerator Laboratory, we have completed a study of the decay of 3.6-hour ^{173}Ta to levels in ^{173}Hf. The low-lying high-spin states in ^{173}Hf were recently studied in the ^{171}Yb(α,2nγ) reaction,[1] and although the perturbed rotational band built on the $7/2^+$[633] Nilsson state was clearly indicated there remained several ambiguities concerning the lowest-lying states and band-head transitions between the several Nilsson states involved. It was therefore appropriate to carry out a detailed study of the ^{173}Ta decay in an effort to resolve those ambiguities.

To produce the ^{173}Ta, the ^{12}C beam from the Yale Heavy Ion Accelerator was used to bombard natural metallic holmium foil rolled to a thickness $\simeq$10 mg/cm^2. Excitation function measurements determined the maximum yield for the desired ^{165}Ho(^{12}C,4n)^{173}Ta reaction to be at 83 MeV. The carrier-free Ta activity was chemically isolated from other elements by the solvent extraction technique described on page 60 of this report.

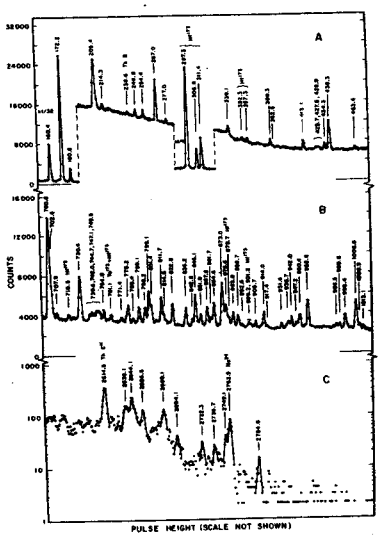

Fig. 1 Selected portions of the γ-ray spectrum from ^{173}Ta decay.

The γ-ray singles spectrum of ^{173}Ta (Fig. 1) was taken in the region 60-4000 keV with a 35 cm^3 coaxial detector (resolution 2.0 keV FWHM at 660 keV). The lower-energy portion of the spectrum was studied with a 3-mm deep Si(Li) detector (resolution 200 eV FWHM at 6 keV). In addition, γ-γ coincidence data have been acquired with a second detector, 15 cm^3 in volume. Three-parameter (E_{γ_1}-E_{γ_2}-t) coincidence events were digitized and recorded serially on magnetic tape for later sorting.

In order to obtain reliable information on the Q-value of ^{173}Ta, a β^+-γ coincidence experiment was performed in which a 3x3" NaI(Tl) crystal served as the γ-ray detector and a 1x1" anthracene crystal was used for registering the positrons. The end-point energy of the positron group coincident with the most prominent group of γ-rays near 170 keV was found to be 2480$\pm$150 keV.

To establish the coincidence relations among the low energy transitions in ^{173}Hf, an e^--γ coincidence experiment has also been carried out with a surface barrier silicon detector (500μ depletion depth, resolution 5 keV FWHM at 624 keV) and the 35 cm^3 Ge(Li) device. As isomeric states were expected for these low-energy transitions, the time spectrum was sorted according to selected e^--γ coincidence gates. The half-lives of the 107.2-keV ($5/2^-$[512]) and 197.5-keV ($7/2^+$[633]) levels were determined to be 182$\pm$20 and 160$\pm$40 ns, respectively. Details of the lower-lying levels in ^{173}Hf are shown in Fig. 2. It will be noted in Fig. 2 that the 197.5-keV level is in fact a closely-spaced doublet, presumably composed of the $7/2^+$[633] bandhead and the $7/2^-$ member of the $5/2^-$[512] rotational band. The lifetime measured for the 90.3-keV transitions from this state would therefore arise from the $7/2^+$[633]$\rightarrow$$5/2^-$[512] E1 component, since the intraband $7/2^-\rightarrow5/2^-$ M1 is not expected to have such a long half-life.

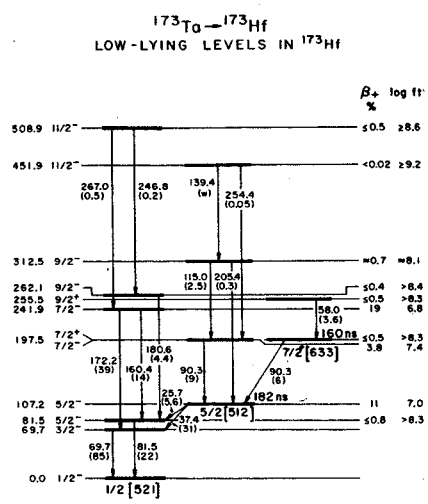

Fig. 2 The level structure of ^{173}Hf below 600 keV as determined from ^{173}Ta decay data.

Multipolarities have been assigned to the more prominent transitions on the basis of the photon intensities measured in this work and the conversion electron intensities of Ref. 2. Rotational states built on the ground $1/2^-$[512]

Nilsson orbital and the $5/2^-[512]$ and $7/2^+[633]$ bands were observed. Spin and parity assignments have been made for several higher-lying levels on the basis of log(ft)'s, γ-ray intensities, and conversion coefficients. The complete decay scheme for ^{173}Ta is shown in Fig. 3.

The lifetime of the $7/2^+[633]$ state in ^{173}Hf provides the second measurement of an absolute E1 transition rate betweeen the $7/2^+[633]$ and $5/2^-[512]$ intrinsic states, ^{173}Yb being the other case for which experimental data are available. Such ΔK=1 E1 transitions are well-known to exhibit unusual branching intensity patterns that result from numerous small components contributing to the total E1 transition amplitude. As a consequence, their Nilsson-model hinderance factors $[F_n=B(E1)_N/B(E1)_{exp}]$ can vary over many orders of magnitude.

It is now commonly recognized that the Coriolis interaction is a principal contributor to such large fluctuations in ΔK=1 E1 strengths between the same intrinsic states. In the case of ^{173}Hf the strongly admixed $5/2^+[642]$ component in the $7/2^+[633]$ band presumably gives rise to a large $5/2^+[642] \rightarrow 5/2^-[512]$ amplitude that adds coherently to the principal $7/2^+[633] \rightarrow 5/2^-[512]$ component. But inclusion of such Coriolis-admixed components in a more detailed Nilsson calculation is still often incapable of explaining observed E1 transition rates in such cases. We have considered the simple first-order correction to the E1 transition moment:

$$B(E1) = \frac{3}{4\pi} e^2_{eff} \left(\frac{\hbar}{m\omega_o}\right) [a_{7/2^+}(\tfrac{7}{2}\,1\,\tfrac{7}{2}\,-1|\tfrac{5}{2}\,\tfrac{5}{2})$$

$$(U_{7/2^+}U_{5/2^-} - V_{7/2^+}V_{5/2^-})G(E1;7/2^+\rightarrow 5/2^-)$$

$$+a_{5/2^+}(\tfrac{7}{2}\,1\,\tfrac{5}{2}\,0|\tfrac{5}{2}\,\tfrac{5}{2})(U_{5/2^+}U_{5/2^-} - V_{5/2^+}V_{5/2^-})$$

$$G(E1;\ 5/2^+\rightarrow 5/2^-)]^2$$

where the even parity subscripts refer to the wave amplitudes for the strongly Coriolis-mixed Ω=5/2 and 7/2 members of the $i_{13/2}$ family of neutron orbitals, the $(U_iU_f - V_iV_f)$ are the usual E1 pairing reduction factors for the orbitals involved, and G(E1) is calculated in the Nilsspn scheme as before.

For estimates of the a_{Ω^+} we refer to the results obtained by Hultberg et al.[1] in their fit for the perturbed energies of the $7/2^+[633]$ rotational band excited in the ^{171}Yb(α,2n)^{173}Hf reaction.

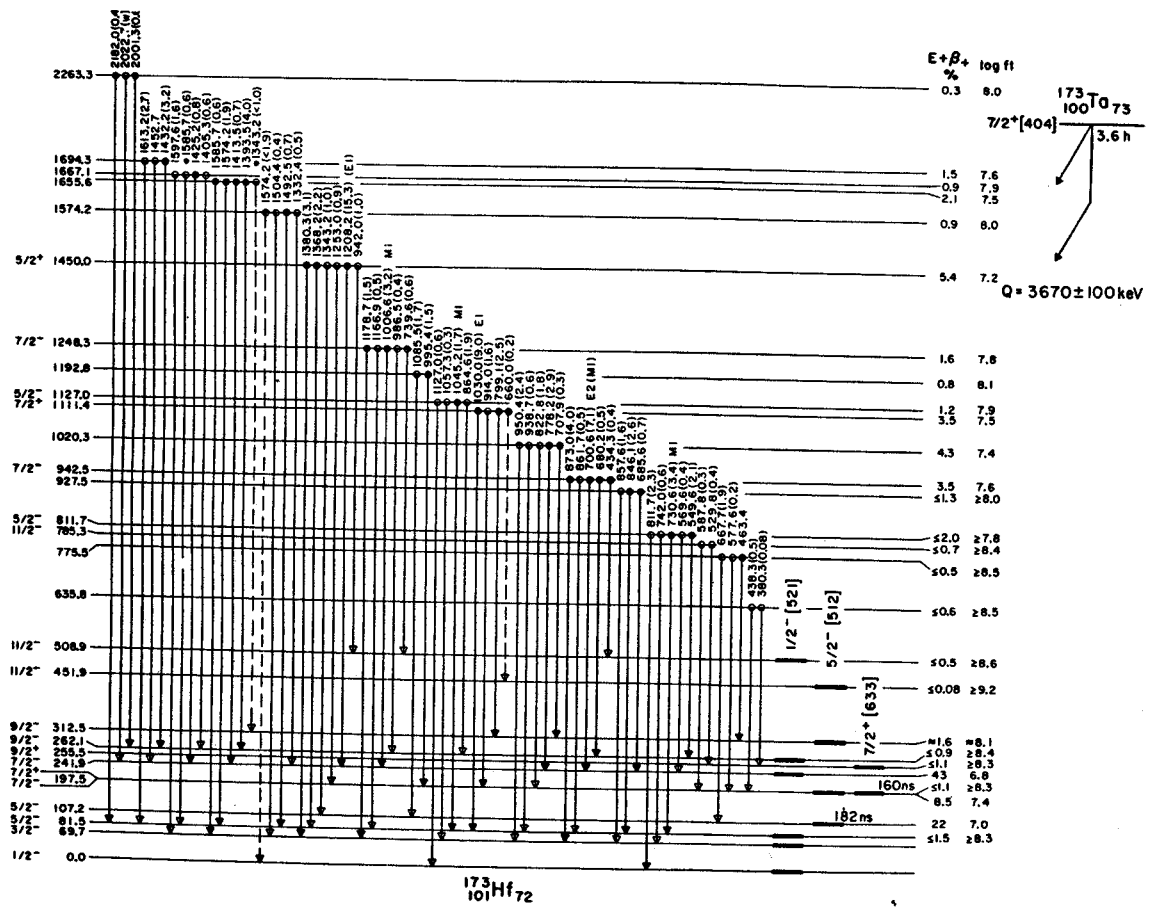

Fig. 3 Decay of ^{173}Ta to levels in ^{173}Hf.

The amplitudes of the $7/2^+[633]$ and $5/2^+[642]$ components contributing to the $7/2^+$ band head are found by these authors to be 0.98 and 0.21, respectively. The results of our calculation are summarized below:

Calculated El Transition Probability for the 90.3-keV $7/2^+[633] \rightarrow 5/2^-[512]$ Transition in ^{173}Hf

Method	$T_{1/2}(El)$ (nsec)	F_N
Nilsson Model*	8.3	24
Nilsson Model with pairing	2300	0.12
Nilsson Model with Coriolis mixing and pairing	410	0.49

*The deformation parameters assumed were $\varepsilon_2=0.26$, $\varepsilon_4=0.02$.

A close examination of the pairing reduction factors in Eq. (1) reveals the extreme sensitivity of the above results to the presumed location of the Fermi surface. Most notably, the factor $(U_{7/2^+}U_{5/2^-}-V_{7/2^+}V_{5/2^-})$ is estimated to be only -0.06. Obviously a small inaccuracy in this quantity could significantly alter our results. The conclusion to be drawn is that we still know relatively little about the many factors which influence $\Delta K=1$ El transitions in such cases.

Further details of the ^{173}Hf levels and transitions may be found in a forthcoming publication.[3]

References

1. S. Hultberg, I. Rezanka, and H. Ryde, to be published.
2. B. Harmatz and T.H. Handly, Nucl. Phys. A121, 481(1968).
3. Submitted to Physical Review C.

* Supported by the USACEC and by the NSF.

** Heavy Ion Accelerator Laboratory, Yale University, New Haven, Conn. 06520

The Decay of ^{177}Ta to Levels in ^{177}Hf*

B.D. Jeltema** and F.M. Bernthal

Recent years have seen intense study of the odd-neutron Hf and W isotopes. Interest in this region has been generated by the presence of low-lying positive parity states associated with the strongly perturbed $i_{13/2}$ family of Nilsson single particle orbitals in these nuclei. Much of the work has employed in-beam γ-ray spectroscopy, primarily using (α,xnγ) reactions on appropriate Yb or Hf targets. For example, work at the MSU Cyclotron Laboratory has detailed the rotational band structure of ^{179}W and ^{181}W,[1] the former of which is an isotone of ^{177}Hf and is characterized by a neutron structure similar to that of ^{177}Hf.

Theoretical analysis of the perturbed rotational-band structure of such nuclei requires as much information as possible about the higher-lying perturbing Nilsson states and their associated rotational bands that mix into the lower-lying bands observed in the (α,xnγ) experiments. This information on higher states can often be obtained from decay scheme studies. Therefore, it was decided to study levels of ^{177}Hf populated in the EC-β^+ decay of ^{177}Ta. The most recent ^{177}Ta decay scheme is that proposed by West, Mann, and Nagle[2] from their work using NaI(Tℓ) scintillation detectors. It seemed reasonable to expect that Ge(Li) detectors might produce significant new data.

The ^{177}Ta sources were prepared by bombarding natural lutetium foil (97.4% ^{175}Lu) with 29 MeV alpha particles produced by the MSU Cyclotron, the predominant reaction being ^{175}Lu(α,2n)^{177}Ta. Typical bombardments were at 1 μa beam current for 15 hours. The source was then allowed to decay for three to four days to allow eight-hour ^{176}Ta to decay from the sample. The tantalum activity was separated from other activities by dissolving the target in 6M HCl, precipitating the lutetium as LuF_3, and then extracting TaF_6^- from the supernate with a small amount of diisopropyl ketone (DIPK). The carrier-free Ta was back-extracted into distilled water to yield a solution which could be evaporated to produce clean "point" sources of high specific activity.

Energies and intensities of γ-rays emitted by the decay of ^{177}Ta were studied using a Ge(Li) detector with a photopeak efficiency of 10.4% at 1333 keV (relative to a 3x3 in NaI(Tℓ) detector). Optimum resolution of this system is 2.1 keV FWHM at the same energy. The ^{177}Ta singles spectra were analyzed using the computer program SAMPO which does a least squares fit of the γ-ray peaks to a Gaussian function with exponential tails. Table I lists the preliminary results of this work.

To determine the cascade relationships of ^{177}Ta decay, γ-γ coincidence experiments have also been performed. Two detectors, each with photopeak efficiencies of approximately 7%, were placed at 180° geometry with the source sandwiched between graded lead absorbers to reduce coincidences due to x-ray and Compton backscatter events. Using the real time computer tasks TOOTSIE and IIEVENT, the addresses of coincidence events were serially recorded on magnetic tape to be recovered later, off-line. In the recovery process, the operator is free to set gates on any part of the spectrum he desires.

Preliminary results of the ^{177}Ta decay experiments are shown in the level scheme (Fig. 1). Previously unknown γ-rays which have been seen in singles and placed in the decay scheme have energies of 494.9, 805.7, and 1002.9 keV. New γ-rays tentatively placed in the decay scheme on the basis of coincidence data include 311.8, 398.3, 257.1, 105.7, 315.7, and 421.1 keV. Transitions of 71.6 and 313.3 keV (seen in singles but not in coincidence) were included in the decay scheme since they are well known from ^{177m}Lu decay.[3] The levels at 1002.9 and 742.0 keV had not been placed before this work. Spin assignments are consistent with those of West *et al.*[2] and with the (d,p)-(d,t) reaction work of Rickey and Sheline.[4]

The proposed level at 741.7 keV is of special interest, since it lies so close to the level at 746.0 keV earlier[2] associated with the $7/2^+[633]$ Nilsson orbital. Our coincidence data clearly show the 420.7- and 424.6-keV transitions to be in coincidence with the 208.3-keV γ-ray, but not with each other. The Ge(Li) singles spectrum of Fig. 2 shows the γ-ray doublet of interest at 421-425 keV. The 420.7-keV transition had early been identified[5] and was tentatively associated with a $3/2^-$ isomer proposed to lie at 420.9 keV.[2] That assignment seems now to have been incorrect, but the apparent large K-conversion coefficient of the 420.7-keV transition is still unexplained. Work on the ^{177}Ta decay is continuing.

References

1. F.M. Bernthal and R.A. Warner, this report p. 65.

2. H.I. West, Jr., L.G. Mann, and R.J. Nagle, Phys. Rev. 124, 527(1961).

3. A.J. Haverfield, F.M. Bernthal, and J.M. Hollander, Nuclear Physics A94, 337(1967).

4. R.A. Rickey, Jr., and R.K. Sheline, Phys. Rev. 170, 1157(1968).

5. B. Harmatz, T.H. Handley, and J.W. Mihelich, Phys. Rev. 119, 1345(1960).

* Supported by the USAEC and the NSF.

** NSF Undergraduate Research Participant, Summer 1972.

TABLE I

Energies and Relative Intensities of γ-rays Seen in ^{177}Ta Decay

Energies (±.2 keV)	Intensity (±10%)
96.7	0.49
113.0	563.
136.7	0.64
177.0	0.19
197.1	0.27
208.3	100.
249.7	3.3
313.3	0.22
321.3	2.3
354.9	0.36
391.6	0.10
420.7	3.8
424.6	12.6
452.9	0.28
491.6	3.5
494.9	0.54
508.0	8.4
526.1	2.0
549.6	0.71
597.8	1.1
604.6	2.6
632.8	3.3
734.4	4.6
736.4	1.8
745.9	25.
805.7	0.27
847.4	2.9
944.5	6.3
1002.9	0.11
1057.7	33.

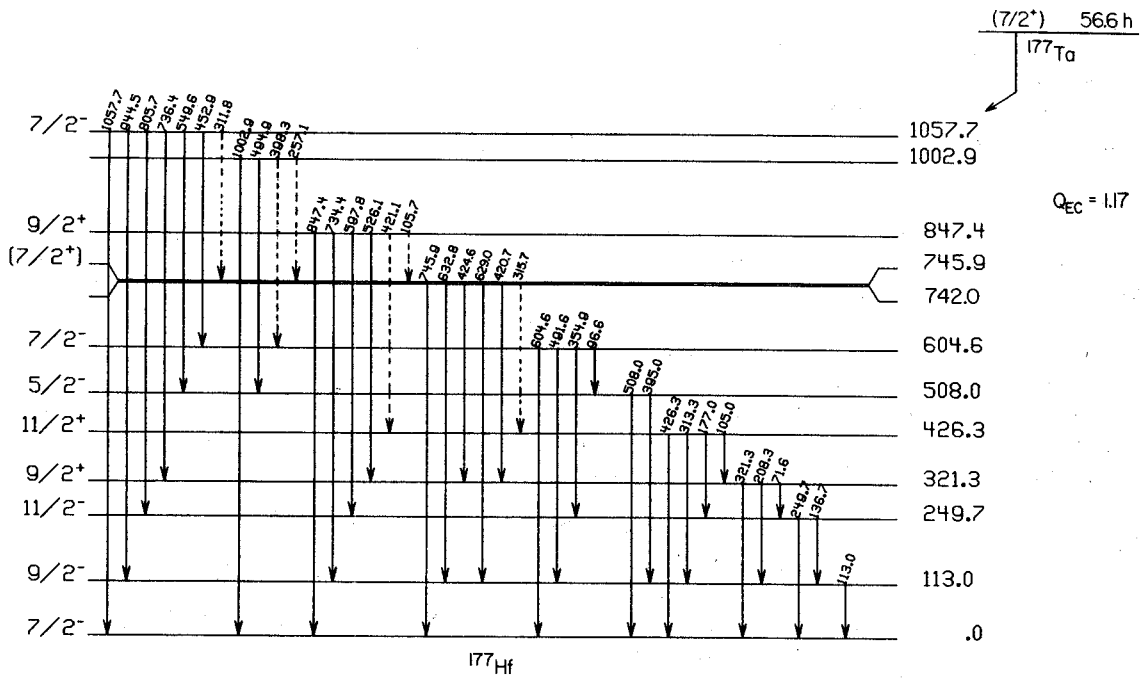

Fig. 1 Decay of ^{177}Ta to levels in ^{177}Hf.

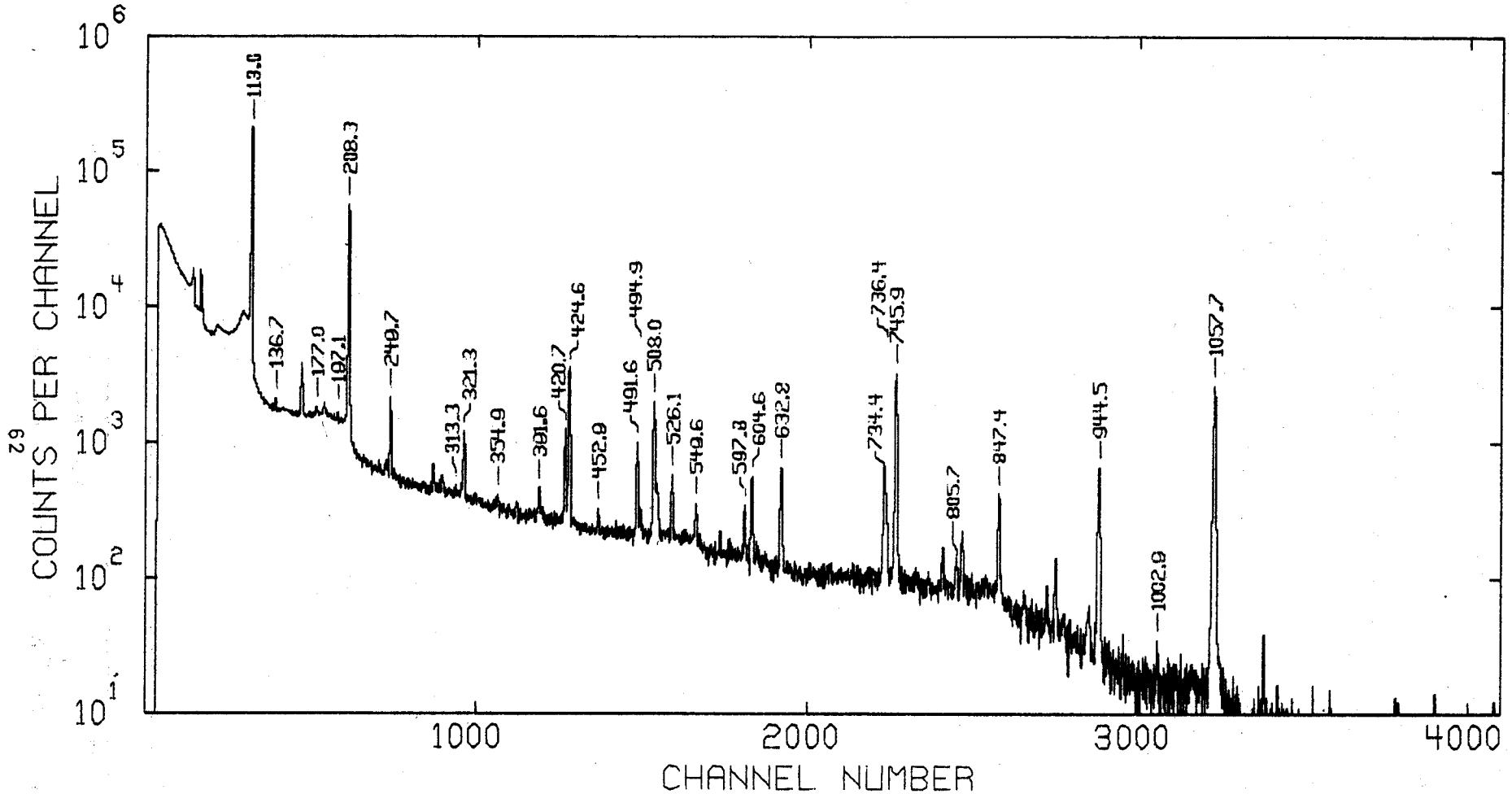

Fig. 2 The γ-ray singles spectrum from decay of ^{177}Ta to ^{177}Hf. Some of the unlabeled peaks also belong to ^{177}Ta decay.

Levels in ^{179}W Populated in the ^{177}Hf(α,2nγ) Reaction*

F.M. Bernthal and R.A. Warner

A study of the rotational band structure of ^{179}W has been completed as the first in the series of (α,xnγ) investigations of the odd-neutron species in the upper reaches of the "rare-earth" region of deformation. The ^{179}W nucleus is particularly interesting because of its apparent similarity to the ^{177}Hf isotone that has been so thoroughly studied as the product of ^{177m}Lu decay. The Coriolis interaction found to exercise so profound an influence on the $i_{13/2}$ family of Nilsson orbitals in other nuclei is no less important in the $9/2^+[624]$ band in ^{179}W. Analysis of the perturbations associated with these orbitals and the effects of those perturbations on the γ-ray decay probabilities, energy-level ordering, and neutron-transfer cross-sections is a principle objective of this program of study.

In the ^{179}W experiments, 26-MeV beams of α-particles from the MSU sector-focused cyclotron were allowed to impinge on a thick, metallic target of ^{177}Hf metal (92% enriched) and the prompt γ-ray spectrum was accumulated in both singles and coincidence modes. Figure 1 shows the prompt singles γ-ray spectrum of ^{179}W obtained with a 43 mm dia. by 26 mm deep Ge(Li) detector with resolution 2.3 keV FWHM and efficiency 6.5% at 1333 keV. Because the target used in this experiment was about 0.5 mm thick, the (α,nγ)^{180}W lines also appear prominently in the spectrum. The problems of γ-ray intensity normalization attendent to such a thick target precluded detailed γ-ray angular distribution measurements, but some useful qualitative data were obtained from complementary ^{181}Ta(p,3nγ) cross-bombardments carried out with thin tantalum targets.

In addition to the γ-ray singles measurements, detailed γ-γ coincidence spectra were obtained with a 2.5% efficient Ge(Li) detector placed at 180° geometry to the 6.5% device already described. Resolving time for the coincidence system was typically ∿20 nsec FWHM, though the cyclotron RF period (∿60 nsec) determines the effective resolving time.

The band structure of ^{179}W deduced from the γ-ray data is shown in Fig. 2. The most notable feature of the level scheme is the large perturbation associated with the $9/2^+[624]$ band.

The structure reported here is in essential agreement with that deduced from independent ^{178}Hf(α,3nγ) and ^{181}Ta(p,3nγ) experiments at Stockholm[1] and Milan.[2] Of special importance to the correct interpretation of the ^{179}W level structure is the placement of the $11/2^+$ level at 372.9 keV. The γ-γ coincidence data clearly indicate the 253-keV transition to be in coincidence with the 120-, 95.9-, and 137.7-keV lines, thus supporting the level sequence shown in Fig. 2 for the low-lying

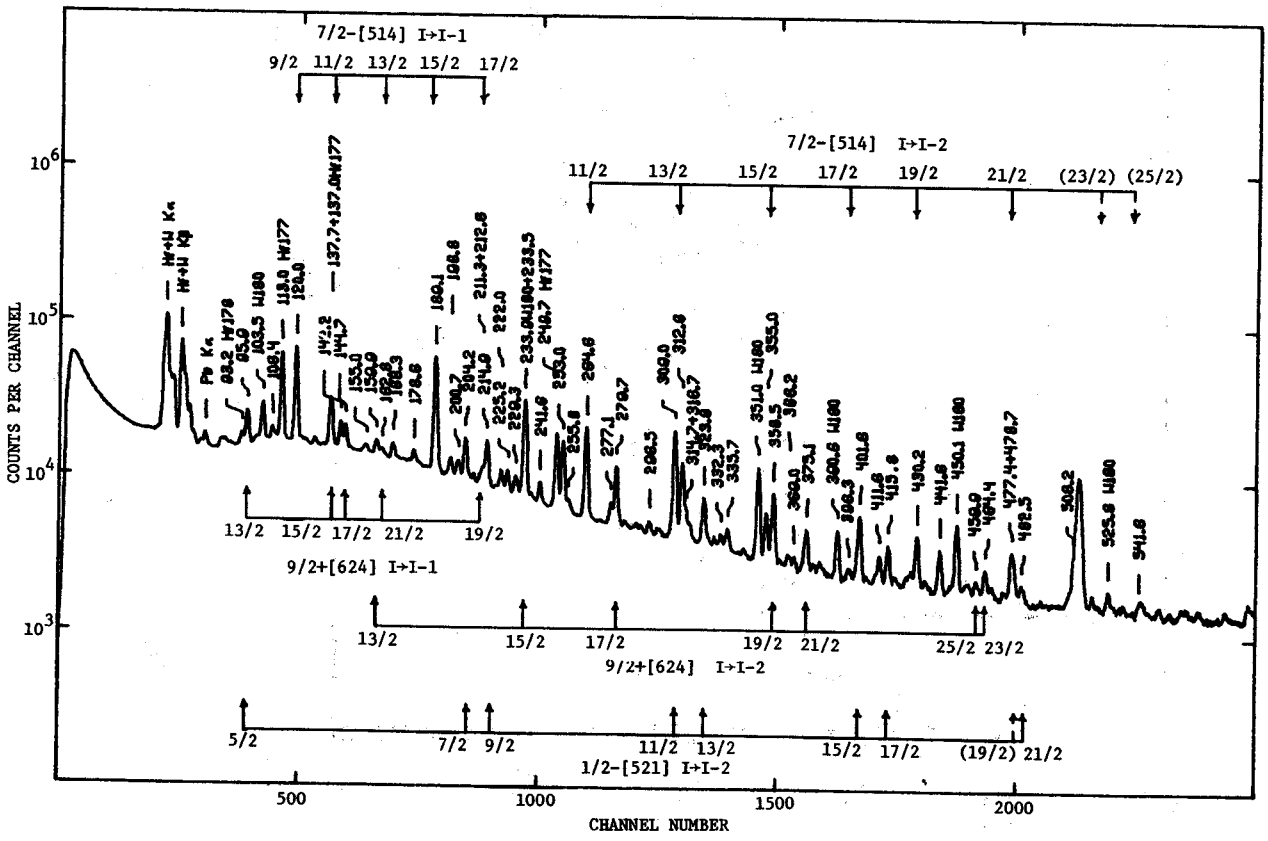

Fig. 1 The ^{177}Hf(α,2nγ)^{179}W in-beam γ-ray singles spectrum.

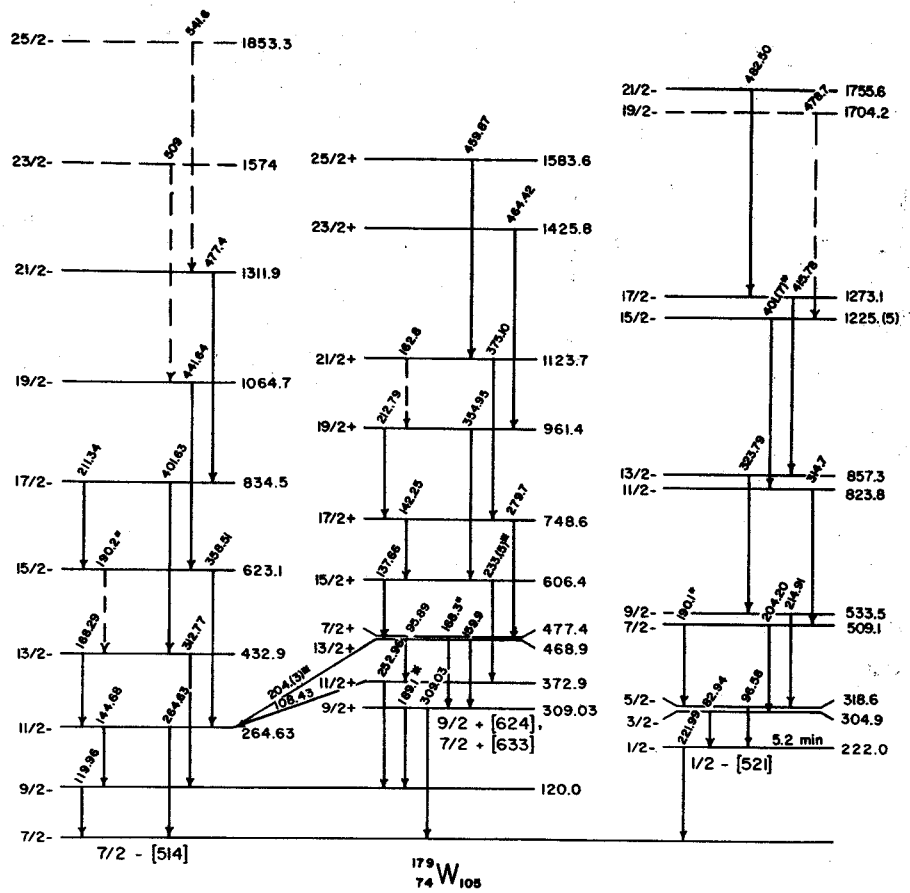

Fig. 2 The level structure of ^{179}W deduced from the $^{177}Hf(\alpha,2n\gamma)$ reaction.

$9/2^+[624]$ band members. In addition, the angular distribution of the 253-keV γ-ray is found in the $^{181}Ta(p,3n\gamma)$ data to be consistent with that expected for a dipole transition.

We also note in Fig. 2 that the even-parity band has substantial $K=7/2^+$ character because of the very close-lying $7/2^+[633]$ state at 477.4 keV. Identification of other members of this $7/2^+$ band would be of considerable importance to the Coriolis band-mixing calculations for ^{179}W. The strong influence of the near-lying $7/2^+[633]$ band on the $9/2^+[624]$ band is seen in Fig. 3 where the magnitude of the perturbations in ^{179}W contrasts sharply with the relatively mild perturbations of the $9/2^+$ band in $^{177,179}Hf$ and ^{181}W.

The perturbed band structure characteristic of this and other Nilsson states emanating from high-j shell-model states can often be described by diagonalizing the complete Coriolis interaction matrix for the rank j+1/2 basis set of Nilsson orbitals. The results of such a calculation should yield eigenvectors that are consistent with those required to explain the neutron-transfer "finger-print" patterns. We have carried out such a calculation for the ^{179}W $9/2^+[624]$ band and are able to reproduce the experimental levels of Fig. 2 to ± 3 keV. provided the Coriolis matrix elements near the Fermi surface are somewhat reduced. Details of the calculation and a comparison of the eigenvectors required to reproduce the observed energy levels with the C_{jl} values implied by the transfer reaction work of Casten et al.[3] will be described in a forthcoming publication.

References

1. Th. Lindblad, private communication (1972).
2. C.B. Birattari, et al., preprint, University of Milan (1972).
3. R. Casten, P. Kleinheinz, P.J. Daly, and B. Elbek, preprint (1971).

* Work supported by the USAEC and NSF.

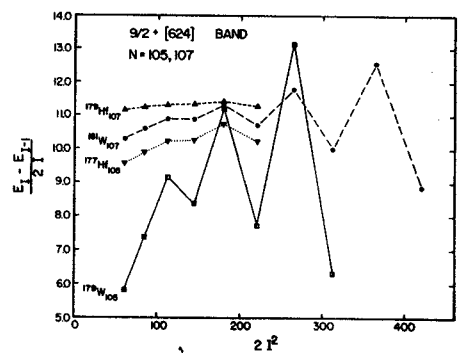

Fig. 3 Plot of $E_I-E_{I-1}/2I$ vs. $2I^2$ for the $9/2^+[624]$ rotational band in N=105 and 107 isotones.

Levels in ^{181}W Populated in the ^{180}Hf(α,3nγ) Reaction *

F.M. Bernthal and R.A. Warner

The in-beam γ-ray spectroscopy work on N=105 ^{179}W has been extended to ^{181}W in order to study further the behavior of the 9/2$^+$[624] band in this and other neutron-deficient nuclei as one moves toward the heavier limits of the "rare-earth" region of deformation. The experimental arrangement for these experiments was quite similar to that already described for the ^{179}W study, except that in this case a ^{180}Hf self-supporting metal foil (~1.3 mg/cm^2) prepared by the argon heavy-ion sputtering technique of Sletten[1] was used as the target material. The thin foil target allowed angular distribution data to be obtained in the ^{181}W experiments to aid in assigning the γ-ray lines to their corresponding bands.

The ^{180}Hf(α,3nγ) reaction was carried out with 35-MeV α-particles from the MSU Cyclotron. A typical singles γ-ray spectrum taken with a 43 mm dia. by 26 mm deep Ge(Li) detector is shown in Fig. 1. Most of the prominent γ-ray transitions have been placed in the ^{181}W level scheme of Fig. 2. Of particular interest is the 92-keV transition which is in coincidence with the γ-ray transitions up to spin 19/2$^+$ in the ground 9/2$^+$[624] band. We therefore have tentatively associated the 92-keV transition with an isomeric state thought to exist at 906 keV. Such a state would presumably be composed of the 9/2$^+$[624] neutron and two of the four proton orbitals 9/2$^-$[514], 1/2$^-$[541], 5/2$^+$[402], and 7/2$^+$[404] known to lie near the Fermi surface in the Z=74 isotopes. If the proposed state is indeed three-particle in character, it should have a relatively long half-life, and experiments to measure the lifetime of the 92-keV line have been undertaken. Preliminary results are consistent with a 906-keV isomer de-exciting to the spin 19/2 member of the 9/2$^+$[624] band. Several other transitions in the ^{181}W spectrum remain unassigned and are presumably associated with the weakly populated 5/2$^-$[512] band or, as some evidence suggests, with a band built on the tentative 906-keV three-particle state.

The assigned locations of the 7/2$^-$[514] and 5/2$^-$[512] band-heads are consistent with the ^{181}Re decay data of Daly *et al.*[2] In Fig. 3 a plot of the 7/2$^-$[514] and 9/2$^+$[624] band energy spacing as a function of I^2 is shown. The perturbation of the 9/2$^+$[624] band is comparable to that seen in ^{177}Hf, but much less than the sharp perturbations characterizing that band in ^{179}W and ^{183}Os (cf. Pg. 63 and Pg. 70 of this report). On the other hand, the normally serene 7/2$^-$[514] band also experiences some minor perturbation near its band-head and at higher spins in ^{181}W. The influence of the very close-lying members of the 5/2$^-$[512] band may be important for the lower-spin perturbations here.

A detailed analysis of the 9/2$^+$[624] band in terms of Coriolis coupling to the other $i_{13/2}$ orbitals is in progress. Our preliminary results reproduce the energies of the 9/2$^+$[624] band members through spin 25/2 to ±1 keV of experiment if one accepts an *ad hoc* attenuation of Coriolis matrix elements near the Fermi surface. Work on the ^{181}W level scheme is continuing.

References

1. G. Sletten and P. Knudson, preprint (1971).

2. P.J. Daly, K. Ahlgren, K.J. Hofstetter, and R. Hochel, Nucl. Phys. A161, 177(1971).

* Work supported by the USAEC and the NSF.

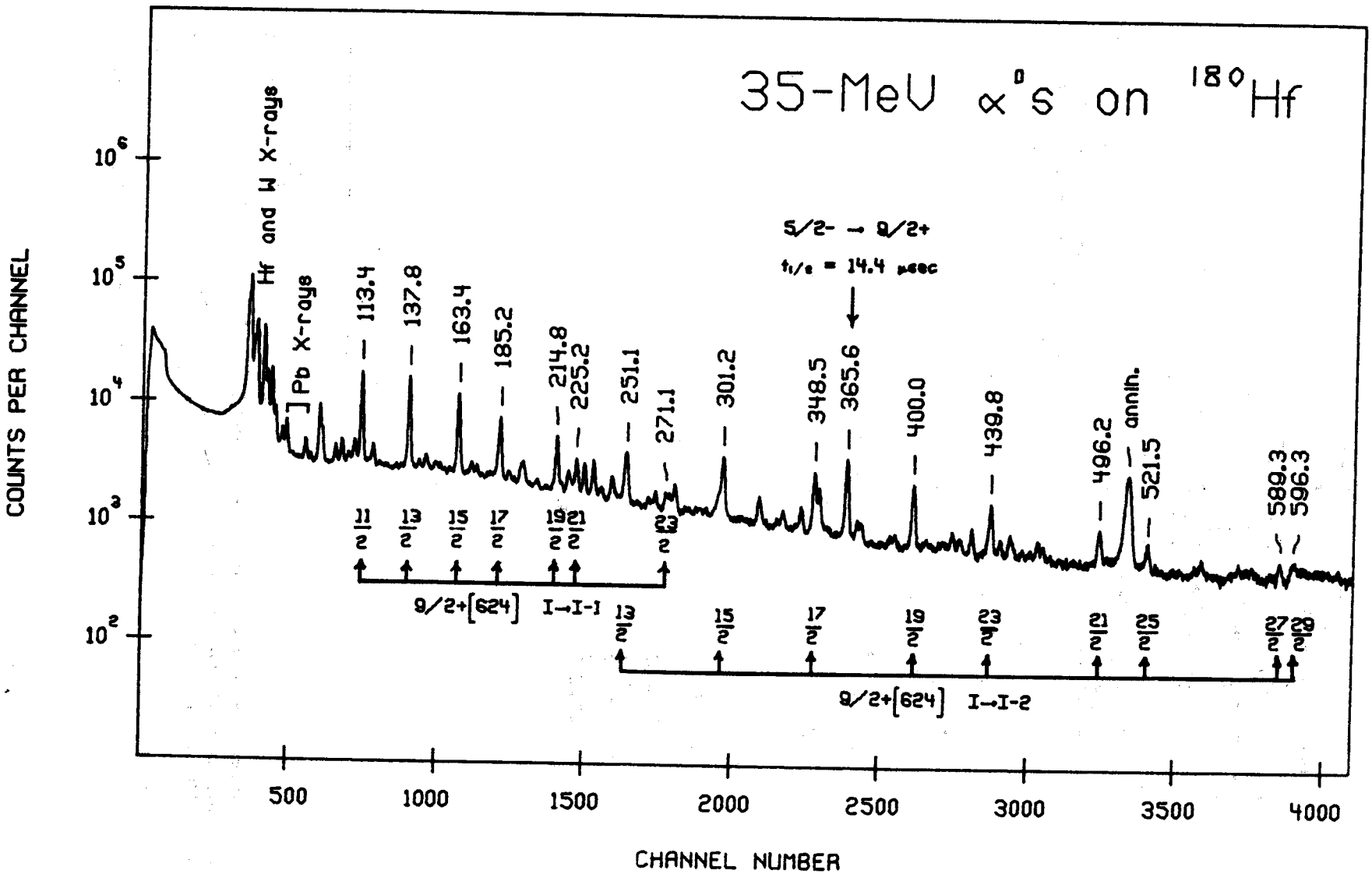

Fig. 1 The prompt singles γ-ray spectrum from the $^{180}Hf(\alpha,3n\gamma)^{181}W$ reaction (35 MeV).

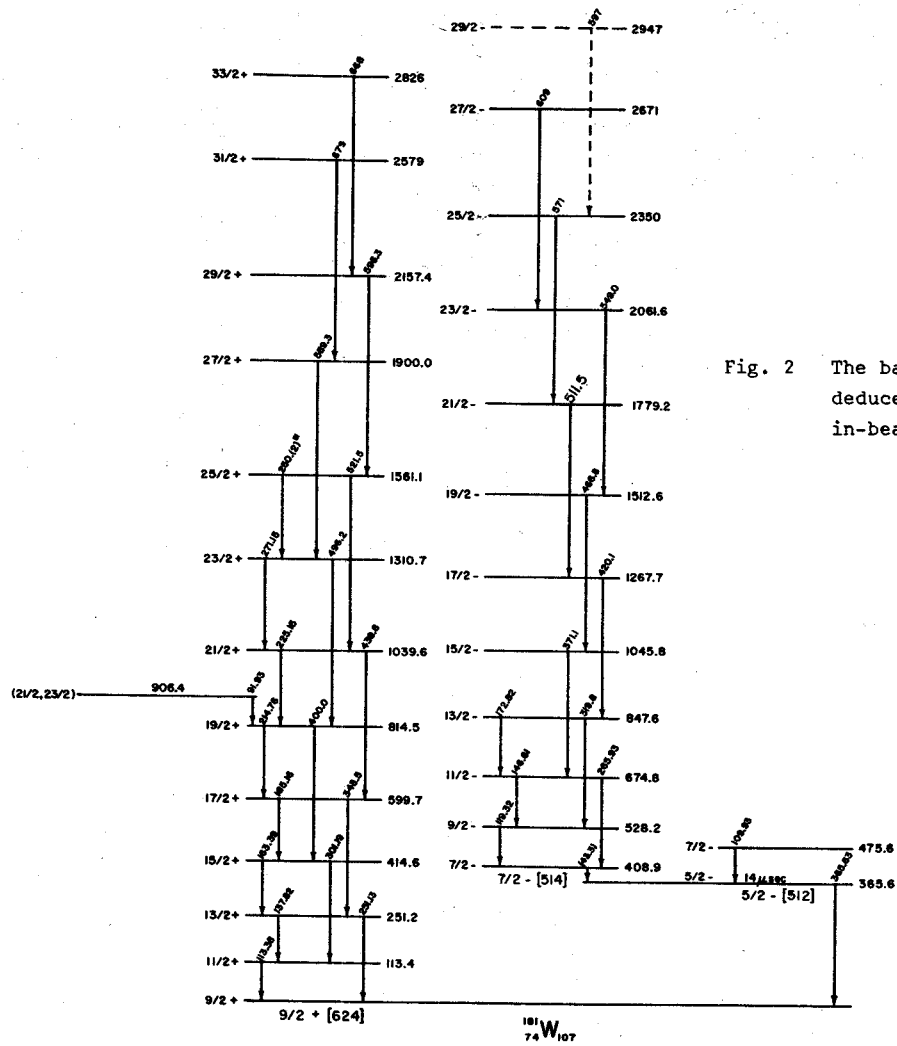

Fig. 2 The band structure of ^{181}W as deduced from the $^{180}Hf(\alpha,3n\gamma)$ in-beam γ-ray spectrum.

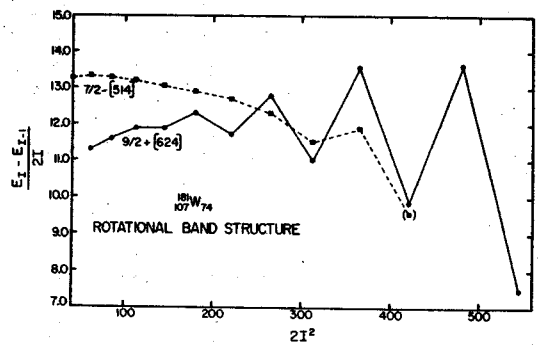

Fig. 3 The rotational energy spacing $E_I-E_{I-1}/2I$ as a function of $2I^2$ for the $7/2^-[514]$ and $9/2^+[624]$ bands in ^{181}W.

Search for the "Phase Transition" Effect at High Spins in Even-Even Nuclei Near the Edge of the Rare-Earth Deformed Region*

R.A. Warner and F.M. Bernthal

Since the early prediction[1] of a phase transition in deformed nuclei and the subsequent discovery[2] of marked increases in nuclear moments of intertia near 14 units of angular moentum for some rare-earth nuclei, there has been considerable speculation regarding the relationship of the prediction to the discovery. A more detailed explanation for the observed phenomenon has recently been offered,[3] and suggests that the behavior seen occurs specfically because of the presence of low-Ω states from the $i_{13/2}$ neutron orbital near the Fermi level in the nuclei studied. Meanwhile more experimental data have become available,[4] demonstrating the effect in a number of nuclei with $88 \leq N \leq 104$.

As it might be argued that all known cases fall within the region allowed by the description of Stephens and Simon,[3] it seemed essential to investgate moments of inertia in which the irregularity would not be predicted (by this model) to occur at such low angular momenta.

The states of interest are produced in (α,xn) reactions on self-supporting metallic foils. Gamma-gamma coincidence data are used to establish the yrast cascades, and γ-ray anisotropies are measured to verify that the transitions observed have angular distributions consistent with the stretched-E2 assignments.

Data have already been obtained on states in ^{180}W and $^{182,184,186,188}Os$. In addition to these nuclei with $N \geq 106$, data have been collected on the N=90 and 92 nuclei $^{154,156}Gd$ in a further attempt to define limits for the region of "backbending" moments of inertia. Some sample coincidence spectra are displayed in Fig. 1, and in Fig. 2 the moments of inertia are plotted versus rotational frequency (according to the convention adopted by Johnson et al.[2]) for those data which have been analyzed.

References

1. B.R. Mottelson and J.G. Valatin, Phys. Rev. Letters 5, 511(1960).
2. A. Johnson, H. Ryde, and J. Sztarkier, Phys. Letters 34B, 605(1971).
3. F.S. Stephens and R.S. Simon, Nucl. Phys. A183, 257(1972).
4. P. Thieberger, A.W. Sunyar, P.C. Rogers, N. Lark, O.C. Kistner, E. der Mateosian, S. Cochavi, and E.H. Auerbach, Phys. Rev. Letters 28, 972(1972). R.M. Lieder, H. Beuscher, W.F. Davidson, P. Jahn, H.-J. Probst, and C. Mayer-Böricke, Phys. Lett. 39B, 196(1972). A. Johnson, H. Ryde and S.A. Hjorth, Nucl. Phys. A179 753(1972). H. Beuscher, W.F. Davidson, R.M. Lieder, and C. Mayer-Böricke, Phys. Lett. 40B, 449(1972).

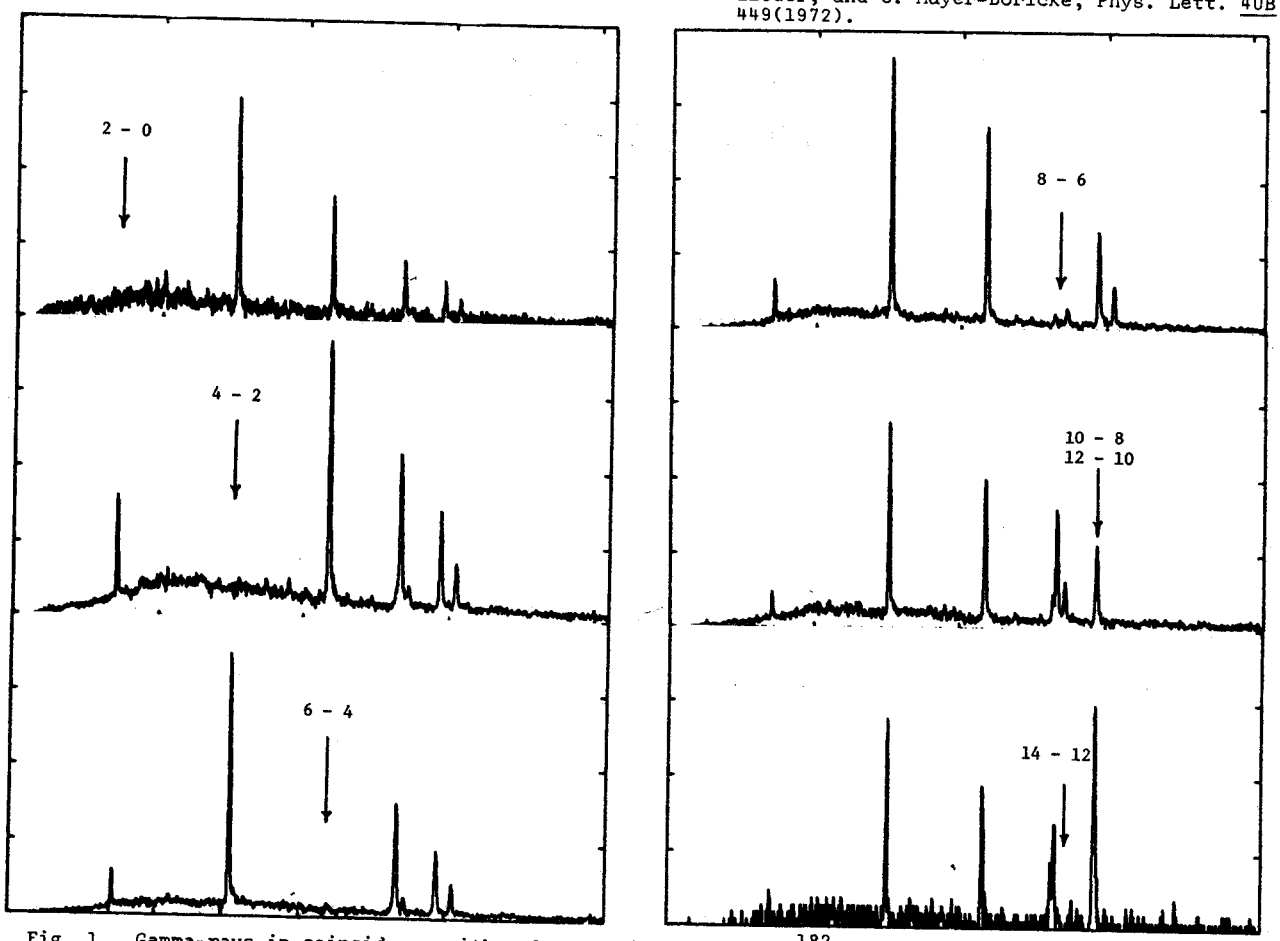

Fig. 1 Gamma-rays in coincidence with selected transitions in ^{182}Os, prepared by the reaction $^{182}W(\alpha,4n)$. The location of the gate for each spectrum is marked. Notice that the 10-to-8-12-to-10 doublet is the only peak appearing in its own gate.

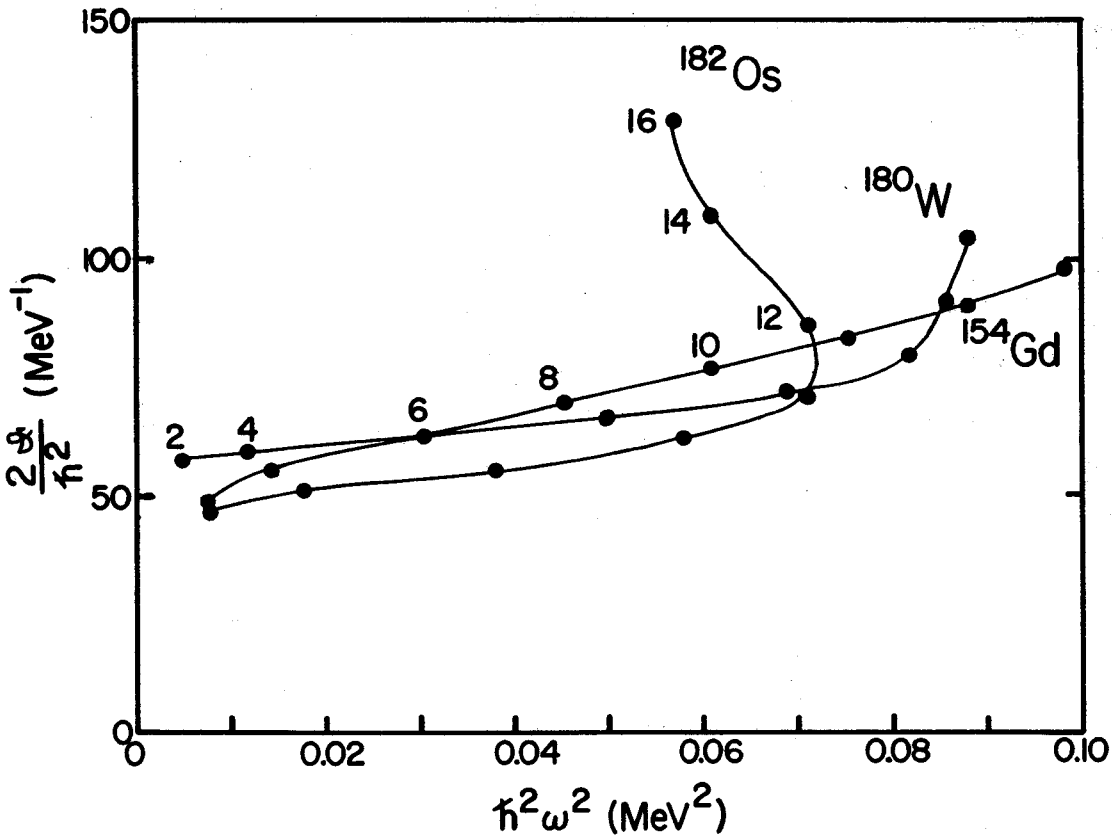

Fig. 2 Moment of inertia plotted against rotational frequency for three of the nuclei being studied.

In-Beam γ-ray Spectroscopy of Odd-A Osmium Isotopes*

F.M. Bernthal, R.A. Warner, C.L. Dors, and G. Sletten**

In-beam (α,xnγ) study of the odd-neutron species in the heavier "rare-earth" deformed region has been extended to the osmium isotopes. The first data obtained have been those for ^{183}Os, produced by the ^{182}W(α,3nγ) reaction (Fig. 1). In this experiment, a self-supporting foil of ^{182}W (94% enriched) prepared at Niels Bohr Institute by the argon-ion sputtering method,[1] was bombarded with 35-MeV α-particles from the MSU Cyclotron. Preliminary analysis of the γ-ray singles and γ-γ coincidence data has identified members of the ground 9/2$^+$[624] rotational band up to spin 29/2 and again we find this band, based on the $i_{13/2}$ family of Nilsson orbitals, to be strongly perturbed—even more strongly than is the corresponding band in ^{179}W. In Fig. 2 we show a plot of the 9/2$^+$[624] band level spacing in ^{183}Os as a function of I^2. Analysis of this highly distorted band structure by the Coriolis matrix diagonalization technique is underway, and data on other low-lying bands in this isotope of Os are being analyzed.

Preliminary data have also been obtained on ^{187}Os from the ^{186}W(α,3nγ) reaction. This isotope should be of particular interest because of the presence at 257 keV of the 11/2$^+$[615] Nilsson orbital. The rotational band associated with this orbital is expected to be strongly populated in the in-beam studies, and should yield valuable further information on the effects of rotation-particle coupling on the band structure associated with the $i_{13/2}$ neutron orbitals in nuclei near the edge of the deformed region. It is worth noting that the increasing complexity and difficulty in interpreting the level structure of nuclei in this and similar regions often requires that decay data be used to supplement the in-beam data. In those cases where the decays of iridium isotopes to the odd-A osmium isotopes are not well understood, we have undertaken complimentary decay-scheme experiments.

References

1. G. Sletten and P. Knudson, preprint (1971).

* Work supported by the USAEC and the NSF.

** The Niels Bohr Institute, University of Copenhagen, Denmark.

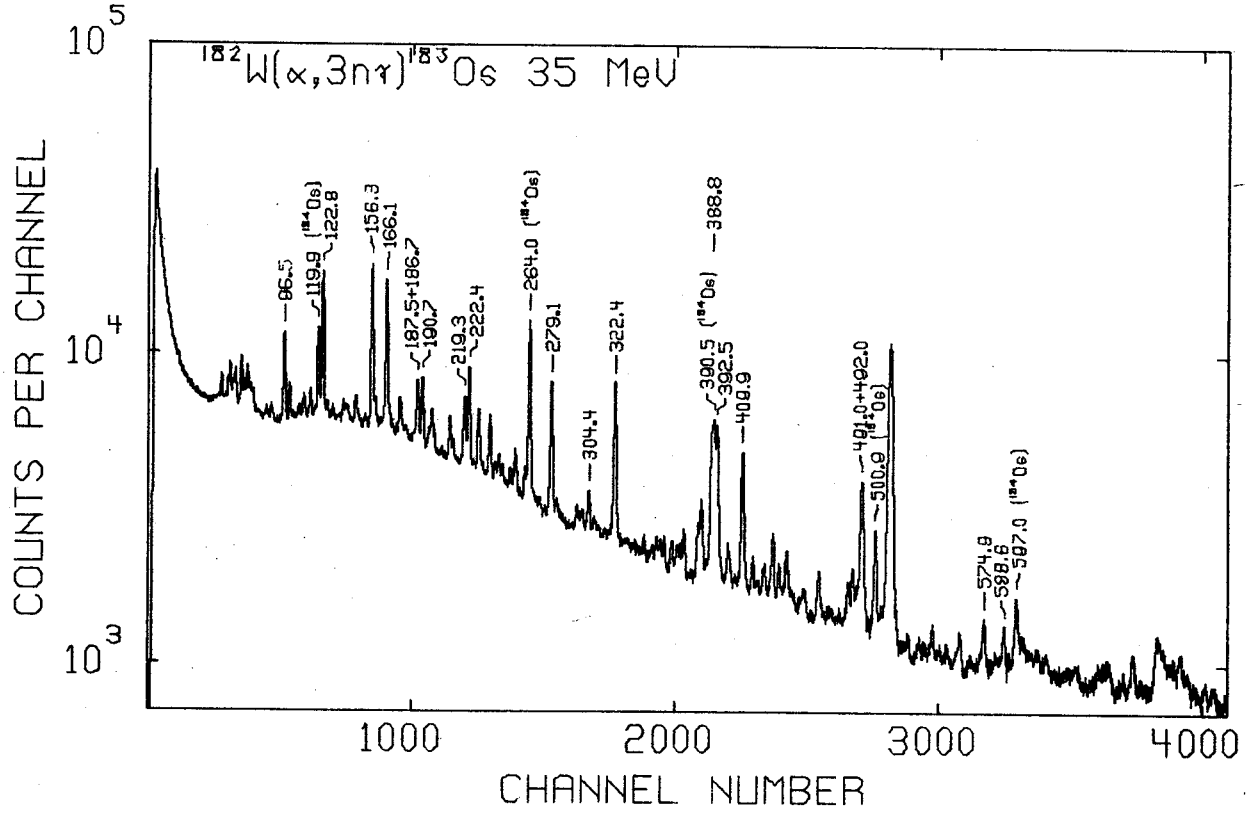

Fig. 1 The γ-ray singles spectrum from the ^{182}W(α,3nγ)^{183}Os Reaction.

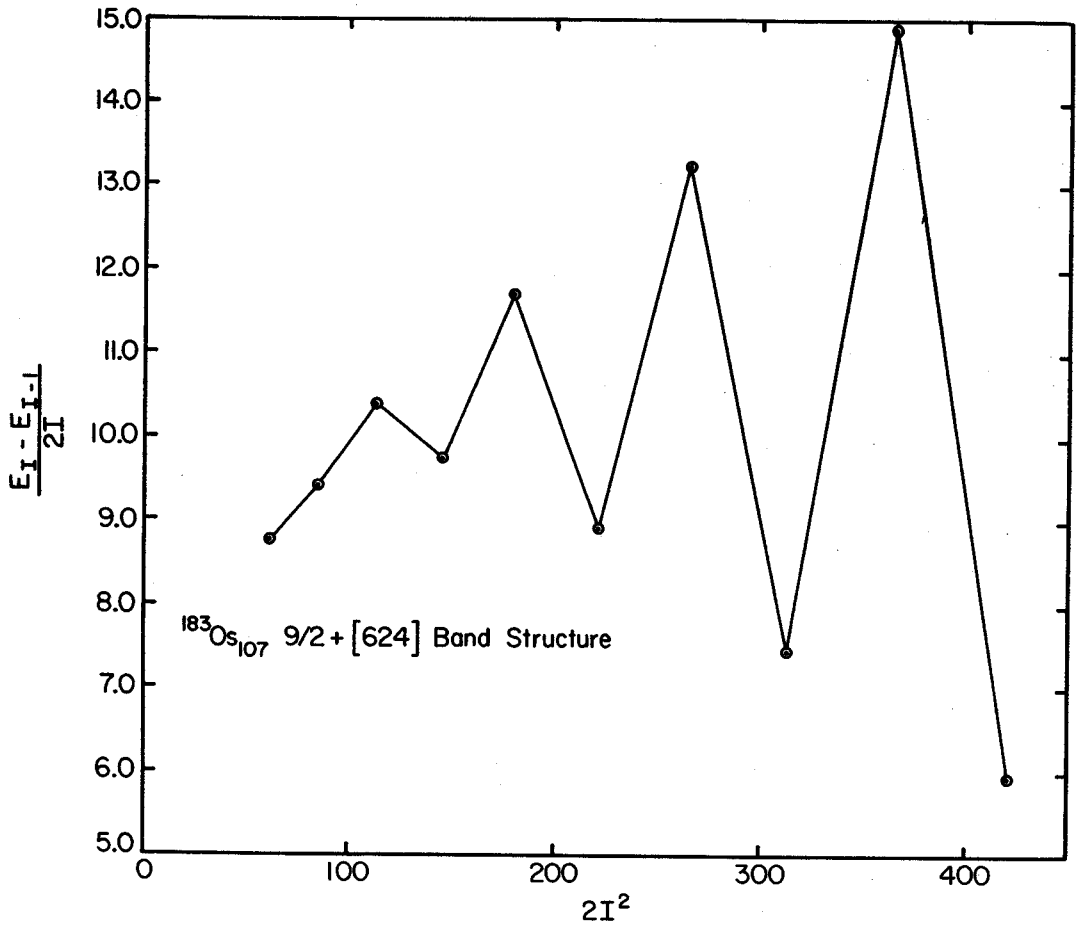

Fig. 2 Plot of $E_I - E_{I-1}/2I$ vs. $2I^2$ for the $9/2^+[624]$ ground band of ^{183}Os.

Levels in ^{199}Hg Populated in the Decay of ^{199}Tl*

G. Mathews** and F.M. Bernthal

In supplement to the early NaI(Tl) work of Bauer, et al.[1] the γ-ray spectrum associated with EC decay of ^{199}Tl (7.4 hour) has been re-investigated with Ge(Li) detectors. Levels in ^{199}Hg have been previously investigated by Coulomb excitation, transfer reactions, and ^{199}Au decay studies. This previous work has recently been summarized in Ref. 2.

We here report tne observation of 17 new γ-rays arising from the ^{199}Tl decay. All of these newly observed transitions have been placed in the preliminary revised ^{199}Tl decay scheme shown in Fig. 1.

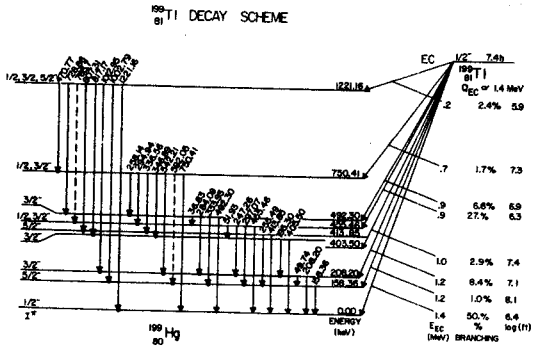

Fig. 1 Proposed scheme for the EC decay of ^{199}Tl to levels in ^{199}Hg.

The ^{199}Tl sources were prepared by the ^{197}Au(α,2n) reaction on gold foils ≈100 mg/cm^2 thick. Typical α-particle beam energy was ≈29 MeV.

Singles γ-ray spectra were taken with a 10.4% efficient Ge(Li) detector having resolution 2.4 keV FWHM and peak-to-Compton ratio ∿35:1 at 1333 keV. A typical singles spectrum is shown in Fig. 2.

The ^{199}Tl peaks were assigned by following their decay rates relative to that of the known 455.5-keV ^{199}Tl γ-ray. Assignments to ^{198}Tl and ^{200}Tl were made in a similar way on the basis of normalization to the 636.8 and 368.0-keV transitions in those decays, respectively. The γ-ray energies and intensities associated with ^{199}Tl decay are summarized in Table 1. A 592.0-keV transition is assigned to ^{199}Tl decay on the basis of coincidence and half-life data, although the strong 591.8-keV ^{200}Tl transition obscures the line in singles. The analysis of all singles data was effected with use of the photopeak fitting code, SAMPO. On the basis of this analysis, the 25 γ-rays listed in Table I have been assigned to ^{199}Tl decay. Also included in the ^{199}Tl decay scheme are low-energy transitions at 36.83, 49.74, and 51.93 keV identified in previous work.[3] The data of Ref. 1 are shown for comparison.

The level scheme of Fig. 1 was constructed with the aid of γ-γ coincidence data acquired with two Ge(Li) detectors positioned at 180° geometry. Data for the complete 4096x4096 coincidence matrix were stored serially on magnetic tape for later analysis. In Fig. 3 we show representative coincidence spectra obtained in this way. The spectra for the 403.5, 492.3, 817.7, and 1062.8-keV transitions show, in part, the basis on which we have assigned new levels at 750.4 and 1221.2 keV in ^{199}Hg populated in the decay of ^{199}Tl. The log(ft) values for EC-β$^+$

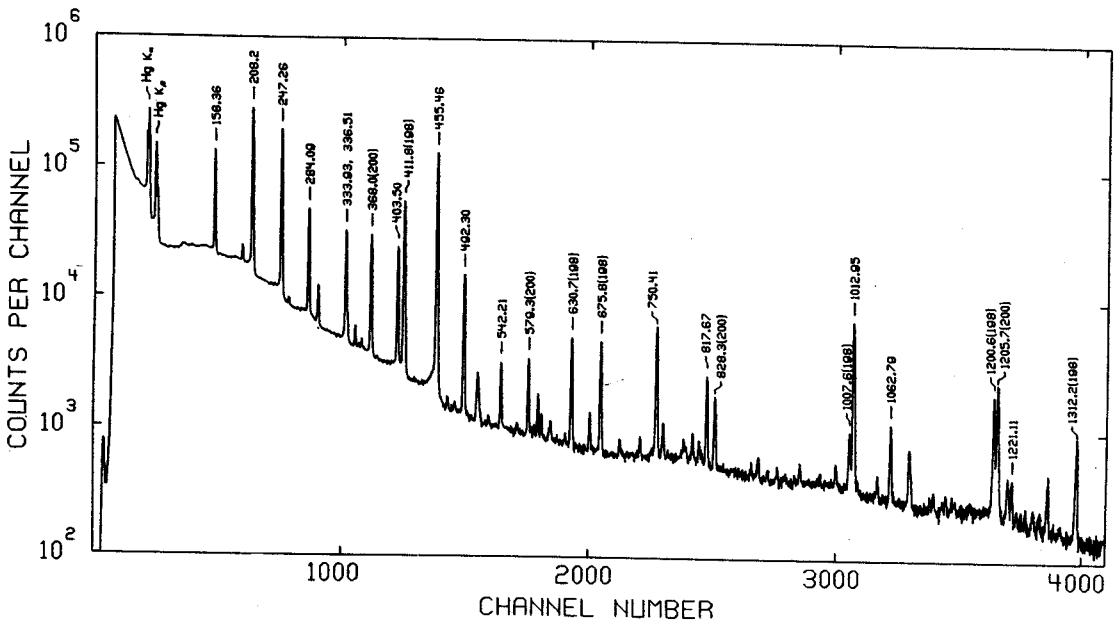

Fig. 2 Gamma-ray singles spectrum from ^{199}Tl decay. Prominent containant lines from ^{198}Tl and ^{200}Tl are identified also.

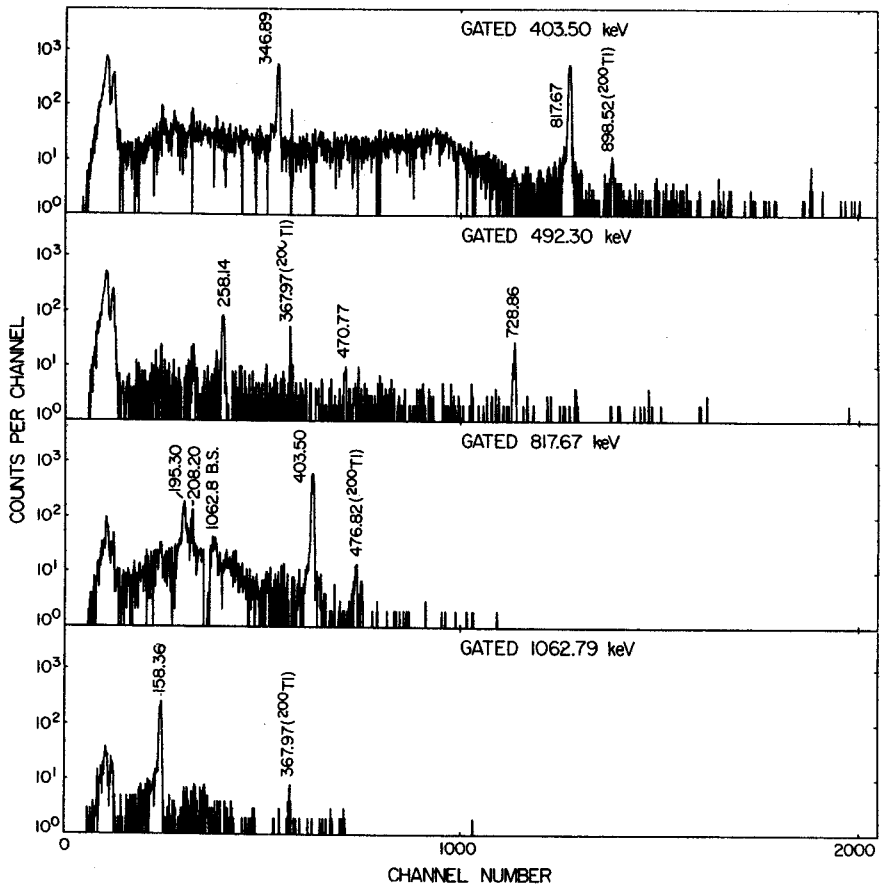

Fig. 3 The 403.5, 492.3, 817.7, and 1062.8-keV γ-γ coincidence spectra from ^{199}Tl decay.

decay of ^{199}Tl have been calculated on the basis of an assumed Q-value of 1.4 MeV derived from β-decay systematics, and a previously measured[4] 50% EC-β^+ feeding to the ^{199}Hg ground state. The tentative spin and parity assignments are consistent with the data compilation of Lewis.[2] It is worth noting that the relatively low log(ft) for EC-decay to the 1221.16-keV level seems to point to an allowed β-decay. If this were the case, then an even parity would be indicated for that state. Such an assignment would be difficult to account for on the basis of elementary shell-model considerations. However, the uncertainty in the 0.2-MeV decay energy makes this log(ft) value somewhat questionable without the aid of precise data on the ^{199}Tl Q-value.

TABLE I

Energies and Relative Intensities of γ-rays from ^{199}Tl Decay

Present Work		Bauer et al.	
Energies (keV)	Intensities (rel)	Energies (keV)	Intensities (rel)
158.36±.05	40 ±.2	158.4	40 ±4
195.30±.05	2.1 ±.2	195.2	7.0±1.4
208.20±.05	9. ±5	208.2	88 ±9
247.26±.05	75. ±4	247.2	68 ±7
255.49±.11	.10±.03	254	
258.14±.10	.58±.06		
284.09±.05	17.8 ±.9	284.0	10 ±2
294.94±.09	.42±.04		
297.07±.06	2.8 ±.3		
333.93±.05	14.2 ±.7	333.9	12.0±2.4
336.56±.08	1.14±.11		
346.89±.08	1.07±.11		
403.50±.05	13.9 ±.7	403.4	3.0±0.6
413.85±.08	1.59±.16		
455.46±.05	100±5	455.1	100 ±10
470.77±.10	.31±.06		
492.30±.05	12.3 ±.6	492.8	8.0±1.6
542.21±.05	2.13±.21		
*592.0 ±.11	<0.8		
728.86±.11	.36±.04		
750.41±.05	8.4 ±.4		
*765.7 ±.15	<.05		
807.31±.11	.40±.04		
817.67±.07	3.26±.20		
1012.95±.05	14.2 ±.7		
1062.79±.07	2.05±.21		
1221.16±.12	.24±.03		

*Observed in coincidence spectrum only.

References

1. R.W. Bauer, L. Grodzins, and H.H. Wilson, Phys. Rev. 128, 694(1962).
2. M.B. Lewis, Nuclear Data Sheets for A=199, B6, 355(1971).
3. B. Jung and J. Svedburg, Nucl. Phys. 20, 630(1960).

* Work supported by the USAEC and NSF.

** Present Address: Chemistry Department, University of Maryland, College Park, Md. This work was submitted in partial fulfillment of the requirements for the Bachelor of Science degree in Chemical Physics at Michigan State University.

Inelastic Scattering from Pb and Bi Isotopes

W.T. Wagner and G.M. Crawley

A high resolution study of inelastic proton scattering on these nuclei is a powerful technique for testing nuclear structure models and the direct reaction mechanism in this region of A. Utilizing dispersion-matching methods with extensive use of the on-line tuning technique of Blosser et al.,[1] exposures have been taken at 35 MeV bombarding energy on nuclear emulsions in the Enge split-pole spectrograph. Results have been obtained for the three isotopes ^{207}Pb, ^{208}Pb, and ^{209}Bi at angles between 10° and 100° with a typical resolution of less than 10 keV (FWHM). A spectrum of ^{208}Pb is displayed below.

This spectrum reveals the collective states of ^{208}Pb as well as the weakly excited levels. Even with the small exposure length a number of unnatural parity states are evident; the 4^- state at 3.475 MeV of excitation is discernible as well as the 6^- and the 4^- states at 3.920 and 3.961 MeV, respectively. The background is small and discrete structure is apparent up to about 7.4 MeV excitation energy where ^{208}Pb becomes unstable to neutron decay.

For the doubly-magic nucleus, ^{208}Pb, extensive shell model theories have been constructed giving nuclear wave functions for both the natural and unnatural parity states. Some work has also been done on ^{207}Pb and ^{209}Bi. With the direct reaction scattering codes available and the reasonably well understood two nucleon effective interaction, the natural parity state wave functions given by microscopic theory can be tested. Including the effects of knock-on exchange, core polarization, and the tensor and spin-orbit two nucleon force will permit a thorough investigation of the theory. Further, observation of the unnatural parity states should allow determination of the tensor and $\underline{L}\cdot\underline{S}$ components of the force since scattering into such states is apparently sensitive to these two components especially at higher energies. The low background of typical spectrograph data encourages a search for the giant dipole and quadrupole states. The strengths of these resonances spread over a considerable region of excitation energy (about 2 MeV), both having weak but strongly forward peaked angular distributions on the order of 500 μb/sr maximum at this energy.

Although the odd mass nuclei are essentially single particle in behavior, inelastic scattering gives information on their collective characteristics. Indeed, the low-lying multiplets in ^{207}Pb and ^{209}Bi have been successfully described by the weak coupling model so that analysis of higher lying states would be interesting.

Elastic scattering from these nuclei will also be studied so that optical model parameters needed for inelastic scattering calculations can be obtained. The feasibility of using a position sensitive wire proportional counter in the spectrometer focal plane for this less resolution-dependent study of elastic and collective states is currently being determined.

References

1. H.G. Blosser, G.M. Crawley, R. deForest, E. Kashy, and B.H. Wildenthal, Nucl. Instr. and Methods 91, 61(1971).

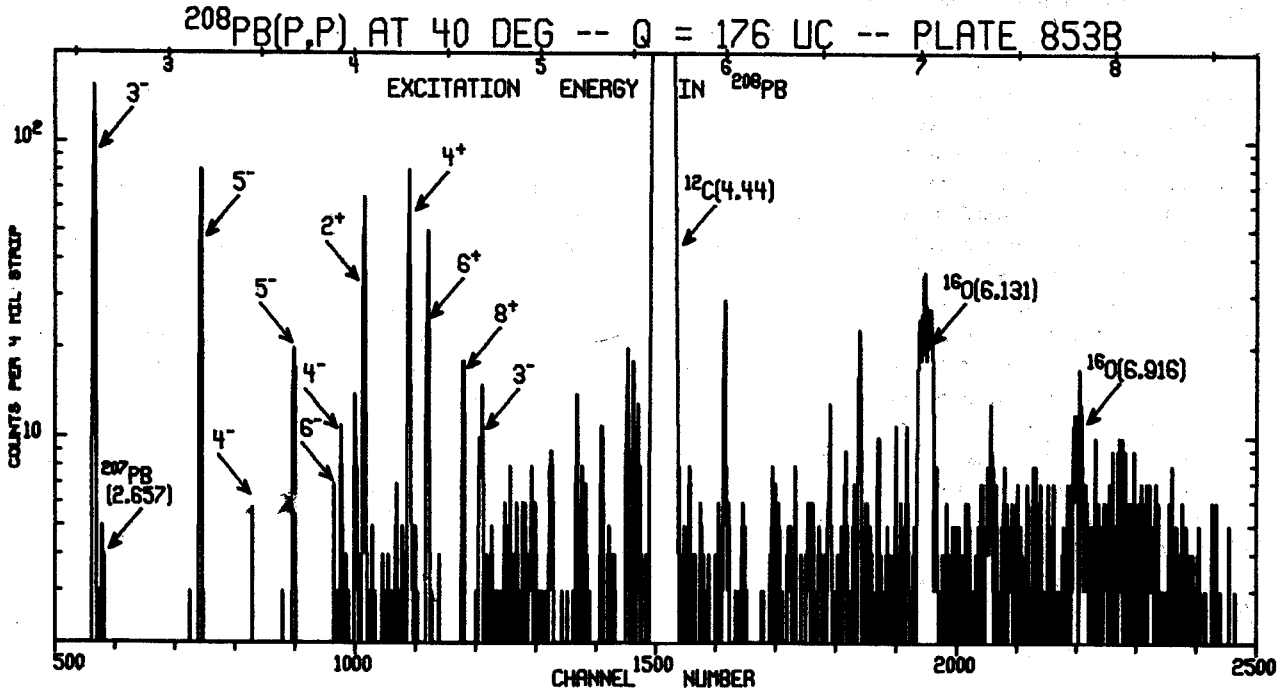

The Pb isotopes are a region of the nuclear chart which is especially well suited to test the shell model in detail for several reasons: (1) ^{208}Pb is believed to be a relatively good closed core. (2) The neutron single particle states are known from the ^{208}Pb(p,d)^{207}Pb reaction. (3) Assuming the shell model and using a reasonable basis, all the Pb isotopes should be calculable using these known single particle energies and only the T=1 part of the two-body interaction. Except for renormalization effects, and assuming charge symmetry, this T=1 interaction depends only on proton-proton scattering, not on the less well determined proton-neutron scattering.

In order to make such a test, the (p,d) and (p,t) reactions are being studied on all the stable Pb isotopes using both nuclear emulsions and the position sensitive proportional counter in the focal plane of a magnetic spectrometer. By using the identical experimental set-up for studying both reactions on all four targets, we are able to measure relative cross sections on the various isotopes to a few percent. Hence, we can accurately deduce spectroscopic factors for the (p,d) reaction on the lighter Pb isotopes relative to those for single hole states seen in the ^{208}Pb(p,d)^{207}Pb reaction. Such a procedure eliminates many of the usual ambiguities in conventional DWBA analysis.

The ^{208}Pb(p,d)^{207}Pb and ^{207}Pb(p,d)^{206}Pb Reaction

W.A. Lanford and G.M. Crawley

The study of ^{208}Pb(p,d)^{207}Pb reaction provides the basis for understanding the (p,d) reactions on the lighter isotopes of Pb. The strong states seen in this reaction correspond to the $3p_{1/2}$, $2f_{5/2}$, $3p_{3/2}$, $1i_{13/2}$, $2f_{7/2}$, and $1h_{9/2}$ single neutron hole states. The study of the transitions to these single hole states provides a calibration of the DWBA analysis (both in strength and angle dependence) which makes the analysis of the (p,d) reaction on the lighter isotopes of Pb less ambiguous. In addition, many states are seen excited in this reaction; the strength to these non-single neutron hole states indicates some of the limitations of shell model calculations based on a ^{208}Pb closed core. It is also possible that these weak transitions result from multi-step processes in the reaction mechanism.

Since the ^{207}Pb ground state corresponds to a $p_{1/2}$ neutron hole outside ^{208}Pb, the ^{207}Pb(p,d)^{206}Pb reaction excites states in ^{206}Pb with configurations of the form $(p_{1/2})^{-1}x(L_j)$ where L_j stands for the available single neutron hole states (the same ones which are strongly excited in ^{208}Pb(p,d)^{207}Pb). Shown in Fig. 1 are spectra of the ^{208}Pb(p,d)^{207}Pb and ^{207}Pb(p,d)^{206}Pb reactions observed with the position sensitive proportional counter. These spectra are plotted with a common Q-value scale (approximately), and are labeled with the dominant L-value as determined by the angular distributions.

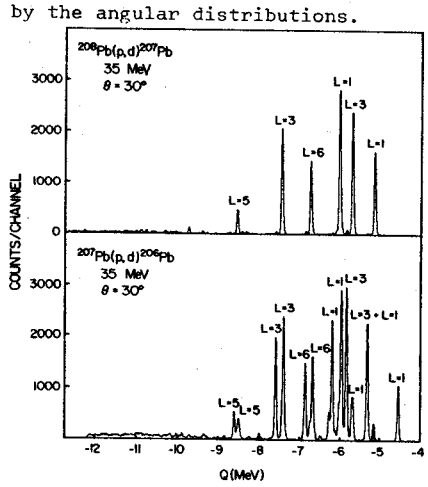

Fig. 1 Spectra of the ^{208}Pb(p,d)^{207}Pb and ^{207}Pb(p,d)^{206}Pb reactions observed with the position sensitive proportional counter in the focal plane of the magnetic spectrometer. The spectra have a common Q-value scale (approximate).

It turns out that the strong states observed above 2.0 MeV have very simple shell model configurations of $(p_{1/2})^{-1}$ weakly coupled to the $i_{13/2}$, $f_{7/2}$, and $h_{9/2}$ single neutron hole states. This can be seen by looking at highest L=6, 3, and 5 transitions shown in Fig. 1. Note that the strength in the ^{208}Pb(p,d)^{207}Pb reaction to these states is split to close doublets in the ^{207}Pb(p,d)^{206}Pb reaction. The low-lying states have more mixed configurations.

The ^{206}Pb(p,d)^{205}Pb and ^{204}Pb(p,d)^{203}Pb Reactions

W.A. Lanford

These experiments conducted with the identical experimental setup and the ^{208}Pb(p,d)^{207}Pb reaction provide spectroscopic data on the lighter isotopes of Pb with which to test the shell model. Shown in Fig. 2 are spectra of the ^{206}Pb(p,d)^{205}Pb and ^{204}Pb(p,d)^{203}Pb reaction observed with the position sensitive proportional counter. These spectra are plotted on a common Q-value scale (approximately). Previous measurements[1] of the ^{206}Pb(d,t)^{205}Pb reaction led to spectroscopic factors which were in serious disagreement with shell model predictions. Preliminary analysis of our results indicates very good agreement between theory and experiment.

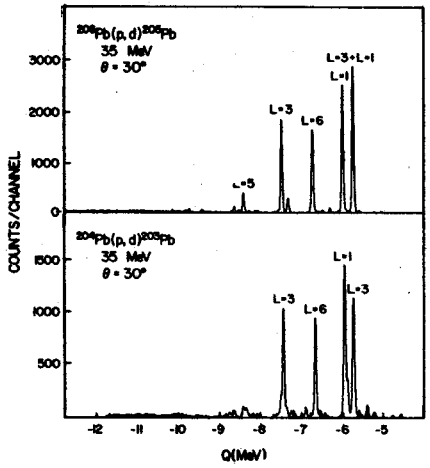

Fig. 2 Spectra of the $^{206}Pb(p,d)^{205}Pb$ and $^{204}Pb(p,d)^{203}Pb$ reactions observed with the position sensitive proportional counter in the focal plane of the magnetic spectrometer. The spectra have a Common Q-value scale (approximate).

It is interesting to note that, except for the lowest L=1 and L=3 transitions, the spectra look very much like the $^{208}Pb(p,d)^{207}Pb$ spectra shown in Fig. 1. Notice that the L=1, 6, 3, and 5 transitions occur at about the same Q-value in all reactions. This is a further indication of how good simple shell model calculations should be for these isotopes. In the simplest model of a spherical shell model with a very weak residual interaction, except for the strength to the lowest L=1 and L=3 transitions, the (p,d) reaction on all the even isotopes of Pb should be the same. Preliminary evaluation of the strengths to the $p_{3/2}$, $i_{13/2}$, $f_{7/2}$, and $h_{9/2}$ orbits indicates that this is not too far from the case.

Reference

1. Robert Tickle and John Bardwick, Phys. Rev. 178, 2006(1969).

The (p,t) Reaction on the Stable Isotopes of Lead

W.A. Lanford

The (p,t) reaction is being studied on all the stable Pb isotopes using a 35 MeV proton beam. The triton spectra are recorded using either nuclear emulsions or the position sensitive proportional counter in the focal plane of our split-pole magnetic spectrometer. Figure 3 shows spectra of the (p,t) reaction on ^{208}Pb, ^{207}Pb, ^{206}Pb, and ^{204}Pb. The spectra are aligned so as to have a common energy (Q-value) scale.

The results are being analyzed using the two-nucleon DWBA code DWUCK and the shell model wave functions of McGrory[1] for ^{208}Pb, ^{206}Pb, and ^{204}Pb. Figure 4 shows DWBA fits to the data for the $^{208}Pb(p,t)^{206}Pb$ reaction to the lowest 0^+, 2^+, and 4^+ states of ^{206}Pb. Each calculated cross-section has an independent normalization. Also shown is the transition to the 3^+ unnatural parity state at 1.339 MeV.

McGrory's shell model wave functions were used to predict the relative intensities of states of a given J^π in the $^{208}Pb(p,t)^{206}Pb$ and $^{206}Pb(p,t)^{204}Pb$ reactions. Figure 5 shows the comparison

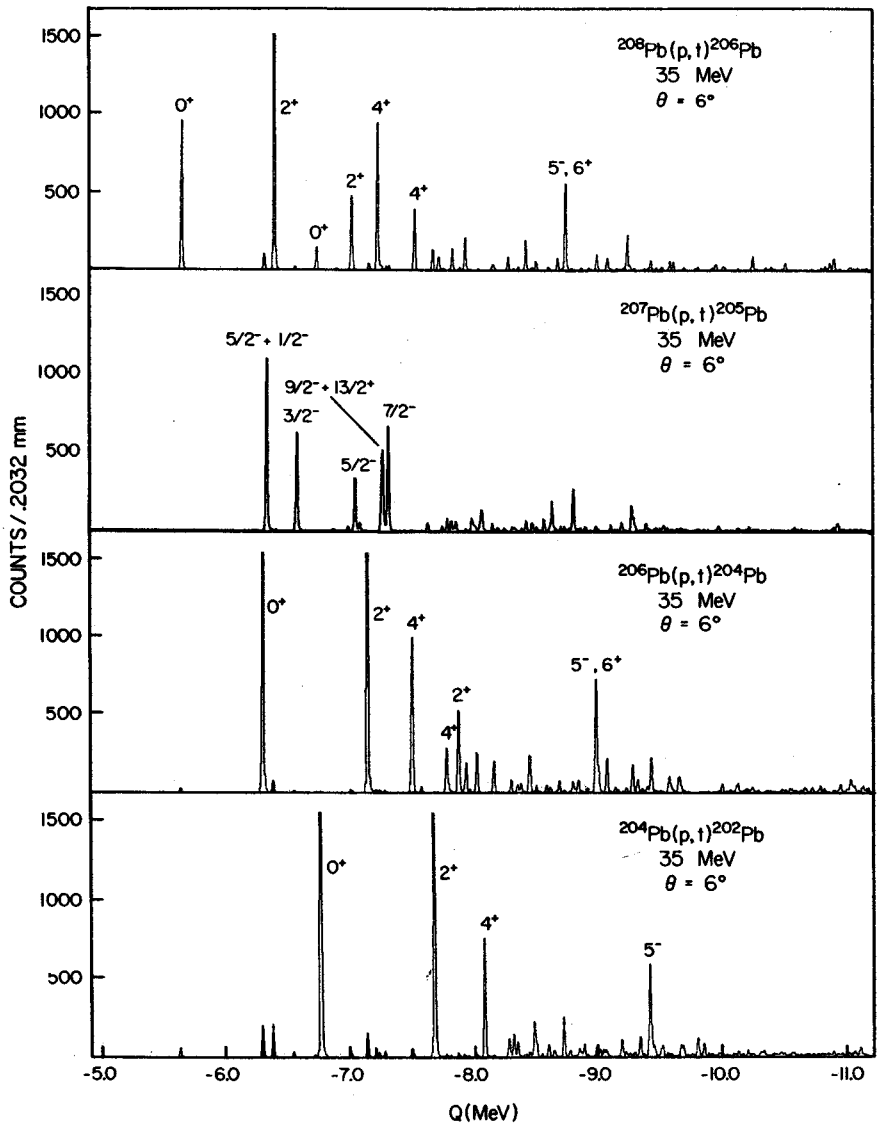

Fig. 3 Spectra of the (p,t) reaction on the stable isotopes of lead. All spectra have a common Q-value scale.

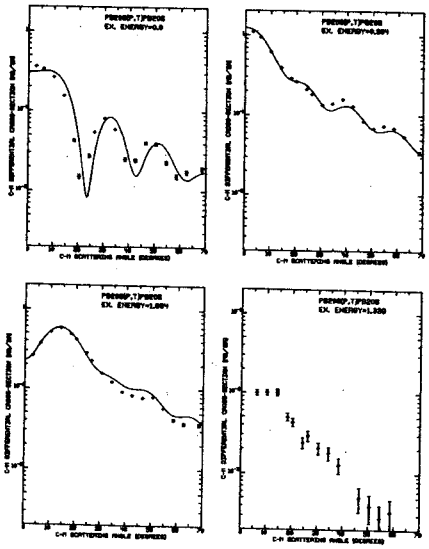

Fig. 4 Experimental and DWBA calculations for the angular distributions of the ^{208}Pb(p,t) reaction to the lowest 0^+(0.0 MeV), 2^+(0.804), 4^+(1.684), and 3^+(1.339) states in ^{206}Pb.

between these predictions and the experiment for 0^+, 2^+, and 4^+ states. Note there is generally good agreement for the relative cross-sections of different L-transfers.

References

1. J.B. McGrory, ORNL, private communication, August 1972.

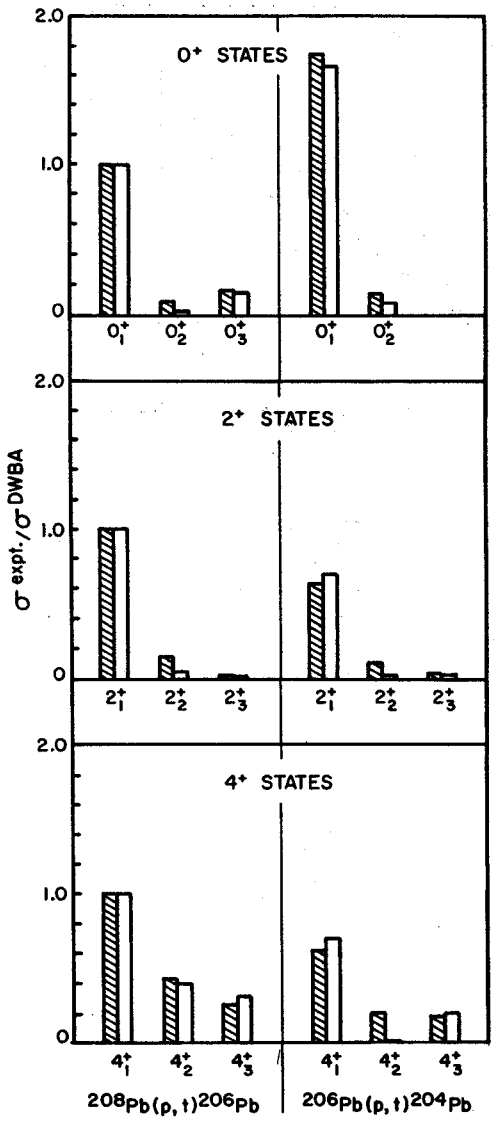

Fig. 5 The comparison of theory and experiment for the cross-sections to the 0^+, 2^+, and 4^+ states in ^{206}Pb and ^{204}Pb. Theory and experiment are normalized for the lowest states in ^{208}Pb(p,t)^{206}Pb reaction.

High Resolution Study of the Particle-Hole Multiplets in ^{208}Bi from the ^{209}Bi(p,d) Reaction at 35 MeV

G.M. Crawley, W. Lanford, E. Kashy, and H.G. Blosser

Recent discussions of the effective two nucleon force obtained from the two particle spectra of nuclei near closed shells[1] has again focussed attention on such nuclei. One important example near the doubly magic nucleus ^{208}Pb, is the nucleus ^{208}Bi with a proton outside the ^{208}Pb core and a neutron hole in the core. In the present experiment, we have studied ^{208}Bi by the reaction ^{209}Bi(p,d) using the high resolution capability of the Michigan State Cyclotron. In the simplest picture of this reaction, we expect to reach states which consist primarily of a proton in the $h_{9/2}$ orbit coupled to neutron holes in the $2p_{1/2}$, $1f_{5/2}$, $2p_{3/2}$, $0i_{13/2}$, $1f_{7/2}$, and $0h_{9/2}$ orbits.

The present experiment extends the previous work[2,3] to the important $[\pi h_{9/2}, \nu^{-1} h_{9/2}]$ multi- and also with the better resolution available with the MSU Cyclotron facility checks the spin parity assignments from the (d,t) reaction. A further motivation for the experiment was the clear differentiation of angular momentum transfers provided by the angular distributions of deuterons in the (p,d) reaction with 35 MeV protons. This allows easy identification of the members of a multiplet and serves as an indication of any mixture of different ℓ values in a particular transition. Finally a careful comparison was made of the present ^{209}Bi(p,d)^{208}Bi reaction with a ^{208}Pb(p,d)^{207}Pb experiment carried out at the same energy, with the same apparatus to check the strength in the ^{208}Bi multiplets compared to the transition strength for the single hole states in ^{207}Pb.

The experiment was carried out using the 35 MeV proton beam from the Michigan State University isochronous cyclotron. The reaction products were analyzed in an Enge split-pole spectrograph and the deuterons were detected in NTA and NTB, 25 microns nculear emulsions. Thin mylar absorbers were placed in front of the plates to eliminate tritons. The bismuth target used was 100 μgm/cm^2 thick evaporated onto a 20 μgm/cm^2 carbon backing.

Before making exposures the total resolution was optimized by passing first the elastically scattered protons and then the deuterons from the ground state of the ^{208}Pb(p,d) reaction, into the speculator system[4] in the focal plane of the magnet. A total resolution of less than 5 keV FWHM for scattering angles from 6° to 50° was obtained [Fig. 1]. Two exposures were taken at each angle, one for the p and f multiplets and the other longer exposure to obtain adequate statistics on the $h_{9/2}$ and $i_{13/2}$ multiplets. In order to fully exploit the high resolution it was necessary to scan the nuclear emulsion in 100 micron steps and in some regions of close doublets to reduce the step size of the scan to only 50 microns.

The results in general agree quite well with the previous measurements especially for the f and p multiplets. Some differences were observed in the $[\pi h_{9/2}, \nu^{-1} i_{13/2}]$ multiplet where the states at 1.708 MeV and 1.844 MeV are assigned spin parities of 5 and 4 respectively opposite to the previous values. No evidence of a state with the the correct ℓ transfer was found near 2.72 MeV where the 2^- member of this multiplet was reported.[3] This state may appear instead at 3.057 MeV or perhaps as a close doublet with the 1^+ state at 2.892 MeV.

The $[\pi h_{9/2}, \nu^{-1} h_{9/2}]$ multiplet appears to be comparitively pure and a number of spin parities can be assigned especially for the strong states. A publication is currently being prepared on this work.

References

1. J.P. Schiffer in the Two-Body Force in Nuclei, Ed. Sam M. Austin and G.M. Crawley, Plenum Press, 1972, p. 205.

2. J.R. Erskine, Phys. Rev. 135, B1110(1964).

3. W.P. Alford, J.P. Schiffer, and J.J. Schwartz, Phys. Rev. Letters 21, 156(1968), and Phys. Rev. C3, 860(1971).

4. H.G. Blosser, et al., Nucl. Instr. and Methods 91, 61(1971).

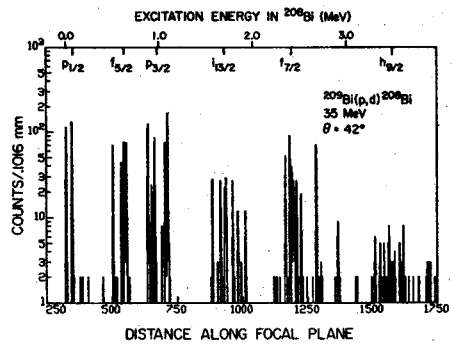

Fig. 1 Spectrum of the ^{209}Bi(p,d)^{208}Bi reaction recorded at 42° with E_p=35 MeV. The energy scale at the top of the figure shows the location of the Q-values of the ^{208}Pb(p,d)^{207}Pb reaction to the indicated single particle states.

Nuclear Theory

H. McManus, G. Bertsch, J. Borysowicz

I. Reactions (Bertsch)

The (^{3}He,t) reactions was found in some cases to be dominated by an intermediate α state, in calculations done with Schaeffer (visitor, 1971). This explains unusual features found in (^{3}He,t) reactions to antianalog states, discovered at this lab. More thorough calculations have been done here by de Takacsy (visitor, 1972). At present the main effort is with a graduate student, Poon, to ulitize simple semiclassical methods to treat multistep reactions. With another visitor, Auerbach, theoretical corrections were made to the decay of analog states. The techniques and wave functions might be useful in the analysis of the (p,n$\bar{p}$) reaction, which also has unusual features. This is under study.

II. Collective States (Bertsch)

We are investigating the properties of giant collective modes from a qualitative point of view. It has been shown that these states should be narrower than non-collective states.

III. Effective Operators and Effective Forces (McManus)

As collective states in closed-shell nuclei are one of the simplest types of nuclear excitation perturbative calculations of both effective force and effective charge for particle-hole states were tried: also calculation of effective charges assuming MSDI is effective force. (With M. Dworzecka, Research Associate 71-72). This formalism was used to compare e-e' and p-p' for collective states of ^{40}Ca using for p-p' experiments done here (G.R. Hammerstein, Research Assistant 71-72 with M. Dworzecka). Various other studies of effective operators were: effects of core polarization in (p,p') on Ca, Sr, Y, and Pb (with G.R. Hammerstein, F. Petrovich, and J. Borysowicz); extraction of effective charge from e-e' in s-d shell. (G.R. Hammerstein with Larson and Wildenthal); and comparison of e-e' with p-p' in Tin and Lead region (G.R. Hammerstein with R. Howell) using p-p' experiments done here and elsewhere. Most of this has spilled over in one form or another into analysis done by experimentalists here. Also attempted were tests of semiclassical methods in e-e' (with G.R. Hammerstein) and in π-nucleon scattering (with H.K. Lee, visitor 1972).

IV. Mesonic Effects in Nuclei (McKellar, visitor,71)

A stimulating visit by Bruce H.J. McKellar (71) increased our knowledge of mesic exchange currents in nuclei. While here McKellar found a generalization of Siegert's theorem limiting the role of exchange currents in parity non-conserving electromagnetic transitions, and completed other problems on the nucleon-nucleon force, including the parity violating part. Bertsch has applied the theory of the pp reaction and found an effect of possible significance to the solar neutrino problem.

V. Cluster Model and Few Bodies (Borysowicz)

Structure of ^{16}O and ^{12}C has been investigated using the α-cluster model of Brink. No agreement with the elastic electron scattering is found when harmonic-oscillator clusters are used. Cluster with primitive correlations lead to a better agreement. This leads to the study of ^{3}He, where N-N correlations can be taken into account more precisely, We found that N-N correlations stronger than usually assumed give a better fit to the elastic-electron scattering. The 3-body scattering problem is investigated in the framework of Faddeev eqs. Different methods are tried for the resulting integral eqs. (with J. Hetherington, N. Larson, and K. Gilbert).

Compound and Direct Neutrons Produced by Proton Bombardment

T. Amos and A. Galonsky

Because of Coulomb-barrier effects, evaporation of neutrons comprises almost 100% of the probability for decay of a heavy compound nucleus. More than 50% of direct emissions initiated by proton bombardment can be expected to be neutrons. Therefore, a study of neutron emission should reveal the major features of the reaction mechanisms induced by proton bombardment.

Using thick targets of C, Al, Cu, Ag, Ta, and Pb, bombarded by protons of energy 22, 30, and 40 MeV, we have measured absolute neutron spectra at 0°, 30°, 60°, 90°, 120°, and 150°. The measurements were made by the time-of-flight method with a liquid scintillator. Gamma rays were suppressed by pulse-shape discrimination. The neutron energy range covered was 0.5-40 MeV. The lower limit, 0.5 MeV, took us well below the Maxwelliah peak in the evaporation part of each spectrum. This is an important improvement over our earlier data because the peak is a distinguishing feature of an evaporation spectrum and it is reassuring to actually see it in the data. Also, without the peak it would not be possible to integrate the spectra to obtain the total neutron production. Because of the non-linear pulse-height response of the scintillator with respect to neutron energy, we had to detect pulses with a range of 600 in size in order to cover the factor of 80(0.5-40 MeV) in neutron energy.

As a sample of the experimental results we present all of the Ta data in Fig. 1. Although

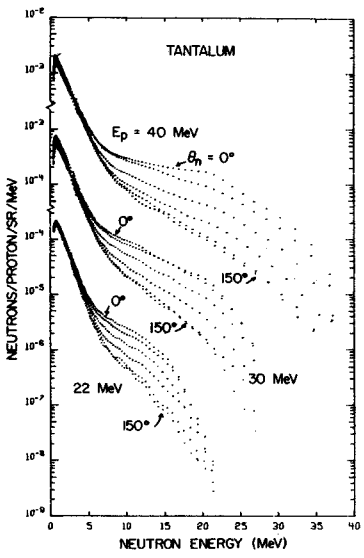

Fig. 1

manipulations of the data for comparisons with theoretical models have been made, the qualitative essence of the physics (for Ta) is all in Fig. 1. At each proton bombarding energy the data tell us there are two distinct reaction mechanisms at work. At low neutron energies we have the same absolute spectrum at all neutron angles. This is the isotropy expected of a compound-nucleus reaction. Furthermore, the spectrum has a peak around 1 MeV followed by an exponential fall off. A simple thermodynamic calculation of evaporation leads to such a spectrum (even when integrated through the thick target). Above about 5 MeV the data break sharply from the evaporation exponentials giving two differences: many more high-energy neutrons than could result from evaporation and a sharply forward peaked angular distribution. These are the characteristics one expects of direct reactions.

A final aspect to be noted from Fig. 1 is the strong increase in neutron yield at all energies with increasing proton bombarding energy. The total yields, that is, integrations over neutron energy and angle, are shown in Fig. 2 for all of our targets and energies. Also shown are data obtained at E_p=18 and 32 MeV[1] by a completely different and completely integral experimental technique, the so-called manganese-bath technique.

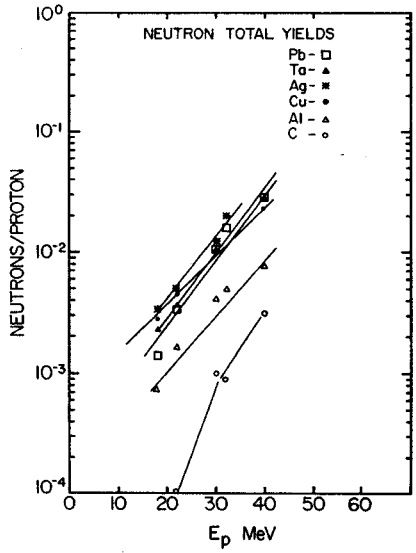

Fig. 2

In making a more quantitative analysis of the data we have had to allow for a sequence of neutron emissions from an excited compound nucleus. For each 10 MeV of proton bombarding energy about one neutron is boiled off. We followed this sequence of emissions and excitations of the residual nuclei on the computer and integrated the proton energy through the target in order to fit the compound-nucleus data. There were only two parameters, the radius, which controlled the normalization, and the level-density parameter, a, which controlled the shape of a spectrum. We used a simple degenerate-gas model

in which $U=aT^2$, where U is the excitation energy of the residual nucleus and T is the temperature. For Ta, T≈1-1/2 MeV. By trial and error we were able to get good fits to the evaporation data from Cu, Ag, Ta, and Pb. The values of a so obtained are plotted against mass number, A, in Fig. 3.

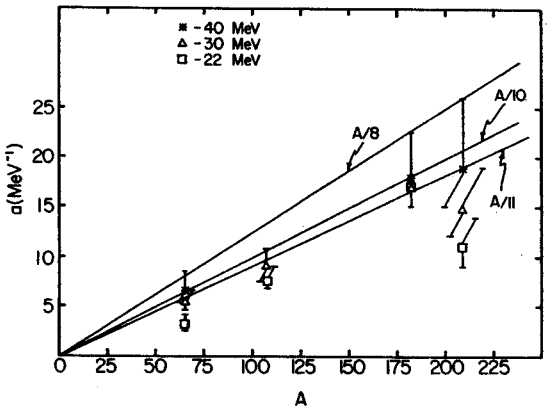

Fig. 3

The degenerate gas model predicts the value a=A/10 if r_o=1.4 F. A summary of low-energy data[2] shows that A/8 is a good average fit. A comparison between Ta and Pb indicates a lower level density in doubly-magic Pb in the 22- and 30-MeV data. Apparently the shell closures have an effect, but it diminishes with increasing excitation energy. We could not perform a sensible fit to the Al data because there was no clean separation of an evaporation from a direct spectrum. The carbon data did not appear to be part of any systematics.

By extrapolating the evaporation exponentials and subtracting from the observed spectra we extracted a direct or non-compound spectrum for each proton energy and neutron angle for Cu, Ag, Ta, and Pb. It is easy to imagine the results by looking at Fig. 1. Models of these neutrons, pre-equilibrium models, have been developed recently.[3] As presently constituted, these models are incapable of predicting an angular distribution for the emitted neutrons (our data, Fig. 1 for example, show a strong angular dependence). In order to make some comparison between theory and experiment we have integrated our spectra over neutron angle. We have also subtracted spectra so that we have data at E_p=35 MeV (subtracting 30-MeV spectra from 40-MeV spectra) and E_p=26 MeV (subtracting 22-MeV spectra from 30-MeV spectra). Because the neutron yields rise rapidly with energy, these subtractions are small. Most of the neutron production in the 22-MeV data occurs in the first few MeV below 22 MeV. The average proton energies for these spectra were taken to be the energy at which one half of the production had occurred, namely, 18.0, 20.1, 18.2, and 18.8 MeV for Cu, Ag, Ta, and Pb, respectively. The 26-MeV spectra (including the evaporation parts) are shown in Fig. 4. Except for carbon they are remarkably

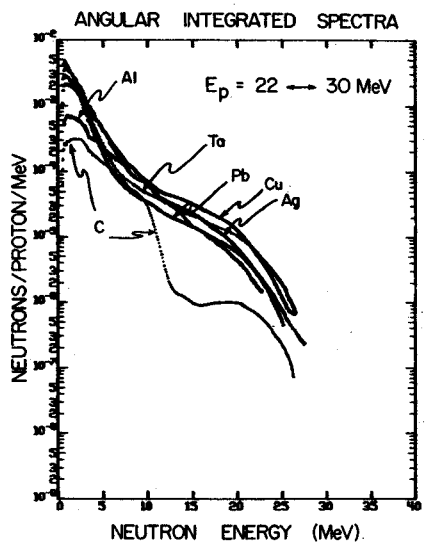

Fig. 4

similar to each other. In Fig. 5 the Ta data are compared with results of a pre-equilibrium calculation obtained through the courtesy of M. Blann, University of Rochester. Beyond the peak due to equilibrium evaporation, which is not included in Blann's calculation, there is excellent agreement in absolute values and fair agreement in the shapes.

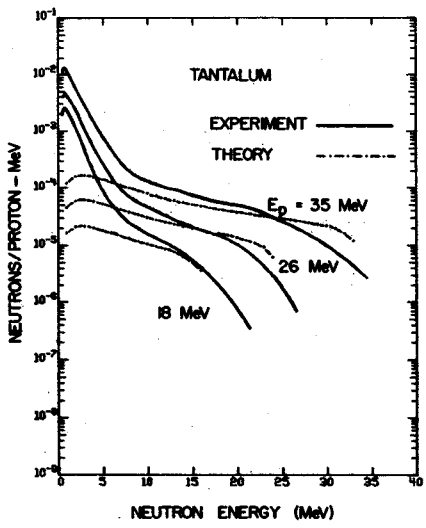

Fig. 5

Finally, we give in Fig. 6 the total probability, integrated over both angle and energy, for a direct, or pre-equilibrium, reaction resulting in the emission of a neutron. We see a dramatic increase with proton energy, but even at 35 MeV direct emission is only ∿20% probable. Compound nucleus reactions dominate. Even when there is a direct emission there will generally be enough excitation energy for equilibrium evaporation of one or more neutrons to follow.

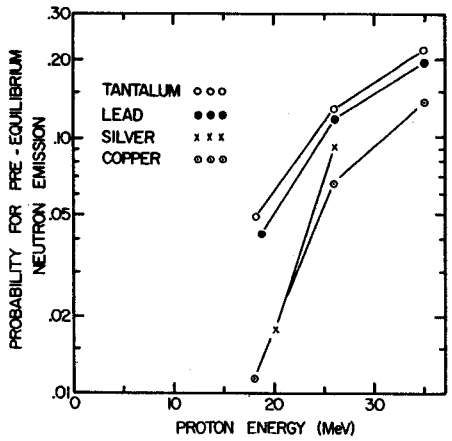

Fig. 6

The energy dependence could be studied more precisely with thin-target data, which we hope to obtain.

References

1. Y.K. Tai, G.P. Millburn, S.N. Kaplan, and B.J. Moyer, Phys. Rev. 109, 2086(1958).

2. David Bodansky, Ann. Rev. Nuclear Sci. 12, 79(1962).

3. M. Blann and A. Mignerey, Nuclear Physics A186, 245(1972) and reference given there.

Fine Structure in Pulse Shape Discrimination

A. Galonsky and T. Amos

In the area of pulse-shape discrimination (PSD) we have discovered the existence of a fine structure in the neutron PSD signature. We observed in our NE213 scintillator 38-MeV neutrons produced by 40-MeV protons in the $^{7}Li(p,n)^{7}Be$ reaction. A contour plot of the two-dimensional PSD display is shown in the figure. The peaks labelled A and C are the ones usually observed. They correspond to gamma rays and neutrons, respectively. Our computer data-taking system, TOOTSIE, allows us to examine the time-of-flight spectrum of any portion of the data shown in the figure.

When this was done for each of the groups A through E, it was found that each of the new groups, B, D, and E, had the neutron (C) time-of-flight spectrum. Our analysis gives the following identifications of the neutron groups: B consists of protons escaping from the end of the scintillator. Its relative importance increases with neutron energy. For a given neutron energy its relative importance decreases with increasing scintillator thickness. C consists of protons recoiling from n-p scattering and stopping within the scintillator. D consists of protons from the $^{12}C(n,p)^{12}B$ reaction, and E consists of α particles from break-up by neutrons of ^{12}C into three α particles. C predominates at low neutron energies, but above 70 MeV the cross section for n-p scattering is less than the cross section for either $^{12}C(n,p)^{12}B$ or $^{12}C(n,n3\alpha)$. In order to determine absolute values of neutron cross sections from a calculation of scintillator efficiency it is necessary to take account of the origin of each of the above groups.

In addition to its use in neutron time-of-flight work, the fine structure in PSD may find application in neutron spectroscopy not involving time-of-flight. Neutron spectroscopy in the upper atmosphere and in the Van Allen belts is one example that comes to mind.

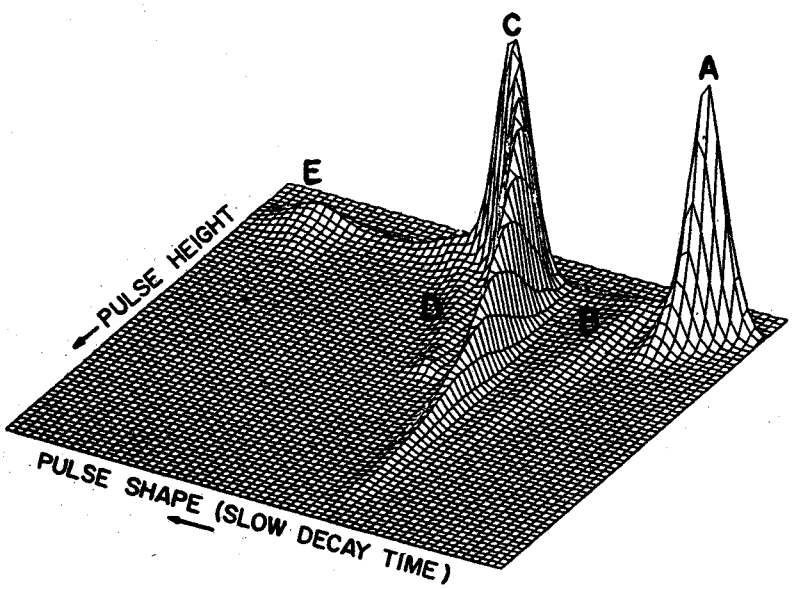

Fig. 1 Contour diagram of 2-dimensional pulse-shape-discrimination data obtained with 38-MeV neutrons incident on NE213 liquid scintillator. The labelled groups are discussed in the text.

C.P. Wolk,* S.M. Austin, J. Bortins, and A. Galonsky

In the last two years we have made a number of technical improvements in our program to use ^{13}N in a study of fixation of nitrogen in algae. This has resulted in the first autoradiograph of ^{13}N fixation of which we are aware.

One major improvement was a switch in the reactions producing ^{13}N from $^{16}O(p,\alpha)$ to $^{13}C(p,n)$. This improved the yield by a factor of five and, because of the lower proton energy required, eliminated the problem of the activiation of the sample holder. Most importantly production of ^{13}NO, which was a significant problem with the O target, did not occur with the ^{13}C target. In the earlier work we had to eliminate the ^{13}NO chemically because algae fix this compound more rapidly than they fix N_2.

We also improved our autoradiography technique by using emulsion sensitization.[1] This reduced the average grain spacing by a factor of two. A photomicrograph of an algae with two tracks from ^{13}N positron decay is shown in the figure. The average grain spacing in this photo is 2 microns.

The objective of the program was to find out if N_2 fixation is accomplished by the heterocysts. There is one heterocyst for about 20 vegetative cells, and there are three heterocysts in the algal filament shown (all three larger, two darker, than the other cells). Based on 10^3 tracks we can now say that the heterocysts are not the sole sites of nitrogen fixation but do perform about 25% of the fixation. We will now go on to try to discover the biochemical products made by the heterocysts and vegetative cells with their assimilated N_2.

References

1. W.H. Barkas, Nuclear Research Emulsions, Academic Press, p. 131(1963).

* AEC Plant Research Laboratory.

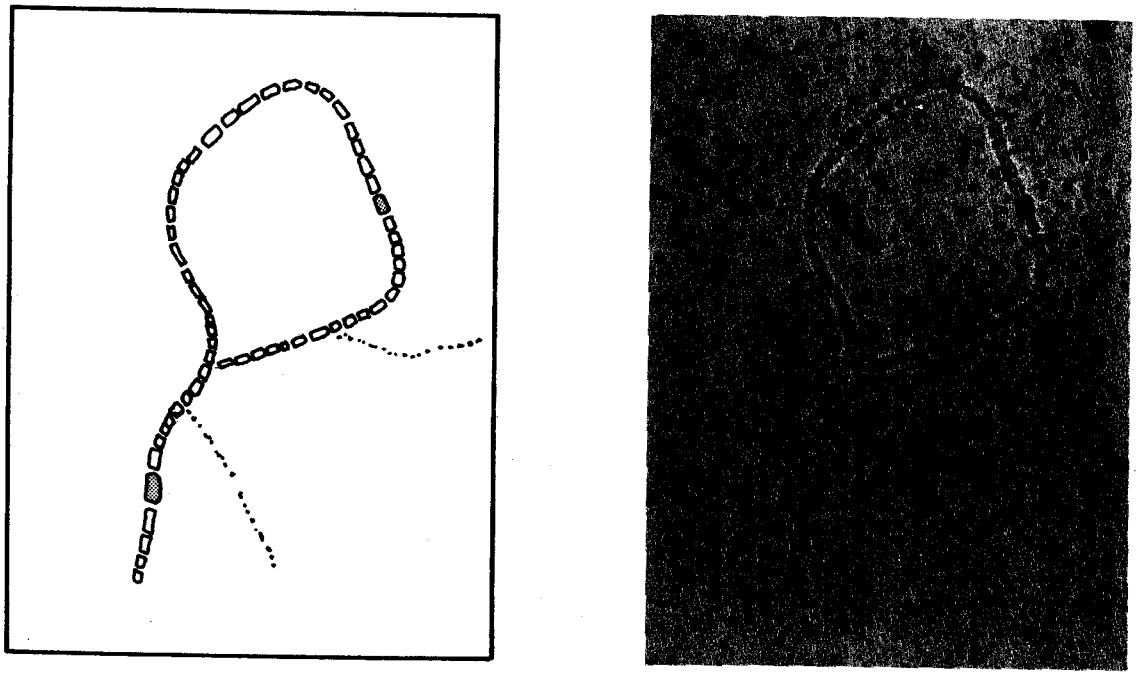

Fig. 1 Photomicrograph of a filament of ^{13}N-fed, blue-green algae. There are two tracks from ^{13}N position decay. Each track originates in a vegetative cell.

Strontium Isotopic Ratios and Trace Element Abundances, Aves Ridge Granities, Caribbean Basin

Charles M. Spooner*

An unusual recovery of about 3500 kgs. of granitic rocks from a dredge haul (12° 20' N Lat., 63° 30' W. Long.) from the Aves ridge has prompted an investigation into the strontium isotopic ratios and trace element geochemistry to determine whether these rocks have a direct origin in the upper mantle or an origin involving anatectic melting of crystal material.

The Aves ridge forms a prominent submarine feature parallel to and about 270 km to the west of the Lesser Antilles. On the basis of seismic refraction studies (Fox et al.[1]), the ridge is composed of a 5 km thick capping series of volcanic and sedimentary rocks overlying a crustal layer with V_p=6.0 to 6.3 km/sec.

Three rock types: a granite, a granodiorite inclusion within the granodiorite and a granophyre were analyzed. Strontium isotopic analyses were performed on a 6-inch, 60° sector, solid source, Nier-type mass spectrometer at the MIT Geochronology Laboratory. The measured $^{87}Sr/^{86}Sr$ for the three rock types are: 0.7038 ± 0.0007, 0.7046 ± 0.0023, and 0.7080 ± 0.0005 respectively, expressed relative to 0.7083 ± 0.0004 for the Eimer and Amend $SrCO_3$ standard. Since all have low Rb/Sr ratios (less than 0.3) and since K-Ar ages range from 89 to 18.5 m.y., the strontium sitopic ratios reported are essentially the initial ratios. Since all the isotopic ratios are lower than that of present-day sea water (about 0.709), equilibration with common strontium in sea water has not taken place. It is reasonable to infer that other trace elements have similarly been unaffected by alteration or contamination.

Trace elements, including many of the rare-earth elements (REE) were analyzed by instrumental neutron activation analysis using facilities kindly provided by the MSU Cyclotron Laboratory. The samples were irradiated in powdered form without prior chemical treatment for up to 3 hours at a thermal neutron flux of $2x10^{12}$ $n/cm^2/sec$ in the MSU Triga reactor. Counting data were collected using a 10% Ge(Li) detector and a 4096 channel ADC using PHOLYPHEMUS. Identification of photopeaks, their integration and comparison with rock standards to yield concentrations was done using a computer procedure outlined by Baedecker.[2] Errors based on counting statistics alone range from 4% to 20% of the amount present. These data are shown in Table I.

When normalized with respect to carbonaceous chondrite abundances, the REE trend shows pronounced light rare-earth enrichment typically found in continental granitic rocks. K/Rb and Zr/Hf ratios show an expected decrease for an internally differentiated series of granties. Strongly lithophile elements, especially Th, show an unexpected decrease in terminal, granophyric stage, probably through removal by a vapor phase. This conclusion is consistent with the petrographic observations (i.e. abundant miarolytic cavities indicative of a gas phase).

The occurrence of granities in the oceanic environment is unusual; however, the great areal extent of the 6.0 to 6.3 km/sec layer throughout the Caribbean basin suggests that granitic rocks may form a substantial fraction of this layer.

The strontium isotopic and trace element results suggest an upper mantle origin from a low Rb/Sr source followed by extensive differentiation (REE results) and near surface emplacement. Perhaps these rocks and the processes forming them are common to primitive continental crusts in which case the Caribbean crust is a proto-continent.

References

1. P.J. Fox, E. Schireiber, B.C. Heezen, The geology of the Caribbean crust: Tertiary sediments, granitic and basic rocks from the Aves ridge. Tectonophysics 12, 89(1971).

2. P.A. Baedecker, Digital methods of photopeak integration in activation analysis, Anal. Chem. 43, 405(1971).

* Department of Geology, MSU. (Supported by the USAEC and the NSF.)

TABLE I

INAA Element Abundances, Aves Ridge Granities, in ppm

	R-1 (inclusion)	R-2 (granite)	R-3 (granophyre)
Na	29600	23700	22200
K	7900	11200	10300
Fe	29600	26100	25700
Mn	249	329	955
Sc	10	14	43
Ba	669	1061	1113
Th	8	8	24
Hf	7	6	25
Zr	215	212	294
Co	138	153	180
La	16	14	32
Ce	33	51	84
Sm	3	17	8
Eu	1	1	3
Lu	0.35	1.2	0.20
K/Rb	767	485	97
K/Th	987	1400	429
Zr/Hf	31	35	12

Nuclear Information Research Associate Program: Data Compilations in the Mass Region A=101-106*

R.R. Todd,** L.E. Samuelson,*** F.M. Bernthal, W.H. Kelly, Wm.C. McHarris, and R.A. Warner

For the past year we have been participating in the Nuclear Information Research Associate Program (NIRA) sponsored by the National Academy of Sciences—National Research Council and funded by the National Science Foundation. Dr. Todd was one of the first group of NIRA's that was selected and he has been working on the compilations of nuclear data of the A-chains A=101-106. At the end of his first year he accepted a permanent faculty position at Western Michigan University. Upon Todd's resignation from the program, Dr. L.E. Samuelson was selected to be the replacement NIRA and is working on the A=104-106 chains.

The compilations for the A=101 and 102 chains are now complete and the results are in the final stages of editing before being submitted for publication. The A=103 compilation will be completed by Dr. Todd later this year.

* Supported by the USAEC and the NSF.

** Now at the Department of Physics, Western Michigan University, Kalamazoo, Michigan 49001

*** Nuclear Information Research Associate. Work supported by the National Science Foundation through the National Academy of Sciencies—National Research Council.

Magnetic Spectrograph

H.G. Blosser, E. Kashy, and J.A. Nolen

The 90-cm Enge split-pole spectrograph has been in operation for about three years. During this period its use has steadily risen; about 60% of total beam time goes to the spectrograph including virtually all of the time devoted to both transfer reactions and inelastic scattering. A continuing series of improvements have added greatly to both the convenience with which the facility can be used and its accuracy.

An absolute calibration system[1] uses a momentum matching procedure to calibrate the spectrograph in terms of known nuclear mass differences. Recent calibration work has been directed to accurate determinations of effective radius of curvature vs. focal plane position. The large contributions of field edges to the total bending make a careful magnet recycling and setting procedure especially important. In addition we have found that the field shape depends on the rate at which the field is changed; for highest accuracy this rate is limited to 1,500 gauss per minute. Careful calibrations at 10 kilogauss have been completed and work at higher fields is in progress.

Many experiments in the spectrograph now utilize one form or another of live focal plane detector so as to minimize the effort and expense required for scanning very high resolution plates (∿0.1 mm lines). The present rather standard live detector configuration uses a resistive wire proportional counter in the focal plane backed by a plastic scintillator for time-of-flight and energy information.[3] The resistive wires typically give 1 mm spatial resolution using charge division and cover 300 mm of focal plane with excellent linearity and stability. The scintillation counter timing window (triggered by the cyclotron rf) makes it possible to study rare particles in the midst of high intensity background. Using this arrangement, clean ^{6}He spectra have been obtained in circumstances where the number of ^{6}He particles entering the proportional counter was a factor of 10,000 less than the alpha particle background. Commercial position sensitive silicon detectors are also sometimes used for live position readout. Such detectors can give spatial resolutions of 0.25 mm over a narrow range and have been used extensively in mass measurements and other narrow range work.

An important contribution to the speed and ease with which the spectrograph can be used has come from the installation of motors and remote readouts on all important spectrograph parameters. These include the focal plane position (up-down and in-out), the target position (angle and height), the entrance aperature (choice of 7) and the scattering angle (∿0.1° accuracy). The beam preparation system also allows independent variation of the energy dispersion on target and the magnification. Two sextupole lenses are also provided for optimum cancellation of aberrations. These remote controls, in conjunction with the previously described resolution meter,[2] allow the user to quickly make fine adjustments in all control elements as required for optimum resolution. At present the best resolution obtained in a reaction experiment is 3.7 keV for ^{12}C(p,t) at 40 MeV and 3.0 keV at 30 MeV for ^{12}C(p,p').

References

1. G.F. Trentelman and E. Kashy, Nucl. Instr. and Methods 82, 304(1970).

2. H.G. Blosser, G.M. Crawley, R. deForest, E. Kashy, and B.H. Wildenthal, Nucl. Instr. and Methods 91, 61(1971).

3. W.A. Lanford, W. Benenson, G.M. Crawley, E. Kashy, I.D. Proctor, and W.F. Steele, BAPS 17, 895(1972).

Accurate Q-Values and Excitation Energies Using Momentum Matching and Photographic Emulsions

G. Hamilton, E. Kashy, J. Nolen, and I. Proctor

Using previously developed momentum matching techniques in conjunction with photographic emulsions in the magnetic spectrograph we are able to determine excitation energies of nuclear levels and ground state Q-values with an accuracy ∿2 keV. Previous measurements at MSU, including calibration of the beam energy analysis system and determination of many new nuclear masses, had utilized solid state or resistive wire proportional counters in the focal plane of the magnetic spectrograph.

The emulsion method eliminates some of the uncertainties of the detector methods. The basic difference is that with the plates all known and unknown states are recorded simultaneously on one plate during a given run. A disadvantage of this method is that more calibration lines are needed in any given measurement because the focal plane calibration must also be treated as an unknown when measurements are not being made at constant ρ in the magnet. This is in practice not a limitation, however, as indicated in the example given below.

All the measurements quoted below were from spectra recorded on 21" long photographic plates with proton and deuteron line widths ∿0.3 mm. The centroids were read directly from the plates using a microscopic with a stepping motor stage drive. The accuracy of the ball screw and reproducibility of the readings combined to give typical centroid uncertainties of ∿0.03 mm except for very weak peaks.

One run consisted of bombarding with 35 MeV protons a thin ^{27}Al target on a C backing. Both protons and deuterons were recorded in the emulsion. The calibration lines are indicated in Table I. In one simultaneous least squares fit to these 6 lines it is possible to determine a) the beam energy to a standard deviation of 2 keV, b) the scattering angle to a standard of 0.03°, c) the absolute radius of curvature of the calibration lines, and d) the two coefficients of a parabolic ρ vs. D calibration curve for this region of the focal plane. We are using a flat plate holder instead of the slightly curve surface specified for the Enge split-pole magnet. Over this 20" section of the focal surface we find a small, but necessary, quadratic term in the ρ vs. D curve but higher order terms have not been justified by the accuracy of the present calibration lines. The correlation matrix resulting from the least squares fit does indicate that the five parameters mentioned above are in fact independently determined.

Tentative new assignments and probable errors resulting from this run are given in Table I. There may be small changes in these numbers before the analysis is finalized.

The current measurement of the ^{15}O mass excess is 2857±1 keV, which agrees with several other recent determinations of this number. The $3/2^-$ hole state in ^{15}O is a very strong and useful line for use as a calibration in future work involving neutron pickup reactions. The well known particle states in the 6 MeV excitation energy region in ^{15}O are extremely weak in pickup reactions, and vice versa.

TABLE I

Preliminary Excitation Energies and Q-Values Extracted via Momentum Matching Technique

Peak	Previous Q (keV)	Fit Q (keV)	Previous E_x (keV)	Fit E_x** (keV)
$^{27}Al(p,d)$	-10833.3±0.9*	10833±1	0.0	0
"			228.2±1.0	228
"			417.0±0.4	418
"			1057.7±0.5	1059
"			1759.2±0.6	1760
"			1850	-
"			2068.7±0.3	
"			2069.5±0.3	2070
"			2071.7±0.8	
"			2365.0±0.5	2366
"	-13378.5±1.2*	-13378±1	2545.2±0.5	2545
"			2660.8±0.4	
$^{16}O(p,d_o)$	-13439.3±0.6	-13441±1	0.0	0
$^{27}Al(p,d)$			2913.2±0.6	2915
"			3159.4±1.0	3161
"			3405 ±5	3403
"			3677 ±8	3680
"			3751 ±8	3753
"			3962 ±10	3962
"			4425 ±8	4430
"			4546 ±8	4547
"			4704 ±8	4705
"			4939 ±8	4941
"			5473,5485,5506	5491
"			5593 ±8	5597
"			5715,5741	5724
$^{12}C(p,d_o)$	-16497.3±1.0	-16497±1	0.0	0
$^{27}Al(p,p_o)$	0.0*		0.0	-1
$^{16}O(p,p_o)$	0.0		0.0	0
$^{14}N(p,p_o)$	0.0		0.0	2
$^{13}C(p,p_o)$	0.0		0.0	1
$^{27}Al(p,p')$			842.9±0.3	844
"			1013.0±0.3	1014
"			2208.9±0.6	2210
"			2732.0±0.8	2734
$^{12}C(p,d_1)$			1995 ±3	2000
$^{27}Al(p,p')$			3003.5±1.0	3003
"			4410 ±2	4404
"			4510.6±0.6	4509
$^{12}C(p,p')$	-4439.2±0.3*	- 4439±1	4439.2±0.3	4439
$^{27}Al(p,p')$			4812 ±2	4810
$^{16}O(p,d_1)$			5177 ±3	6172

*Used as calibration lines.
**Estimated errors are ∿2 keV.

A Charge Division Position Sensitive Proportional Counter System

W.A. Lanford, W. Benenson, G.M. Crawley,
E. Kashy, I.D. Proctor, and W.F. Steele

We have developed, and are extensively using, a position sensitive proportional counter system for use in the focal plane of our split-pole magnetic spectrometer. The system consists of a charge-division position-sensitive proportional counter backed with a plastic scintillation counter. The scintillation counter provides an energy signal and a time signal both of which are used for particle identification. A gas handling and flow system is used to stabilize gas pressure and preserve the purity of the gas. In addition, we have a permanent electronics setup which allows particle identification with (1) the E signal from the scintillation counter, (2) the ΔE signal from the proportional counter, and (3) the time-of-flight (TOF) of the particle in the spectrograph (relative to the rf of the cyclotron). These may be used in any combination by simply changing switches.

The system has the following characteristics: for 45° incident particles. (1) Position resolution of about 1 mm (FWHM along the focal plane), (2) an active length of about 12 inches, (3) a counting rate capability greater than 5×10^3 cps, (4) extremely good particle identification.

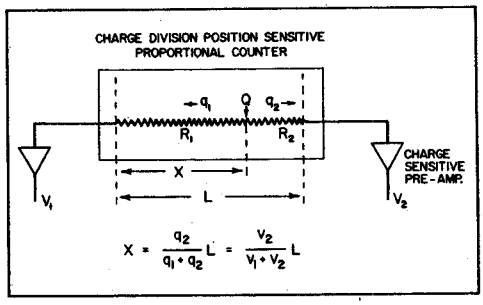

Fig. 1 A schematic representation of a change division, position sensitive proportional counter. The symbol X represents the distance along the counter, and Q is the total charge pulse in the counter which divides into q_1 and q_2 depending on were the event occured.

The proportional counter is a normal transmission mounted proportional counter except (1) the center wire has a relative resistance (∿4KΩ) and (2) the signal from the proportional chamber is measured at both ends of the center wire with charge sensitive pre-amps. Figure 1 shows schematically how the counter works. The charge Q deposited at position X along the center wire divides according to the resistance to the preamps (which look like ground to the high frequency components of the pulse). The signal V_1 and V_2 are shaped (RC∿.5 μs) and fed into computer ADC's. The computer performs the division XE/E to generate X. This counter is similar to those developed at Rochester[1] and Rutgers.[2]

While this system does not allow one to use the full high resolution capability of the dispersion matched cyclotron-magnetic-spectrometer combination, it has been heavily used since it first became operational. Most particle transfer reactions which are presently being studied in the lab (such as (p,d), (p,t), (p,^{3}He), (^{3}He,^{6}He), and (^{3}He,^{7}Be)) use this proportional counter system to take at least some of the data. Often the combination of plate data at a few angles and proportional counter data at the remaining angles is sufficient. Shown in Fig. 2 is a comparison of ^{208}Pb(p,t)^{206}Pb reaction observed with nuclear emulsions and with the proportional counter. While the plate data has higher resolution, in this case almost all the states are resolved by the counter. There are several other spectra taken with this system in other sections of this report. There are some experiments reported, such as (p,^{3}He) and the (^{3}He,^{6}He) reactions which would have been very difficult to study with more conventional techniques but which time-of-flight particle identification puts on an equal basis with other reactions.

References

1. H.W. Fulbright, W.A. Lanford, and R. Markham, to be published.

2. N. Williams, T.H. Kruse, M.E. Williams, J.A. Fenton, G.L. Miller, Nucl. Inst. and Methods 93, 13(1971).

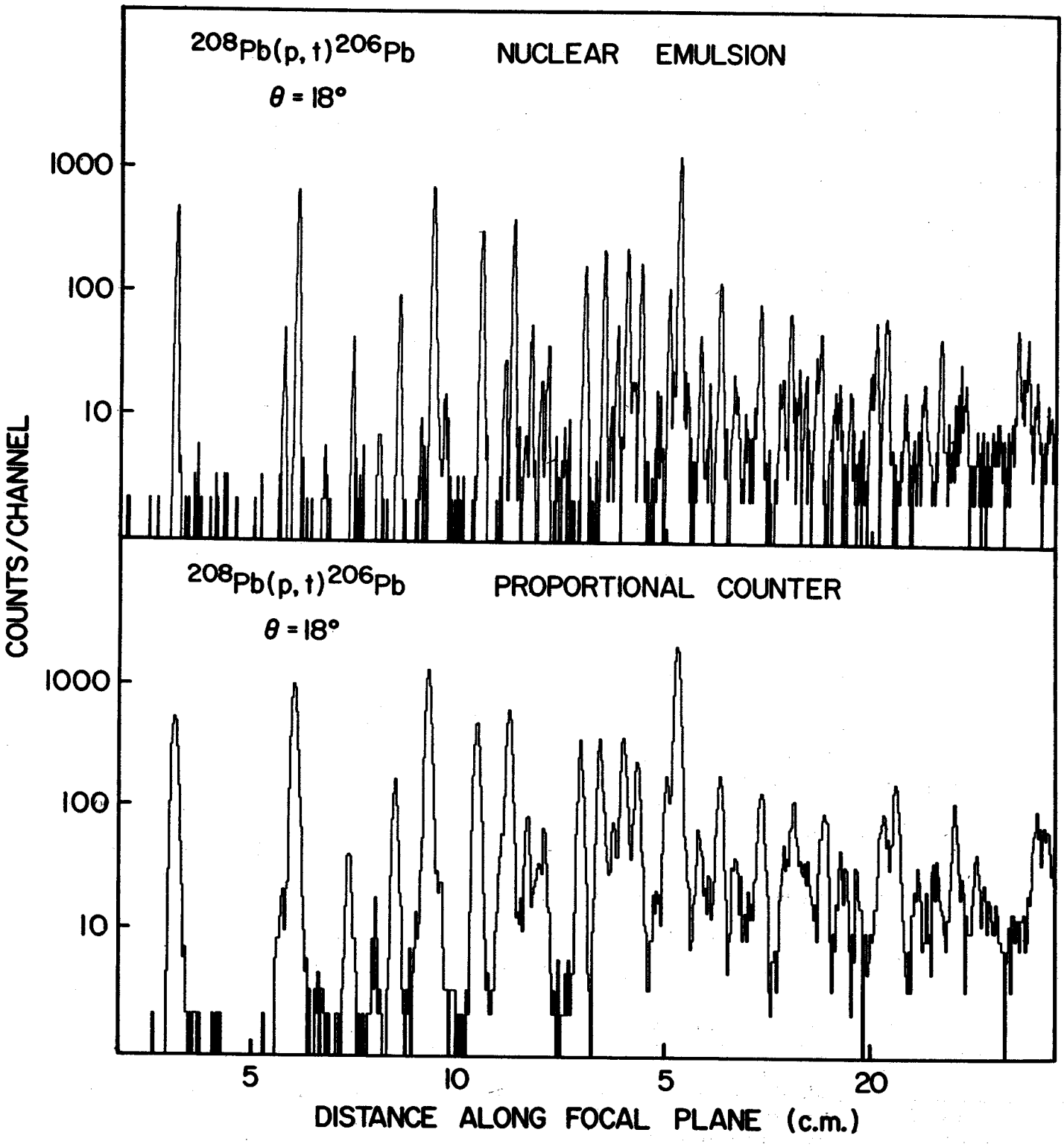

Fig. 2 Spectra of the ^{208}Pb(p,t)^{206}Pb reaction with E_p=35 MeV obtained with a nuclear emulsion (top) and with the position sensitive proportional counter (bottom). The resolution of the data taken with nuclear emulsions is about 15 keV (FWHM) while that taken with the proportional counter is about 30 keV.

Cyclotron Modifications and Improvements

H.G. Blosser, H.P. Hilbert, L.L. Learn, P.S. Miller, P. Sigg, and G. Stork

I. Alumina rf Tuning Bearings

In the spring of 1972 a major cyclotron shut-down was scheduled for the first time in seven years. The primary purpose of this shut-down was replacement of the graphite bearings supporting the main rf tuning panels in the cyclotron cavity, which had gradually deteroirated in the years of operation, as seen in Fig. 1. The basic problem appeared to be a failure of contact fingers designed to shield the bearings from rf, which led to rf heating of the bearing and the melting of the bearing housing. The tuning panels were then free to shift by as much as 2 mm, introducing sudden jumps and instabilities in the rf. The newly installed Alumina bearings do not require protective contacts and the basic wear characteristics of the Alumina are such that we expect an essentially infinite life from the new arrangement.

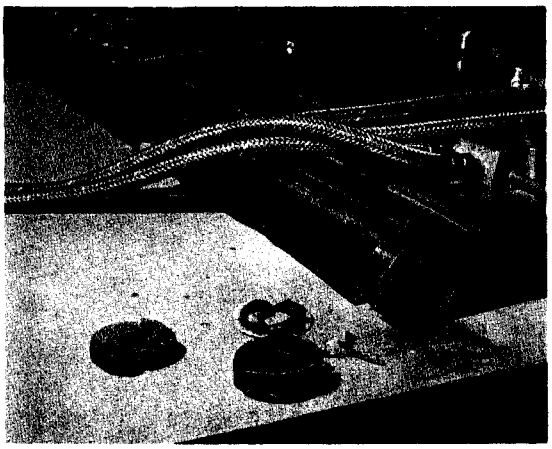

Fig. 1 Old tuning panel bearing components as removed from the Cyclotron in April 1972. One graphite disc (2 are shown) was removed from the bearing mount seen on the panel in the background. The deterioration of the bronze bushing around the graphite insert shown in the foreground is evident.

II. New Centering Coils

During the major disassembly required to change the rf bearings a new set of beam centering coils was installed in the cyclotron. The previous centering coils had been installed in 1967 as an afterthought for the purpose of making control easier. In order to avoid a 6 week shut-down the coils were placed in the dee insulation space thereby adding capacity to the rf system and reducing the useable upper energy of the cyclotron from 56 to 45 MeV. The new coils return the rf system to its original state and we therefore expect the usable energy of the cyclotron to again extend above 50 MeV.

III. New Central Region Design

Acceleration of heavy ions uses the third harmonic mode in our cyclotron, i.e. the orbital frequency of the ions is one-third of the rf frequency. Unfortunately the cyclotron has never given usable third harmonic beams due to the effect of the so-called gap-crossing resonance (a coupling phenonmenon between the longitudinal and transverse motions[1]). The third harmonic gap crossing difficulty was overlooked in the original design studies for the cyclotron, which concentrated on precise, high-energy proton beams as the primary operational objective. Approximately 18 months ago we decided to rectify this design deficiency: detailed study was initiated with the objective of working out an optimized central region for both second and third harmonic acceleration. As this study proceeded, it became clear that the dee angle was an extremely important factor in the gap-crossing resonance difficulties. Figure 2, repeated from last year's annual report, shows the intrinsic orbit centering error plotted vs. dee angle for first, second, and third harmonic acceleration. As the figure clearly indicates, the best dee angle is highly dependent on the harmonic number. After careful consideration of these results and of electrical and mechanical

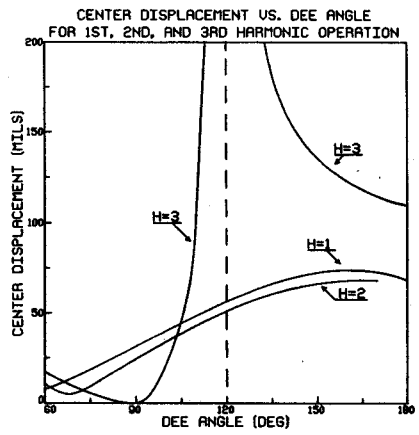

Fig. 2 Effect of gap-crossing resonance on particle orbits in the MSU Cyclotron.

factors, we decided to shift to an interchangeable dee concept in our new design, so that the dee angle could be individually selected for each harmonic and therefore set at the best value. The computing phase of this study has now been completed.[2] New dee configurations for both second and third harmonic acceleration (90° and 60° dees respectively) have been worked out. In brief the results indicate that performance of the third harmonic configuration should match present first harmonic results and second harmonic beams

(deuterons, etc.) should become the most precise of all (assuming equivalent ion source performance in each case).

IV. New Central Plug and Source Mount

In a separated orbit cyclotron the final beam is extremely sensitive to the relative position of the ion source, the source extraction electrode (the puller), and the 180° selection slit. In a standard cyclotron configration the puller is mounted on the dee; such mounting systems are generally rather flimsy and imprecise, and subject to thermal motion as the dee warms or cools. Central region design constraints, however, make it very difficult to devise better puller mounts unless insulators are used, and in the past insulators have generally been viewed as unreliable. Recent insulator development studies at Columbia[3] in connection with the conversion of the Nevis synchrocyclotron, however, imply that Freon-cooled Alumina insulators can now be successfully used for puller mounting. With such an arrangement it would be possible to set the source-puller geometry with great accuracy and thus eliminate the most important contribution to beam instability in our cyclotron. Unfortunately, considering the extremely severe environment in the cyclotron central region, the only way to be really sure of the feasibility of such an arrangement is via a working test.

A first such test was performed about six months ago using an assembly which could be inserted through the cyclotron ion source hole in place of the ion source. In a 72-hour run this test insulator survived without detectable damage. Its voltage holding capability gradually improved throughout the period up to a final value of 48 kilovolts (equivalent to 40 MeV proton operation in our standard turn pattern). Encouraged by this result we have proceeded with the design of a new center plug system for the cyclotron which will carry the ion source, the puller, and the 180° slit on a common 6" diameter plug inserted through a vacuum lock in the lower pole. Construction of this new plug is approximately 50% completed. When it is finished we will be able to subject the Alumina insulators to the ultimate test, namely long-term survival in the presence of an ion source. If the test is successful, insulator-mounted pullers will be introduced in all operating modes of the cyclotron. If the test is unsuccessful, we will revert to the present arrangement of mounting the puller on the dee. Even in this eventuality the new center plug will be a valuable addition since the ion source and the 180° selection slit can be mounted on the plug regardless of the result of the insulator test; the ability to change both of these components through the new lower pole vacuum lock will substantially shorten changeover time from one mode of operation to another.

As a part of the central region work, a new beam probe assembly is being constrcted which will make it possible to shift from a radially sensitive probe to an axially sensitive probe in a few minutes. Such a probe change is required in dealing with coherent vertical oscillations, a beam dynamics difficulty which historically seems to recur every few months in the cyclotron.

V. Interchangeable Dee System

A mechanical design for the interchangeable dee system has been completed; various quick release devices are included which should make it possible to change dees and be back in operation in approximately four hours including pumping time. The radio frequency properties of the various new dees have also been studied in our origional rf mock-up which was returned from Princeton for this purpose. Dee configurations which cover the required frequency range have been worked out for each mode. Results are summarized in Table I. We expect the complete new system to be operational in six to twelve months.

References

1. M.M. Gordon, Nucl. Instr. and Methods NS-18-19, 268(1962).
2. L.L. Learn, H.G. Blosser, and M.M. Gordon, Proc. of the Sixth Interntl. Cyclotron Conference, 1972.
3. J. Rainwater, IEEE Trans. on Nucl. Sci. NS-18, 262(1971).

TABLE I

Frequency Range Results for Various Dees Using Existing Items and Tuning Panels—Results from rf Model

Dee Angle Degrees	Dee Thickness In.	Dee to Linear Spacing In.	Max. Freq. Mhz	Min. Freq. Mhz
60°	2.5	1.375	23.6	17.0
60°	3.5	.875	22.2	14.6
60°	4.0	.625	19.6	12.3
90°	2.5	1.375	21.2	15.5
	4.25	.500	17.5	10.6
120°	2.5	1.375	21.0	13.8
140°	2.5	1.375	19.5	12.7
140°	2.5*	1.375	21.5	14.3
140°	2.5	1.375**	23.6	12.7

* Existing Cyclotron Dees. Model shows coherent shift to lower frequencies due to different tuning panel structure.

** Model study with special Princeton type linear configuration.

Design Study for a Compact 200 MeV Cyclotron

M.M. Gordon, H.G. Blosser, and D.A. Johnson

A preliminary design study has been carried out for a compact cyclotron which would acclerate protons to final energies ranging up to 200 MeV, and other ions to corresponding final energies. This machine would possess the basic structural and operational features of our present 50 MeV cyclotron including the central region geometry, the phase selection slits, and the single turn (100%) extraction system. This cyclotron would provide an excellent tool for nuclear and medical research at a relatively low cost (about two million dollars).

The 200 MeV magnet would have the same gap and the same maximum field strength as our present 50 MeV magnet, and would therefore have about twice the pole diameter (125"). However, this magnet would have four (instead of three) sectors with sufficient spiral to compensate the additional relativistic defocusing.

Realistic field trimming calculations were carried out using a new computer program (Fielder) which showed that excellent results could be obtained with the use of only 17 trim coils. Thus, for 200 MeV protons, the calculated rms phase deviation is less than 3°. Moreover, the total power consumed by the 17 coils would be less than 90 kW in all cases.

The suggested design for the rf system of the 200 MeV cyclotron is closely modelled on the present Maryland and MSU machines. This rf system would operate in the 10-20 MHz range with two dees, about 90° in angular width, allowing for both even and odd harmonic operation. Since these dees would be positioned within the magnet gap, the maximum dee voltage would be restricted to about 70 kV.

As in our present machine, the 200 MeV cyclotron would be equipped with a set of radial slits which reduce the phase width of the transmitted beam down to about 2°. The energy spread within each turn would therefore continue to have the same proportionate value: $(\Delta E)/E=1.5\times10^{-4}$. This implies a final energy spread of 30 keV for 200 MeV protons. and proportionate values for lower energy protons and for other ions. This energy spread is sufficiently small so that single turn extraction would be quite feasible.

Extrapolating the results obtained for our present cyclotron, the 200 MeV proton beam would have exceptionally small emittances, namely: 0.3 mm-mrad radially and 2.5 mm-mrad axially. Because of the increased longitudinal space charge effect, however, the 200 MeV proton beam should be restricted to about 2 micro-amps in order to secure 30 keV energy resolution.

In addition to 200 MeV protons, this cyclotron would produce, for example, 280 MeV helions, 210 MeV alphas, and 290 MeV $^{12}C^{4+}$ ions. The proton (and deuteron) ion source has exceptionally high luminosity so that the high quality beam characteristics given above can be achieved with reasonable beam currents. Since helium and heavy ion sources generally have much lower outputs, some sacrifice could be made in energy resolution and emittance in order to improve the final beam current for these ions.

A more complete discussion of this design study will be found in the proceedings of the Sixth International Cyclotron Conference (Vancouver, 1972), which will soon be published.

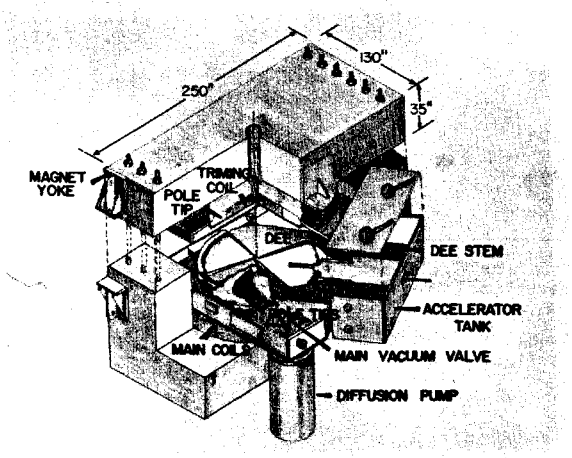

Fig. 1 Compact 200 MeV cyclotron design shown in a cut-away view.

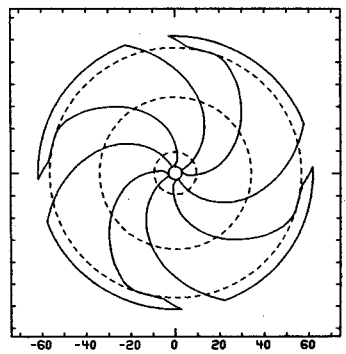

Fig. 2 Schematic diagram of four sector magnet pole tip geometry with scale in inches. Broken circles indicate locations of trim coil nos. 1, 9, and 17.

Progress with the On-Line Isotope Separator*

K.L. Kosanke, Wm.C. McHarris, and H.P. Hilbert

To date our work toward an on-line isotope separation has been directed at two areas of the overall system. First has been the development of our He thermalizer-jet transport (see next section of this report) with a tape transport that will later be used in our complete system. Second has been with our electric quadrupole mass filter. We have directed the initial work on our overall system to these areas because we felt they would each prove to be useful research tools in themselves and could be used before the complete system is operational. The remaining work to be done will be the linking of these two pieces of hardware together.

The on-line mass separation system under construction and its operation are shown schematically in Fig. 1. A collimated cyclotron beam enters the apparatus, striking a thin target (or a series of thin targets) in an atmosphere of helium (1 to 3 atmo. of pressure). Those nuclei near the back of the targets interacting with the beam will be recoiled out of the target into the helium. The recoils are then slowed to thermal energies through collisions in the helium. Recent work by R.D. MacFarlane[1] as well as studies conducted in this lab suggests that the next step is the attachment of the recoils to large molecule clusters (with masses up to 10^8 amu)[2] formed in the plasma generated by the cyclotron beam as it leaves the target passing through the helium atmosphere from impurities in the helium. The recoils then leave the thermalizer attached to these large molecular clusters through a pholyethylene or teflon capillary (0.02 to 0.06 in ID) accelerating to near the sonic velocity of He (∿3 ft/msec). The capillary is run through concrete shielding to a low background area about 40 feet away. At the end of the capillary the helium will be skimmed off using a one or two stage skimmer. Quite efficiency skimming of the helium should be possible just by directing the flow from the capillary at a coinical orifice. The molecular clusters with their horendus masses are extremely well collimate (90% diverage with an angle of less than 3°) and should be passed quite efficiently through the orifice whereas the helium will diverage more rapidly and be largely pumped off. If our pumping capacity is not sufficient to reduce the pressure to $\sim 10^{-5}$ tor after the first skimming stage, a second stage will be added. The molecular clusters will be broken up and the recoils ionized in an RF or DC induced discharge setup in one of the skimming stages with the recoils directed into the ion optics associated with the electrostatic quadrupole.[3] With the quadrupole setup properly only selected masses are transmitted through it.[4] At the exit of the quadrupole the recoils will either be directed into an electron multiplier such that it is possible to obtain a mass scan or onto paper or aluminized mylar tape for conventional nuclear counting.

References

1. R.D. MacFarlane and Wm.C. McHarris, Chap. II.C., "Techniques for the SCudy of Short Lived Nuclei" to be published in Nuclear Reactions and Spectroscopy, ed. by J. Cerny, Academic Press, New York 1973.
2. H.J. Jundas, R.D. MacFarlane, and Y. Fares, Phys. Rev. Letters 27, 556(1971).
3. Electric quadrupole supplied by Extranuclear Labs. P.O. Box 11512, Pittsburgh, Pennsylvania.
4. For a theoretical description of the Electric Quadrupole sec: W. Paul, H.P. Reinhard, and U. von Zahn, Z. Phys. 152, 143(1958).

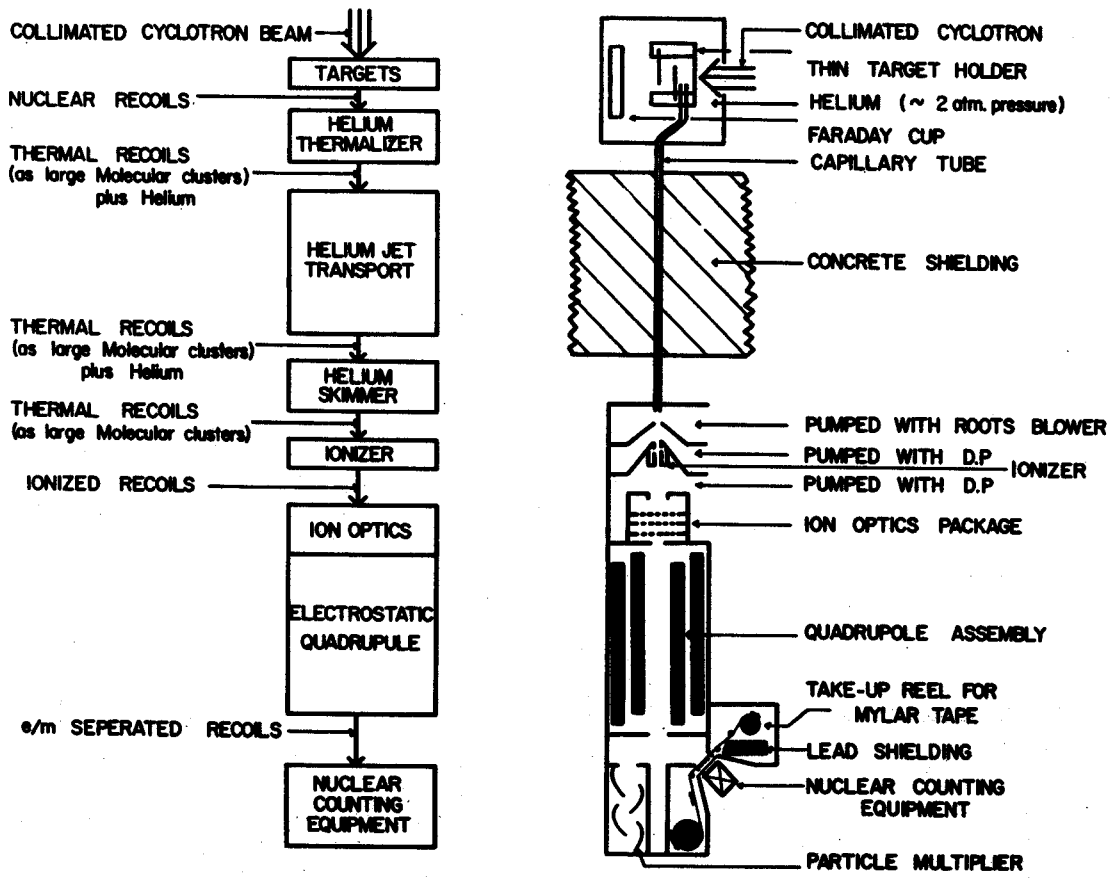

Fig. 1 Block and schematic drawing of on-line mass separator under construction.

Helium Jet System*

K.L. Kosanke, H.P. Hilbert, and Wm.C. McHarris

Our initial motivation for the construction of the helium thermalizer jet transport system was its proposed use as the first stage in an on-line mass filter (preceding section). While this remains the case, the helium thermalizer jet transport system has become a popular research tool in itself. It is being used with increasing frequency for the rapid transport of cyclotron produced activities to a low background area for conventional nuclear counting experiments. We anticipate that the helium jet system will remain an important research tool in and of itself even after we have developed an on-line mass separation capability.

The jet systems we have constructed were paterned after that developed by R.D. Macfarlane,[1] and we are grateful to him for his continued help in developing our system. While we are continuing to use polyethylene capillary (≃45 feet long) we have changed to a larger diameter (0.055" ID) capillary and are using higher pressures (≃3 atm.) of helium doped with small amounts (≃10 ppm) of benzene vapor. This has been done to improve the efficiency of the system and to reduce its transport time. The change to larger capillary was primarily to reduce transit times by reducing the time necessary to sweep the activity recoiling from the back side of the target into the capillary through increasing the flow rate in the capillary. However, this also had the positive effect of increasing transmission efficiency. In the case of ^{26}Si run at 3 atm efficiency increased 32% and the case of ^{23}Mg the efficiency increased 18%.

Before we were using small amounts of benzene vapor added to the helium, the efficiency did not vary much with helium pressure (from 0.3 to 4 atm) but remained at about 5%. Since we started using small admixtures of benzene, the transport efficiency has become sensitive to helium pressure, with the efficiency increasing by about 50% upon increasing the helium pressure from 1 to 3 atmospheres. This also had the positive effect of reducing transport times by increasing the flow rate in the capillary. The

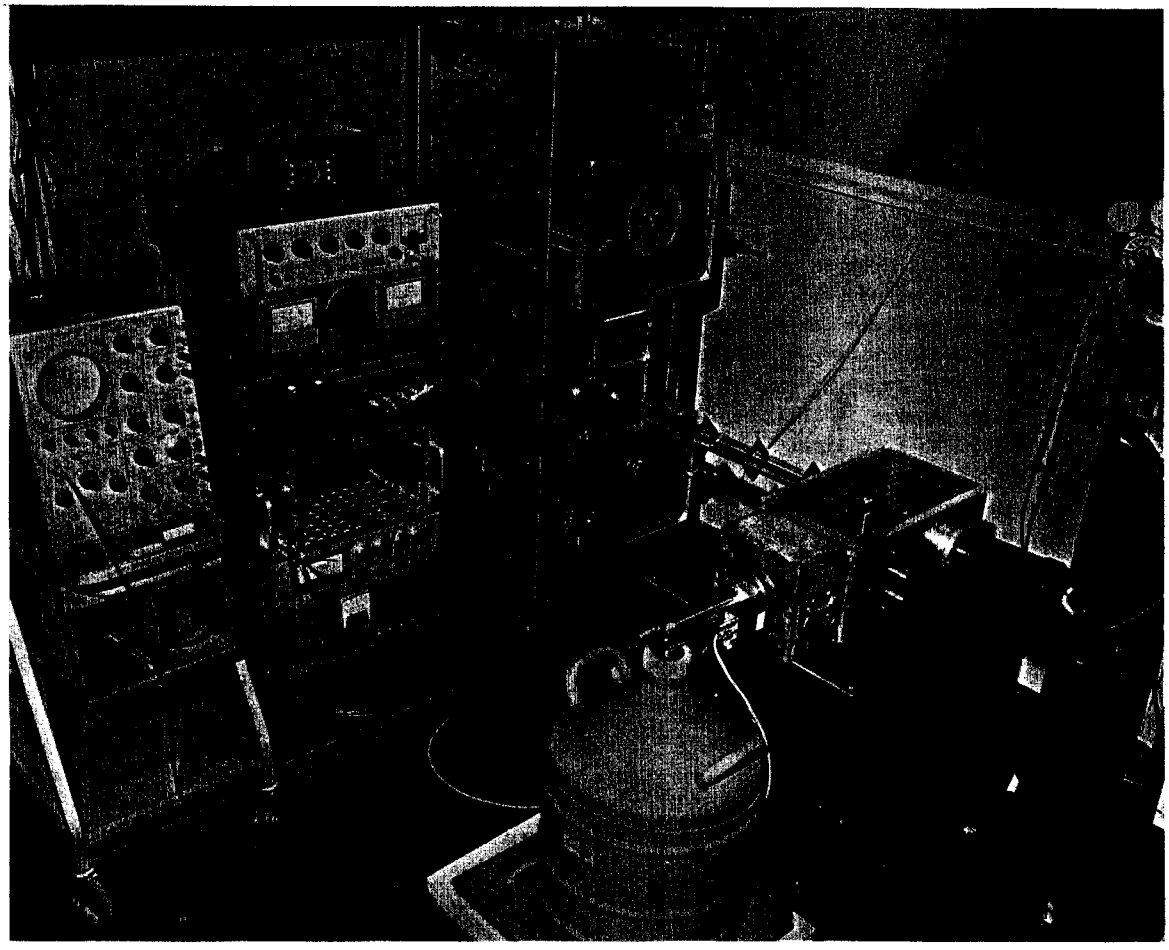

Fig. 1 Typical gamma ray singles experimental set-up using helium thermalizer jet transport system.

largest overall improvement in the helium jet system resulted from the addition of small amounts of impurities to the helium. We are using 10 ppm of benzene vapor added to the helium and obtain efficiencies improved by a factor between 5 and 10. Accordingly the present efficiency of the jet system is 90% for Co recoils. We know that we do not get 100% of the recoils coming out of the capillary to stick on the collecting surface (paper tape in this case). Judging from the radiation background build-up in the detector chamber at the end of the capillary, we believe much of the remaining 10% of the activity lost in the transport process is lost in the process of depositing it on the collecting surface.

All our observations are consistent with Macfarlane's thoughts as to the role of large molecular clusters in the transport of activities with the jet system.[2] He contends that large molecular clusters are formed from impurity molecules in the plasma of the cyclotron beam. (He has determined that the masses of these clusters to extend to $\sim 10^8$ AMU.) Further, the transverse diffiusion rates of these clusters, because of their enormous molecular weights, will be very low (i.e., they diffuse only very slowly to the capillary walls and are therefore lost only at a relatively low rate). Accordingly, high transport efficiency is the result of attachment of thermalized recoils to these molecular clusters.

In an attempt to determine the effect of the pressure in the detector chamber on the transport efficiency of the jet system, we observed that we could run with only a small drop in efficiency even at atmospheric pressure. In a run where a one atmosphere gradient was maintained across the capillary there was only a 30% decreas in the transport efficiency of the jet system upon changing the pressure in the detector chamber from 0.5 mm Hg to 1 atmosphere. Further, it is thought this may be improved by modifying the collecting technique when running at atmospheric pressure. This observation has since lead us to the possibility of preforming relatively fast and sophisticated chemistry with the jet system by catching the activities in aqueous solution. However, it was felt there could be a problem in doing chemistry at this point if the recoil atoms remained attached to the molecular clusters, because the recoils are present only as very small impurities (present only in ppm) in the cluster molecules. In our first attempt at chemistry, the activities resulting from 30-MeV protons on a Zn target were trapped in 2N HCl. Activity was collected for about 30 minutes, then the solution was passed through a column of Dowex-1. A good separation of Zn and Cn was achieved. A second run attempted to set an upper limit on the lifetimes for the recoil-cluster bond. Again we ran using 30-MeV protons on a Zn target. This time the activities were trapped in 8N HCL containing Zn and Cu carriers and fed into a column of Dowex-1 in an attempt at achieving a separation of 32.4-sec. ^{63}Ga from and Zn and Cu activities. We observed an enhancement of better than a factor of 6 over a previous run in which a series of separate Zn targets were irradiated and transported using our pneumatic target transport apparatus (rabbit).[3] In this helium jet transport run there was no attmept made to improve separations by altering any of the experimental parameters from our original guesses. In this run only about 1 second elapsed between entrapment of the activities leaving the capillary in the column eluant and the eluant's leaving the column. Accordingly, it is felt that the major time consuming activity in performing chemistry following the jet system will be involved in physically doing the chemistry and not in freeing recoils from the clusters.

We have observed the nature of the impurity molecules used to generate the molecular clusters can have an effect on the transport efficiency of different recoils. This was observed in a run using 30-MeV protons on an Al target to produce ^{23}Mg through a (p,αn) reaction and ^{26}Si through (p,2n) reaction. Clusters were formed using either benzene vapor or compressed air and water vapor. In each case the activities were transported with improved efficiency. However, the absolute transport efficiency for the ^{23}Mg and ^{26}Si depended on the nature of the cluster impurities. The ^{26}Si transport efficiency increased when changing the benzene vapor to compressed air and water vapor as the major source of impurities, while the ^{23}Mg transport efficiency decreased. Accordingly, the relative yield of ^{26}Si could be made to increase by 36% upon switching to the compressed air and water vapor as the source of impurities.

If it is true in general that transport efficiencies of chemically different recoils in a mixture of recoils are dependent on the nature of the impurities forming the molecular clusters, then not only will it be necessary to consider different sources of impurity molecules to get peak efficiency for the particular recoils to be studied, but also by choosing different impurity molecules it may be possible to make a Z determination of the different recoils by watching their relative transport efficiencies.

In that it was the absolute transport efficiencies that changed inversely in the ^{23}Mg-^{26}Si case and not merely relative transport efficiencies, this suggests that the attachment of recoils to molecular clusters may be occuring at active sites in the clusters that are chemically specific. If this is the case, then it is not

impossible to consider generating cluster molecules using carefully selected impurities such that it would be possible to achieve relatively clean chemical separations ocurring in the short times of the transport process. That is, chemistry performed on a time scale of ~50 msec and performed in such a manner that is fully compatible with placing the helium jet system on-line with an isotope separator. Note, it might be that the cluster molecules required for this would have to be generated off-line, using UV-light[4] or an electric discharge instead of the plasma generated by the cyclotron beam, because their generation required an environment that was incompatible with the efficient transport of activities with the jet system.

References

1. R.D. Macfarlane, R.A. Gouch, N.S. Oakley, and D.R. Torgeson, ORO-3820-2 (1969); Nucl. Instr. and Methods 73, 285(1969).

2. R.D. Macfarlane and Wm.C. McHarris, Chapter II.C., "Techniques for the Study of Short-Lived Nuclei", to be published in Nuclear Reactions and Spectroscopy, ed. by J. Cerny, Academic Press, New York, 1973.

3. G.C. Giesler, Ph.D. Thesis, Michigan State University, COO-1779-55, 1971.

4. K. Wien, Y. Fares, and R.D. MacFarlane, ORO-3820-19, to be published.

* Supported by the USAEC and the NSF.